Engineering multiscale therapeutics for kidney disease

Gary W. Liu

A dissertation

submitted in partial fulfillment of the

requirements for the degree of

Doctor of Philosophy

University of Washington

2019

Reading Committee:

Suzie H. Pun, Chair

Shreeram Akilesh

Stuart J. Shankland

Program Authorized to Offer Degree:

Bioengineering

University of Washington

Abstract

Engineering multiscale therapeutics for kidney disease

Gary W. Liu

Chair of the Supervisory Committee:

Suzie H. Pun

Department of Bioengineering

New therapies are urgently needed to address the growing chronic kidney disease epidemic. Nanoscale materials can enable precision drug delivery to kidney cells, improving the efficacy and safety profile of drug cargo. Renal progenitor cells can be engineered with nanotechnology to more efficiently regenerate lost kidney cells. Part I first motivates glomerular podocytes and proximal tubule cells as therapeutic targets in glomerular injury (Chapter 1). Nanoscale polymers that specifically target proximal tubules are identified (Chapter 2), and a new linker for programmed drug release (Chapter 3) and nanoparticles (Chapter 4) are developed for drug delivery to podocytes. Chapter 5 recommends new work to apply these platforms in therapeutic models. Part II begins with an introduction on renal progenitor cell biology (Chapter 7), and optimizes methods for non-viral gene delivery to these cells (Chapter 8). Chapter 9 recommends future work to use nanotechnology to promote renal progenitor cell survival and function.

Table of Contents

List of Figures

List of Tables

Acknowledgements

This work would not have been possible without the amazing team of mentors, collaborators, friends, and colleagues that I've had the immense pleasure and fortune of working with. A Ph.D. is a culmination of many failed experiments, revised hypotheses, and changed research directions, but working alongside my labmates and mentors has maintained my enthusiasm for academia.

My direct Ph.D. advisor **Suzie Pun**. I've learned so much from working with you these past 6 years, including compassion, grant writing, and patience. Thank you for affording me so much intellectual and experimental latitude, and enabling me to work on projects that I am personally passionate about. We've come a long way in working on kidney projects, from being funded on discretionary funds to now having two full grants supporting our work.

My collaborator and advisor **Stuart Shankland**. Thank you so much for very quickly and early including me in your lab – I've learned so much about the kidneys working directly alongside Shankland labmates and in lab meetings, as well as writing with you on grants and papers. I've enjoyed discussing our lifting routines and complaining about snow days because we can't go to the gym. Thank you for fist-bumping me in the hallways and for looking out for me academically – I really appreciate it.

I would like to thank my reading committee, **Suzie Pun**, **Ram Akilesh**, and **Stuart Shankland**, as well as my supervisory committee, **Suzie Pun**, **Ram Akilesh**, **Ceci Giachelli**, **Jonathan**

Himmelfarb, **Stuart Shankland**, and **Ying Zheng** for their great guidance and advice throughout my Ph.D. work.

My collaborator and mentor **Diana Eng**. You are one of the most passionate, enthusiastic, and energetic scientists that I know. From you I have learned to be optimistic and cheerful despite all odds, and how to greet people with your trademark phrase "Hello, hello!" I have thoroughly enjoyed working alongside you at "zero-dark-thirty" and on the weekends, and learning about your sheep, quail, and chickens!

My collaborator and mentor **Jeffrey Pippin**. I thoroughly agree with Stuart that you are a "walking Wikipedia"! I've lost track of how many of your great suggestions I've used. Thank you for being always prepared and for teaching me the whereabouts of reagents in the Shankland lab, as well as how to dissociate a kidney into a single-cell suspension.

My class and lab mates **Bob Lamm** and **Brynn Olden**. I am incredibly fortunate to have been able to work alongside you – both of you are an incredible fount of scientific creativity, enthusiasm, and energy. We have always dropped whatever we're doing to help each other out, and I think that really emphasizes that we're always up to help each other despite working on very different projects. I will always remember our "Engineering Meetings" and grant "writing" sessions!

My classmates **Shijie Cao**, **Yoon Jung Choi**, **Zhongdi Chu**, **Pak Khumwan**, **Efren Lee**, **Jason Miklas**, **Nuttada "Paper-based" Panpradist**, and **Ida Su**. We've had so much fun hanging out and getting Korean BBQ, boba tea, and dim sum.

My Seattle friends **Atticus Crowe**, **Steven "Momo" Gennaoui**, **Melanie Kong**, and **Brian Wojcik**. Thank you for reminding me that there is life outside of the lab, and for making sure that I have some semblance of a work-life balance. I have thoroughly enjoyed our Pokemon Go adventures and nights of karaoke, movies, trashy Palentine's, and board games.

My card buddies **Ian Cardle**, **Shijie Cao**, **Zhongdi Chu**, **Steven "Momo" Gennaoui**, **Ray Ilian**, **Drew Sellers**, **Meilyn Sylvestre**, **Lucy Yang**, **Bert Xue**, and others. I always look forward to our 80/120 Points sessions as they are one of my favorite ways to carry on a family tradition and destress. Thank you all for playing with me and bringing so much food!

My parents, **Tracy Wu** and **Kefeng Liu**, and my sisters **Anna** and **Janet Liu**. Thank you so much for all of your support throughout these years. I've learned so much about hard work and perseverence from my family and **Janet** – thank you for updating me on what's current in video games.

The undergraduate students that I've had the great privilege and honor of mentoring: **Soren Johnson**, **Ritika Jain**, **Tom McIlwain**, **Allie Carreno**, **Jonathan Yu**, and **Rio Hoshi**. Thank you for your tireless energy, thoughtful questions, and direct contributions to these projects.

Past Pun Lab members: **Yilong Cheng**, **Paul Elias**, **Yu-Shen Lin**, **Dave Chu**, **Chay Ngambenjawong**, and **Christine Wang**. Thank you for your enthusiasm, mentorship, and dedication to the lab environment and culture.

Current labmates: **Shixian Lyu** – you are one of the most efficient scientists I know! Thank you for working with me on these kidney projects. I've learned so much from our collaboration. **Alex Prossnitz** – thank you for taking up the project during your rotation studies. It has been a great honor working with you and mentoring you.

My friend and labmate **Meilyn Sylvestre**. Thank you for your incredible enthusiasm, energy, and fearless leadership in the lab. You have been a close friend and confidante in the lab – everyone needs a Meilyn Sylvestre in their life. It has been an immense privilege mentoring you and watching you grow as a scientist.

Ian Cardle and **Lucy Yang**: it has been an immense pleasure going on intermittent and required 30 min scientific discussions in the field!

Drew Sellers: thank you for your creativity in puns, jokes, wordplay, and bringing up music that nobody knows anymore!

The rest of the Pun Lab members: **Nataly Kacherovsky**, **David Peeler**, **Albert Yen**, **Emmeline Cheng**, **Dan Lee**, **Audrey Olshefsky**, and **Trey Pichon** – thank you for the helpful discussions, mentoring, teaching, and everything you do to maintain the the lab.

Dedication

To my family:

my mom and dad,

and my sisters.

Part I

Nanoscale technologies

for drug delivery to the kidneys

Chapter 1

Technologies to enable kidney cell-specific drug delivery

Abstract

The chronic kidney disease (CKD) epidemic is exacerbated by the lack of effective interventions to arrest disease advancement. A leading cause of CKD is loss of glomerular podocytes, which causes proteinuria that damages multiple renal cell types including podocytes, renal progenitors, and tubules. Current treatments include long-term immunosuppression, which result in serious side effects that complicate the initial kidney disease. These treatments have also been found to have direct, protective effects on podocytes, suggesting that their therapeutic efficacy may be independent of immunosuppression. Nanoscale drug carriers could enable precision drug delivery to specific cell types within the kidney and therefore improve side effect profiles. This work develops new technologies for targeted drug delivery to glomerular podocytes and proximal tubule cells.

1.1 Burden of chronic kidney disease (CKD)

The silent CKD epidemic afflicts 850 million people worldwide and costs the United States a staggering $114 billion per year.[1] CKD is challenging to detect due to a lack of overt clinical symptoms until kidney injury has advanced to an unrescuable state.[2,3] Indeed, less than 10% of patients are aware that they have CKD in its early stages. Due to a lack of effective interventions to arrest disease progression, many patients will progress to kidney failure and require dialysis. These patients face a grim prognosis: poor five-year survival rates (<40%) and dialysis-related complications and morbidity.[1,4] There is an urgent need for new therapies to arrest CKD progression and prevent kidney failure.

1.2 Podocytes as a therapeutic target

A leading cause of CKD is loss and dysfunction of glomerular podocytes, highly specialized and terminally differentiated epithelial cells of the glomerular filtration barrier that form filtration slit diaphragms that are essential to kidney filtration function.[5] Podocyte dysfunction leads to permeability of the glomerular filtration barrier and subsequent proteinuria, which impairs the differentiation capability of podocyte progenitors,[6] causes tubular cell injury and death,[3,7,8] and injures remaining podocytes,[9] exacerbating disease progression.

Human and experimental studies have shown that reduced podocyte number directly underlies focal segmental glomerulosclerosis (FSGS) and declining kidney function,[10,11] and hereditary

FSGS is caused by genetic mutations that broadly disrupt the podocyte cytoskeleton.[12,13] Therapies should therefore aim to protect and regenerate these cells during disease to halt CKD progression.

Despite limited evidence to support an immune system-mediated cause for minimal change and most forms of FSGS,[14,15] the frontline therapy is long-term immunosuppression therapy that delays, but is unable to halt, disease advancement. The long-term remission rate remains poor, with 60-70% of patients relapsing after steroid tapering or withdrawal.[16] Patients develop serious side effects such as obesity, hypertension, infection, and nephrotoxicity that complicate the disease.[17,18] Direct therapeutic modulation of glomerular podocytes could be efficacious while sparing patients these toxic side effects.

Many lines of evidence support podocyte-targeted drug delivery as a clinically viable approach: (*1*) podocytes are actively endocytotic and upregulate macropinocytosis in disease, which may augment internalization of drug carriers;[19-22] and (*2*) clinically used immunosuppressants as well as experimental drugs have direct effects on podocytes by protecting the actin cytoskeleton against protease and cytotoxin injury, discussed more in-depth in the following section.

1.3 Direct drug effects on podocytes

To motivate direct drug delivery to podocytes as a viable strategy, the targeted drug should exert direct therapeutic effects on these cells. Recent findings suggest that clinically used

immunosuppressants as well as experimental drugs have direct effects on glomerular podocytes themselves, and that their efficacy may be independent of systemic immunosuppression.

1.3.1 Glucocorticoids

Many reports now show that glucocorticoids have direct effects on podocytes. In cultured murine podocytes, the glucocorticoid dexamethasone (DEX) preserved podocyte viability and function by upregulating pro-survival proteins and maintaining F-actin content and organization during puromycin aminonucleoside (PAN) injury.[23,24] DEX also enhanced survival of cultured human podocytes during extended culture.[25] In animals with experimental FSGS, glucocorticoid treatment reduced the degree of glomerulosclerosis and decreased the number of apoptotic podocytes.[14]

1.3.2 Calcineurin inhibitors

Similarly, the immunosuppressive calcineurin inhibitor cyclosporine A (CsA) has been shown to have direct effects on the podocyte actin cytoskeleton.[26] CsA inhibits calcineurin-mediated dephosphorylation of synaptopodin, which ultimately prevents synaptopodin cleavage by cathepsin L. As synaptopodin is a regulator of actin dynamics and stress fiber formation,[27] preservation of synaptopodin is critical to mitigate disease-induced actin dysregulation in podocytes.

1.3.3 Proteins

The anti-CD20 monoclonal antibody, rituximab (RTX), has induced long-term remission in intractable, steroid-sensitive nephrotic syndrome with reduced toxicity compared to current frontline treatments.[16,28,29] Although RTX induces B cell depletion, no correlations between B cell recovery and disease relapse have been able to be made.[29] Recently, Fornoni *et al* reported that RTX binds directly to glomerular podocytes.[30] In addition to CD20, RTX also binds SMPDL-3b,[31] a protein that appears to be functionally distinct from CD20. By binding to SMPDL-3b on podocyte cell membranes, RTX prevents patient serum-induced SMPDL-3b downregulation and disruption of the actin cytoskeleton in cultured podocytes.

The fusion protein abatacept (CTLA-4-Ig) has also induced long-term remissions in patients with B7-1 (CD80)-positive biopsies.[32] In cultured podocytes, B7-1 expression leads to cellular migration due to inactivation of β1 integrin, which is reversed by abatacept treatment. Therefore, abatacept binding to B7-1-expressing podocytes *in vivo* and activation of β1 integrin is likely the therapeutic mechanism for clinical remission.

1.3.4 Experimental drugs

Advancements in high-throughput podocyte drug screens have led to the identification of drug candidates that preserve podocyte viability and morphology against cytotoxic compounds or cellular stressors. Examples include GDC-0879, a $BRAF^{V600E}$ inhibitor that induces pro-survival

MEK/ERK signaling;[33] and pyrintegrin, a β1 integrin agonist that prevents PAN-mediated disruption of F-actin, focal adhesions, and β1 integrin.[34]

The small molecule Bis-T-23 induces actin polymerization within podocytes through dynamin oligomerization.[35-38] Dynamin oligomers displace gelsolin caps on actin filament ends, enabling elongation and polymerization of the filament. Bis-T-23 reduced proteinuria in multiple animal (zebrafish, mouse, rat) models of inducible (LPS, PAN) and genetic causes (CD2AP and PKCε KO) of nephrotic syndrome. However, the ubiquitous expression of dynamin II precludes systemic administration of Bis-T-23 as a treatment option in patients.[39,40] A new linker chemistry is developed for stimulus-triggered Bis-T-23 release in Chapter 3.

1.4 Engineering cell-specific targeting

As discussed in Section 1.2, proteinuria has downstream consequences on multiple kidney cell types: podocytes, podocyte progenitors, and tubular cells. An effective treatment to halt CKD will likely require combinatorial technologies to target each of these cell types. In Part I, we develop nanoscale materials for targeted drug delivery podocytes and proximal tubule cells, with a focus on podocyte delivery technologies as podocyte injury results in and is caused by proteinuria.

Nanoscale drug carriers (polymers, nanoparticles) can significantly alter the biodistribution of drug cargo, therefore improving safety and side effect profiles. In Part I of the thesis work, we

identified polymer properties that resulted in the preferential accumulation of polymers in kidney proximal tubules. For podocyte drug delivery applications, we developed a pH-sensitive drug linker for programmed release of Bis-T-23 after drug carrier internalization, as well as nanoparticle drug carriers that recognize glomerular podocytes via antibodies. Such a platform can significantly expedite progress toward halting and reversing FSGS by enabling clinical translation of new classes of small molecule and biologic drugs, "rescuing" drug candidates that have failed due to poor solubility or systemic toxicity, or improving the side effect profile of clinically used drugs.

1.4.1 Passive targeting of polymers to proximal tubules

"Passive targeting" is the preferential accumulation of drug carriers in tissues due to a pairing of the biology of interest and the material properties of the drug carrier, such as size and charge. Anecdotal reports have revealed that materials with anionic charge and size less than 50 kDa accumulate within the kidneys: the Ghandehari group has reported that linear anionic polymers with size ~43 kDa accumulate in the kidneys for up to 4 weeks.[41] While these studies have provided some insights for designing kidney-accumulating materials, a rigorous definition of what polymer architecture, charge, and size promotes kidney accumulation remains to be reported. Given the size- and charge-selectivity of the glomerular filtration barrier,[42,43] these parameters are likely critical in designing kidney-targeting materials. One of the fundamental goals of this work is to define material properties that promote kidney accumulation by passive targeting, and is evaluated in Chapter 2. This is a manuscript published in *Biomaterials*.

1.4.2 Programmed Bis-T-23 release in cultured podocytes

An important component of targeted drug delivery is spatial and temporal control of drug release. Ideally, drugs are conjugated or loaded onto their carriers in a manner that minimizes drug release during circulation to mitigate drug loss and side effects, and release drug after cellular binding and uptake. Drug linkers have been engineered to be sensitive to local cues (pH, enzymes, or redox) within the target tissue or cell for programmed drug release.[44,45]

The experimental drug Bis-T-23 contains catechol groups, which can be conjugated to polymeric drug carriers by reaction with boronic acid side chains on the polymer to form a reversible ester bond. Boronic acids bind tightly to diols, and reactions with catechols (such as Bis-T-23) are especially favored due to the aromatic hydroxyl groups (association constant K_{eq} ~ 830 M^{-1} and 4.6 M^{-1} for catechols and D-glucose, respectively).[46] The conjugated Bis-T-23 can then be released by bond-breaking triggered by acidic pH. Therefore, the drug remains in an inaccessible, pro-drug form during circulation, but is released in active form after cellular internalization into acidic intracellular vesicles. Part of this work seeks to develop and optimize acid-sensitive Bis-T-23 release after uptake into podocytes (Chapter 3). This is a manuscript published in *ACS Biomater. Sci. Eng*.

1.4.3 Active targeting of nanoparticles to glomerular podocytes

"Active targeting" utilizes molecular recognition between the drug carrier and target cell through a conjugated ligand, such as an antibody, peptide, or aptamer that binds to a specific cellular

protein or receptor.[47-49] While passive targeting drives bulk organ-level accumulation of nano-sized drug carriers (10-200 nm), active targeting increases intracellular uptake of drug carriers into target cells within the organs.[50-53] Here, the polyclonal sheep anti-mouse podocyte antibody developed by the Shankland group was utilized to enable molecular recognition of podocytes and subsequent uptake of nanoparticle drug carriers (Chapter 4).[54]

1.4.4 Future perspectives

The technologies developed here can significantly enable control over drug pharmacokinetics. In Chapter 5, new applications of anionic polymers for targeted drug delivery to proximal tubule cells are proposed. In podocyte-targeting work, two projects are proposed: one to evaluate the *in vivo* efficacy of drug-loaded nanoparticles, and the other to optimize nanoparticle passive targeting properties for optimal accumulation in glomerular podocytes.

1.5 Acknowledgments

This work was supported by the Office of the Assistant Secretary of Defense for Health Affairs through the Peer Reviewed Medical Research Program under Award Numbers PR151175 and PR151965, and by the National Science Foundation Graduate Research Fellowship Program under Grant No. DGE-1256082 to GWL. Opinions, interpretations, conclusions, and recommendations are those of the authors and are not necessarily endorsed by the Department of Defense or the National Science Foundation.

References

1. Saran, R., *et al.* US Renal Data System 2018 Annual Data Report: Epidemiology of Kidney Disease in the United States. *American Journal of Kidney Diseases* **73**, A7-A8 (2019).
2. Tuot, D.S., *et al.* Chronic Kidney Disease Awareness Among Individuals with Clinical Markers of Kidney Dysfunction. *Clinical Journal of the American Society of Nephrology* **6**, 1838-1844 (2011).
3. Szczech, L.A., *et al.* Primary care detection of chronic kidney disease in adults with type-2 diabetes: the ADD-CKD Study (awareness, detection and drug therapy in type 2 diabetes and chronic kidney disease). *PLoS One* **9**, e110535-e110535 (2014).
4. Sarnak, M.J. & Jaber, B.L. Mortality caused by sepsis in patients with end-stage renal disease compared with the general population. *Kidney Int* **58**, 1758-1764 (2000).
5. Pavenstadt, H., Kriz, W. & Kretzler, M. Cell biology of the glomerular podocyte. *Physiol Rev* **83**, 253-307 (2003).
6. Peired, A., *et al.* Proteinuria impairs podocyte regeneration by sequestering retinoic acid. *J Am Soc Nephrol* **24**, 1756-1768 (2013).
7. Ding, X., *et al.* Numb Protects Human Renal Tubular Epithelial Cells From Bovine Serum Albumin-Induced Apoptosis Through Antagonizing CHOP/PERK Pathway. *J Cell Biochem* **117**, 163-171 (2016).
8. Nolin, A.C., *et al.* Proteinuria causes dysfunctional autophagy in the proximal tubule. *Am J Physiol Renal Physiol* **311**, F1271-F1279 (2016).
9. Agrawal, S., Guess, A.J., Chanley, M.A. & Smoyer, W.E. Albumin-induced podocyte injury and protection are associated with regulation of COX-2. *Kidney International* **86**, 1150-1160 (2014).
10. Kriz, W. & Lemley, K.V. A potential role for mechanical forces in the detachment of podocytes and the progression of CKD. *J Am Soc Nephrol* **26**, 258-269 (2015).
11. Wharram, B.L., *et al.* Podocyte depletion causes glomerulosclerosis: diphtheria toxin-induced podocyte depletion in rats expressing human diphtheria toxin receptor transgene. *J Am Soc Nephrol* **16**, 2941-2952 (2005).
12. Jefferson, J.A. & Shankland, S.J. The pathogenesis of focal segmental glomerulosclerosis. *Adv Chronic Kidney Dis* **21**, 408-416 (2014).
13. Rood, I.M., Deegens, J.K. & Wetzels, J.F. Genetic causes of focal segmental glomerulosclerosis: implications for clinical practice. *Nephrol Dial Transplant* **27**, 882-890 (2012).
14. Zhang, J., *et al.* Podocyte repopulation by renal progenitor cells following glucocorticoids treatment in experimental FSGS. *Am J Physiol Renal Physiol* **304**, F1375-1389 (2013).
15. Mathieson, P.W. Minimal change nephropathy and focal segmental glomerulosclerosis. *Semin Immunopathol* **29**, 415-426 (2007).
16. Ruggenenti, P., *et al.* Rituximab in steroid-dependent or frequently relapsing idiopathic nephrotic syndrome. *J Am Soc Nephrol* **25**, 850-863 (2014).
17. Greenbaum, L.A., Benndorf, R. & Smoyer, W.E. Childhood nephrotic syndrome--current and future therapies. *Nat Rev Nephrol* **8**, 445-458 (2012).

18. Gipson, D.S., *et al.* Management of childhood onset nephrotic syndrome. *Pediatrics* **124**, 747-757 (2009).
19. Yoshikawa, N., *et al.* Glomerular podocyte vacuolation in focal segmental glomerulosclerosis. *Arch Pathol Lab Med* **110**, 394-398 (1986).
20. Eyre, J., *et al.* Statin-sensitive endocytosis of albumin by glomerular podocytes. *Am J Physiol Renal Physiol* **292**, F674-681 (2007).
21. Chung, J.J., *et al.* Albumin-associated free fatty acids induce macropinocytosis in podocytes. *J Clin Invest* (2015).
22. Inoue, K. & Ishibe, S. Podocyte endocytosis in the regulation of the glomerular filtration barrier. *Am J Physiol Renal Physiol* **309**, F398-405 (2015).
23. Wada, T., Pippin, J.W., Marshall, C.B., Griffin, S.V. & Shankland, S.J. Dexamethasone prevents podocyte apoptosis induced by puromycin aminonucleoside: role of p53 and Bcl-2-related family proteins. *J Am Soc Nephrol* **16**, 2615-2625 (2005).
24. Ransom, R.F., Lam, N.G., Hallett, M.A., Atkinson, S.J. & Smoyer, W.E. Glucocorticoids protect and enhance recovery of cultured murine podocytes via actin filament stabilization. *Kidney Int* **68**, 2473-2483 (2005).
25. Xing, C.Y., *et al.* Direct effects of dexamethasone on human podocytes. *Kidney Int* **70**, 1038-1045 (2006).
26. Faul, C., *et al.* The actin cytoskeleton of kidney podocytes is a direct target of the antiproteinuric effect of cyclosporine A. *Nat Med* **14**, 931-938 (2008).
27. Asanuma, K., *et al.* Synaptopodin regulates the actin-bundling activity of alpha-actinin in an isoform-specific manner. *J Clin Invest* **115**, 1188-1198 (2005).
28. Ruggenenti, P., *et al.* Rituximab in idiopathic membranous nephropathy. *J Am Soc Nephrol* **23**, 1416-1425 (2012).
29. Sinha, A. & Bagga, A. Rituximab therapy in nephrotic syndrome: implications for patients' management. *Nat Rev Nephrol* **9**, 154-169 (2013).
30. Fornoni, A., *et al.* Rituximab targets podocytes in recurrent focal segmental glomerulosclerosis. *Sci Transl Med* **3**, 85ra46 (2011).
31. Perosa, F., Favoino, E., Caragnano, M.A. & Dammacco, F. Generation of biologically active linear and cyclic peptides has revealed a unique fine specificity of rituximab and its possible cross-reactivity with acid sphingomyelinase-like phosphodiesterase 3b precursor. *Blood* **107**, 1070-1077 (2006).
32. Yu, C.C., *et al.* Abatacept in B7-1-positive proteinuric kidney disease. *N Engl J Med* **369**, 2416-2423 (2013).
33. Sieber, J., *et al.* GDC-0879, a BRAF(V600E) Inhibitor, Protects Kidney Podocytes from Death. *Cell Chem Biol* **25**, 175-184 e174 (2018).
34. Lee, H.W., *et al.* A Podocyte-Based Automated Screening Assay Identifies Protective Small Molecules. *J Am Soc Nephrol* (2015).
35. Gu, C., *et al.* Regulation of dynamin oligomerization in cells: the role of dynamin-actin interactions and its GTPase activity. *Traffic* **15**, 819-838 (2014).
36. Gu, C., *et al.* Dynamin Autonomously Regulates Podocyte Focal Adhesion Maturation. *J Am Soc Nephrol* **28**, 446-451 (2017).
37. Schiffer, M., *et al.* Pharmacological targeting of actin-dependent dynamin oligomerization ameliorates chronic kidney disease in diverse animal models. *Nat Med* (2015).

38. Gu, C., *et al.* Direct dynamin-actin interactions regulate the actin cytoskeleton. *EMBO J* **29**, 3593-3606 (2010).
39. Sontag, J.M., *et al.* Differential expression and regulation of multiple dynamins. *J Biol Chem* **269**, 4547-4554 (1994).
40. Allison, S.J. Chronic kidney disease: Actin cytoskeleton alterations in podocytes: a therapeutic target for chronic kidney disease. *Nat Rev Nephrol* **11**, 385 (2015).
41. Borgman, M.P., *et al.* Tumor-targeted HPMA copolymer-(RGDfK)-(CHX-A"-DTPA) conjugates show increased kidney accumulation. *J Control Release* **132**, 193-199 (2008).
42. Ferrell, N., *et al.* Basal lamina secreted by MDCK cells has size- and charge-selective properties. *Am J Physiol Renal Physiol* **300**, F86-90 (2011).
43. Jeansson, M. & Haraldsson, B. Glomerular size and charge selectivity in the mouse after exposure to glucosaminoglycan-degrading enzymes. *J Am Soc Nephrol* **14**, 1756-1765 (2003).
44. Chu, D.S., *et al.* MMP9-sensitive polymers mediate environmentally-responsive bivalirudin release and thrombin inhibition. *Biomater Sci* **3**, 41-45 (2015).
45. Aryal, S., Hu, C.M. & Zhang, L. Polymer--cisplatin conjugate nanoparticles for acid-responsive drug delivery. *ACS Nano* **4**, 251-258 (2010).
46. Springsteen, G. & Wang, B. A detailed examination of boronic acid–diol complexation. *Tetrahedron* **58**, 5291-5300 (2002).
47. Danhier, F., Feron, O. & Preat, V. To exploit the tumor microenvironment: Passive and active tumor targeting of nanocarriers for anti-cancer drug delivery. *J Control Release* **148**, 135-146 (2010).
48. Wang, C.E., Stayton, P.S., Pun, S.H. & Convertine, A.J. Polymer nanostructures synthesized by controlled living polymerization for tumor-targeted drug delivery. *J Control Release* **219**, 345-354 (2015).
49. Bareford, L.M. & Swaan, P.W. Endocytic mechanisms for targeted drug delivery. *Adv Drug Deliv Rev* **59**, 748-758 (2007).
50. Farokhzad, O.C. & Langer, R. Impact of nanotechnology on drug delivery. *ACS Nano* **3**, 16-20 (2009).
51. Pirollo, K.F. & Chang, E.H. Does a targeting ligand influence nanoparticle tumor localization or uptake? *Trends Biotechnol* **26**, 552-558 (2008).
52. Kirpotin, D.B., *et al.* Antibody targeting of long-circulating lipidic nanoparticles does not increase tumor localization but does increase internalization in animal models. *Cancer Res* **66**, 6732-6740 (2006).
53. Pun, S.H., *et al.* Targeted delivery of RNA-cleaving DNA enzyme (DNAzyme) to tumor tissue by transferrin-modified, cyclodextrin-based particles. *Cancer Biol Ther* **3**, 641-650 (2004).
54. Hauser, P.V., *et al.* Novel siRNA delivery system to target podocytes in vivo. *PLoS One* **5**, e9463 (2010).

Chapter 2

Determination of polymer properties that drive kidney accumulation

Gary W. Liu, Alexander N. Prossnitz, Diana G. Eng, Yilong Cheng, Nithya Subrahmanyam, Jeffrey W. Pippin, Robert J. Lamm, Chayanon Ngambenjawong, Hamidreza Ghandehari, Stuart J. Shankland, and Suzie H. Pun

Abstract

Controlling polymer properties that drive tissue-specific accumulation is critical in engineering targeted drug delivery systems. For kidney disease applications, targeted drug delivery to renal cells that reside beyond the charge- and size-selective glomerular filtration barrier could have clinical potential. However, there are limited reports on polymer properties that might enhance kidney accumulation. Here, we studied the effects of molecular weight and charge on the *in vivo* kidney accumulation of polymers in health and disease. We synthesized a panel of well-defined polymers by atom transfer radical polymerization to answer several questions. First, the biodistribution of low molecular weight (23-27 kDa) polymers composed of various ratios of neutral:anionic monomers (1:0, 1:1, 1:4) in normal mice was determined. Then, highly anionic (1:4 monomer ratio) low and high molecular weight (47 kDa) polymers were tested in both normal and experimental focal segmental glomerulosclerosis (FSGS) mice, a model that results in loss of glomerular filtration selectivity. Through these studies, we observed that kidney-specific polymer accumulation increases with anionic monomer content, but not molecular weight; experimental FSGS increases kidney accumulation of anionic polymers; and anionic polymers accumulate predominantly in proximal tubule cells.

[1]Adapted with permission from GW Liu, AN Prossnitz *et al.* Glomerular disease augments kidney accumulation of synthetic anionic polymers. *Biomaterials* 178, 317-325 (2018). Copyright 2018 Elsevier.

2.1 Introduction

Polymeric carriers have been applied in drug delivery to improve circulation time, alter biodistribution, reduce metabolism, and facilitate cellular internalization of drug cargo.[1-5] The pharmacokinetics of polymeric carriers and their cargo depend on polymer properties including molecular weight, dispersity, charge, functionalization, and self-assembled size and shape.[6-9] Studies investigating polymer structure and resulting biodistribution have mainly focused on exploiting the enhanced permeability and retention effect for cancer applications.[10-12] However, polymeric carriers for kidney diseases remain relatively understudied despite the clinical potential of such technologies. For example, targeted drug delivery to glomerular podocytes could improve the standard of therapy for common glomerular diseases such as minimal change disease and focal segmental glomerulosclerosis (FSGS), and drug delivery to tubular epithelial cells may be strategic for acute kidney injury and polycystic kidney disease treatment.[13,14] The major challenge is that these cell populations reside beyond the multi-layered glomerular filtration barrier, which comprises the innermost endothelial cells, a middle glomerular basement membrane, and the outer podocytes.

Given that the glomerular filtration barrier is both size- and charge-selective, these two parameters are likely critical when designing drug carriers to target cells past the barrier. Nanoparticle studies by the Davis group have revealed that gold nanoparticles of size ~75 nm target the kidney mesangium,[15] and polycation-siRNA polymeric nanoparticles accumulate and disassemble in the anionic glomerular basement membrane.[16] However, the polymer physical properties required to cross this barrier for kidney targeting applications remain to be critically

defined. Kamada *et al*. observed that hydrolyzed poly(vinylpyrrolidone-*co*-dimethyl maleic anhydride) copolymers of molecular weight approximately 10 kDa were anionic and distributed in kidneys up to 4 days after administration, with uptake primarily in proximal tubule cells.[17] Similarly, Borgman *et al.* reported that *N*-(2-hydroxypropyl)methacrylamide (HPMA) copolymers, functionalized with cyclo(RGDfK) targeting peptides and anionic penta-carboxylic acid residues, distributed preferentially in the kidneys compared to the designed target, tumors, and were retained up to 10 days after administration.[18] Recently, Bruni *et al*. reported on a panel of poly-*ε*-caprolactone and poly(ethylene glycol) methyl ether methacrylate star co-polymers (10-27 kDa), which exhibited evidence of kidney clearance *in vivo*.[19] While these reports have revealed in broad strokes that polymers with anionic charge and molecular weight less than 50 kDa accumulate in the kidneys, a rigorous evaluation of the individual and combined effects of polymer molecular weight and charge has yet to be reported.

Advances in controlled radical polymerization techniques have enabled polymer synthesis with precise control over molecular weight, dispersity, architecture, and chemical composition.[20] In this work, we used atom transfer radical polymerization (ATRP) to synthesize a panel of polymers to examine the effect of anionic charge density and molecular weight on kidney accumulation and distribution in mice. We first tested the effect of charge using a panel of low molecular weight (LMW) polymers, and then examined the effect of molecular weight in normal mice and mice with experimental FSGS, a model that results in loss of filtration size-selectivity and proteinuria.[21] Here, we report that highly anionic, LMW polymers preferentially accumulate in the kidneys and are internalized into proximal tubule cells. Conditions of experimental FSGS enhance accumulation of anionic LMW polymers.

2.2 Materials and methods

2.2.1 Materials

Poly(ethylene glycol) methyl ether methacrylate monomer (average molecular weight = 300 Da, OEGMA), *N*,*N*'-dicyclohexylcarbodiimide (DCC), 2,2'-bipyridyl (BPY), 2-mercaptoethanol, copper (I) bromide, 4-dimethylaminopyridine (DMAP), and *N*,*N*,*N*',*N*'',*N*''-pentamethyldiethylenetriamine (PMDETA) were purchased from Sigma-Aldrich. 2,2'-dipyridyl disulfide and *tert*-butyl methacrylate monomer (tBuMA) were purchased from TCI America. α-bromoisobutyric acid was purchased from Fluka. OEGMA and tBuMA were passed through a basic alumina column to remove inhibitors before polymerization. Cy3-maleimide was purchased from Lumiprobe.

2.2.2 Polymer synthesis and characterization

A pyridyl disulfide-terminated ATRP initiator was synthesized as previously described.[22] The initiator was purified by column chromatography, and purity was confirmed by ^{1}H NMR. In a typical polymerization, the ATRP initiator, ligand (PMDETA or BPY), and monomers (OEGMA and tBuMA) were dissolved in solvent and added to a round-bottom flask. The solution was purged with Ar gas for 10 min. After, solid CuBr was rapidly added, and the solution was purged again. The following reaction conditions were carried out for each polymer (mol ratios): (*i*) LMW 1:4 and HMW 1:4, initiator:PMDETA:OEGMA:tBuMA:Cu(I) = 1:1:40:160:1, [monomer] = 3 M, in anisole, 60 °C for 4 or 8 h, respectively; (*ii*) LMW 1:1,

initiator:PMDETA:OEGMA:tBuMA:Cu(I) = 1:1:400:400:1, [monomer] = 2 M, in methyl ethyl ketone, room temperature for 2 h; (*iii*) LMW 1:0, initiator:BPY:OEGMA:tBuMA:Cu(I) = 1:1.2:667:0:1, [monomer] = 2 M, in ethanol, 50 °C for 6 h. HMW and LMW 1:4 polymers were precipitated into cold hexanes; LMW 1:1 and LMW PEG polymers were precipitated in cold ether. Polymers were collected by centrifugation and vacuum-dried for at least 24 h, and characterized for molecular weight and dispersity (*Đ*) via gel permeation chromatography (GPC) as previously described.[23] Purity and monomer ratios in the statistical copolymers were assessed with ^{1}H NMR. The integrated signals of the terminal methyl groups of the OEGMA (3 protons) and the *tert*-butyl groups of the tBuMA (9 protons) were compared.

For the synthesis of the HPMA copolymers, the co-monomers *N*-(2-hydroxypropyl) methacrylamide (HPMA),[24] *N*-methacryloylaminopropyl-2-amino-3-(isothiourea-phenyl) propyl-cyclohexane-1,2-diamine-*N,N-N′,N′,N″,N″*-pentaacetic acid (APMA-CHX-A″-DTPA),[25] and 5-[3-(methacryloylaminopropyl)thioureidyl] rhodamine (APMA-rhodamine) were synthesized using established methods. APMA-rhodamine was adapted from the synthesis of APMA-FITC,[26] substituting rhodamine-isothiocyanate instead of fluorescein-isothiocyanate. Copolymerization was performed using free radical copolymerization, using azobisisobutyronitrile (AIBN) as an initiator. The reaction was carried out in a nitrogen-purged sealed glass ampule for 24 h and 50 °C. For the control copolymer, the following feed ratio in mole percent was used: HPMA:APMA-CHX-A"-DTPA:APMA-rhodamine (98:0:2). For the DTPA-containing (anionic) copolymer the following ratio was used: HPMA:APMA-CHX-A"-DTPA:APMA-rhodamine (88:10:2). Initiator concentration was 5 mg of initiator per 100 mg total monomers in both syntheses, in 500 μL of MeOH. Copolymers were purified through dialysis against dH_2O and

lyophilized. Copolymers were characterized for molecular weight and dispersity using size exclusion chromatography. Co-monomer content was measured using UV-Vis spectroscopy. For the control copolymer, rhodamine fluorescent label content was determined to be 0.156 mmol/g. For the anionic copolymer, rhodamine content was determined to be 0.863 mmol/g and DTPA monomer content was found to be 0.598 mmol/g.

2.2.3 Polymer deprotection and fluorescent labeling

Polymers containing tBuMA were deprotected in trifluoroacetic acid, to remove the *tert*-butyl groups and reveal carboxylic acids, for 2 h with stirring. After, polymers were precipitated in cold ether, collected by centrifugation, and vacuum-dried overnight. Polymers were then dissolved in molecular-grade H_2O pH 8, dialyzed against dH_2O for 24 h, and lyophilized. The deprotected polymers were prepared for dye conjugation by reducing the disulfide bond present in the initiator. Polymers were dissolved in PBS-EDTA, purged with Ar for 10 min, and a 1000-fold molar-excess of dithiothretriol (DTT) was added. The reaction was left overnight. Polymers were desalted using a PD-10 desalting column (GE), dissolved in a 2:1 PBS-EDTA:DMSO solution, purged, and a 5× molar-excess of Cy3-maleimide dye (Lumiprobe) dissolved in *N*,*N*-dimethylformamide was added. After 24 h, labeled polymers were dialyzed against dH_2O for 1.5 wk.

2.2.4 Polymer biodistribution studies

All animal experiments were executed in compliance with the University of Washington IACUC guidelines. For the initial LMW polymer biodistribution study, polymers (4 nmol) dissolved in PBS were injected in 7-week old mice via retro-orbital route. After 7 d, animals were sacrificed, perfused with PBS, and major organs (heart, lungs, liver, spleen, and kidneys) were harvested. Organ fluorescence was quantified by a Xenogen IVIS using ex/em = 535/580 nm. Regions of interest were drawn across each organ for quantification, and total radiant efficiencies were normalized by organ weight. Statistical analyses were performed using GraphPad Prism and R software. Experimental FSGS was induced in 9-week old male BALB/c mice (Jackson Laboratory) via two intraperitoneal injections (10 mg/20 g mouse) of a cytotoxic anti-podocyte antibody 24 h apart. HMW and LMW polymers (4 nmol) were injected as above on day 7 after disease induction, and animals were sacrificed for organ fluorescence quantification on day 14 as described above.

2.2.5 Tissue processing and imaging

Kidney tissues were fixed in 4% PFA, washed with PBS, and incubated overnight with 30% sucrose/PBS at 4 °C. Tissues were then embedded in OCT and frozen in an ethanol/dry ice bath. After cryosectioning, tissues were stained with DAPI and mounted with Fluoromount-G (SouthernBiotech). Confocal images were taken as previously reported.[27] Images were captured using a Leica TCS SPE II laser scanning confocal microscope (Solms, Germany) with a HCX PL APO 40×/1.30 oil objective, at 1024×1024 pixel format with 8-bit intensity resolution. Sets

of 8 serial images were collected at 2-μm step size. The acquisition wavelengths were: DAPI excitation 405 nm, emission 380-468 nm; Cy3 excitation 561 nm, emission 576-644 nm. Masson's trichrome and silver staining were performed using standard methods. Images were collected at 600× magnification.

2.2.6 Urine albumin and creatinine quantification

Spot urines were collected on various days before and throughout experimental FSGS induction. Urine albumin content was quantified by radial immunodiffusion as previously described,[28] and creatinine quantified using a creatinine assay kit (Cayman Chemical).

2.2.7 HK-2 cell culture and polymer characterization

The human proximal tubule cell line HK-2 was cultured in K-SFM (ThermoFisher Scientific) and maintained as described by ATCC. For confocal imaging of polymer uptake, HK-2 cells were seeded on bovine collagen I (Corning)-coated glass coverslips in a 24-well plate at 4×10^4 cells/well. After overnight incubation, media was replaced with fresh media or polymer dissolved in media to 1 μM for 2 h. After, cells were washed three times with PBS, and then fixed and stained with DAPI using standard methods. Confocal images were collected as described above.

For viability studies, HK-2 cells were plated in a 96-well plate at 5×10^3 cells/well. After overnight incubation, media was replaced with fresh media or polymer dissolved in media to 1

μM. After 1, 3, or 7 d treatment, cells were washed with PBS, and viability was assayed by MTS/PMS (Promega) according to manufacturer instructions.

HK-2 cells were plated in a 24-well plate at 3-4×10^4 cells/well for uptake characterization studies and tested after overnight incubation. To test the effects of temperature on uptake, media was replaced with polymer dissolved in media to 1 μM, and cells were incubated for 1 h at 37 °C or on ice (4 °C). Cells were then washed 3× with PBS, lifted with trypsin, resuspended in 1% BSA/PBS, and analyzed by flow cytometry. For competition studies, cells were first incubated with 1 mg/mL dextran sulfate (Sigma-Aldrich) in media for 30 min, and then incubated with 1 μM polymer in the presence of 1 mg/mL dextran sulfate for 2 h. Cells were then processed for flow cytometry as described above. Flow cytometry was performed using an Attune NxT Flow Cytometer (ThermoFisher Scientific). At least 1×10^4 cells were analyzed by FlowJo software, using mean fluorescence intensity as a measure of polymer uptake.

2.3 Results

2.3.1 Polymer panel synthesis and characterization

We designed a polymer panel of copolymers with varying ratios of anionic and neutral monomers synthesized by ATRP, with different degrees of polymerization (**Table 2.1**). Importantly, this approach yields well-defined polymers with tailored anion densities and molecular weights while keeping other properties constant. The hydrophilic, small molecular

weight (~300 Da) monomer oligo(ethylene glycol) methyl ether methacrylate (OEGMA) was selected, as OEGMA-based polymers have been shown to exhibit favorable circulation times, low protein-binding properties, and reduced immunogenicity due to shorter ethylene glycol repeats.[29-32] The second monomer, *tert*-butyl methacrylate (tBuMA), yields methacrylic acids (MAA, anionic in charge) after deprotection. The monomer tBuMA was selected as an alternative to direct MAA polymerization, as MAA is insoluble in many organic solvents. Organic ATRP presents several advantages over aqueous ATRP, and results in polymerizations with less synthetic complexity and higher quality materials.

Table 2.1 Summary of p(OEGMA-*co*-MAA) copolymers. Number average molecular weight (M_n) and dispersity ($Đ$) values were determined by gel permeation chromatography. Polymer compositions were determined by ^{1}H NMR. PDS, pyridyl disulfide-terminated ATRP initiator.

Polymer	Composition	OEGMA:tBuMA feed ratios	OEGMA:tBuMA measured ratios	M_n (Da)	$Đ$
LMW 1:0	p($OEGMA_{76}$)-PDS	100:0	N/A	23,000	1.125
LMW 1:1	p($OEGMA_{70}$-*co*-MAA_{70})-PDS	50:50	1:1.1	27,000	1.140
LMW 1:4	p($OEGMA_{39}$-*co*-MAA_{157})-PDS	20:80	1:3.5	25,000	1.370
HMW 1:4	p($OEGMA_{74}$-*co*-MAA_{296})-PDS	20:80	1:5.4	47,000	1.400

By varying the ratio of the two monomers and the polymerization time, p(OEGMA-*co*-MAA) copolymers with defined OEGMA:MAA ratios and molecular weights were synthesized (**Table 2.1** and **Figure 2.1**). Polymers with fixed molecular weight but varying anionic MAA content (0%, 50%, and 80%) were prepared to test the effect of charge on biodistribution. Two target molecular weight ranges were synthesized: low molecular weight (LMW) polymers of 20-25 kDa, and high molecular weight (HMW) polymers of 45-50 kDa. These two molecular weight regimes, which are either below or approximately at the renal filtration cutoff of ~50 kDa,[33] respectively, were utilized to investigate the effect polymer molecular weight on kidney

distribution. For biodistribution and tissue distribution analyses, polymers were fluorescently labeled with Cy3 fluorophore via a stable thioether bond by reduction of the disulfide bond of the pyridyl disulfide-terminated ATRP initiator and subsequent reaction with Cy3-maleimide (**Figure 2.1**).

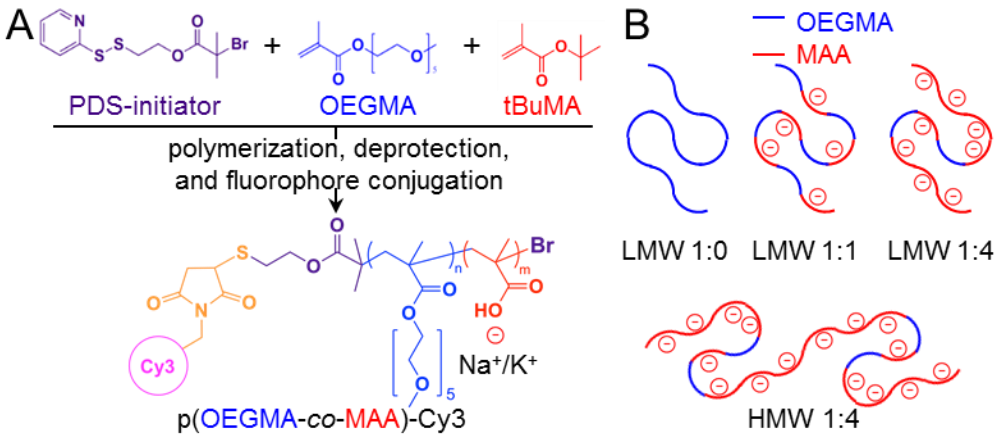

Figure 2.1 Schematics of polymer synthesis and composition. **A.** Concise synthesis scheme of polymers. Polymerization was performed with a pyridyl disulfide (PDS)-terminated ATRP initiator and OEGMA and tBuMA monomers. Deprotection and fluorophore conjugation of polymers yield p(OEGMA-*co*-MAA)-Cy3. **B.** Cartoon schematic of the tested polymers. Polymers were named based on molecular weight and monomer composition. LMW, low molecular weight; HMW, high molecular weight; 1:0, polymer comprising 100% OEGMA monomer; 1:1, polymer comprising 50%/50% of OEGMA and MAA, respectively; 1:4, polymer comprising 20%/80% of OEGMA and MAA, respectively. Blue lines represent OEGMA monomer, and red lines represent MAA monomer.

LMW polymers ranged in number average molecular weight (M_n) from 23-27 kDa, and HMW polymers had M_n of 47 kDa, as determined by gel permeation chromatography (GPC). All polymers exhibited dispersity ($Đ$) < 1.5. Within a molecular weight regime, the MAA monomer fraction during polymerization was varied at 0%, 50%, and 80%, resulting in polymer OEGMA:MAA ratios of 1:0 (homopolymer pOEGMA), 1:1, and 1:4, respectively. Monomer ratios within the copolymers, as determined by ^{1}H nuclear magnetic resonance spectroscopy

(NMR), were in good agreement with the feed ratios and suggest similar reactivity of the two co-monomers under the polymerization conditions used (**Table 2.1** and **Figure S2.1**).

2.3.2 Biodistribution of LMW polymers in normal mice

The effect of polymer charge on kidney accumulation was first determined by evaluating the biodistribution of LMW 1:0, 1:1, and 1:4 copolymers 7 days post intravenous injection. This time point is significantly past the circulation half-life of similarly sized polymers (generally $t_{1/2}$ < 24 h)[34,35] and was intentionally selected to measure organ accumulation. Fluorescence intensities of the three polymers prior to injection were comparable (**Figure S2.2**). Polymer distribution to major organs (heart, lungs, liver, spleen, kidneys) was determined by whole organ fluorescence imaging after perfusion.

The LMW polymers exhibited a statistically significant increasing linear trend (*p*-value < 0.0001) in both kidney and liver fluorescence trending with MAA content (anionic charge), with LMW 1:4 > 1:1 > 1:0 (**Figures 2.2A** and **2.2B**). Preferential kidney accumulation was quantified by normalizing the fluorescent signal in the kidneys by that in the liver. LMW 1:4 exhibited the greatest kidney/liver fluorescence ratio compared to other treatments (**Figure 2.2C**). The distribution of labeled polymers in the kidney was determined by confocal microscopy. Fluorescence was primarily detected in the kidney cortex, intracellularly in proximal tubule cells as identified by morphology and proximity to glomeruli structures (**Figure 2.3**). LMW 1:4 copolymers exhibited the most fluorescent staining as well as deposition in kidney glomeruli. In further confirmation of the role of anionic charge on kidney accumulation, *N*-(2-

hydroxypropyl)methacrylamide (HPMA) copolymers modified with anionic diethylenetriaminepentaacetic acid chelator (DTPA) exhibited greater kidney/liver fluorescence compared to HPMA control polymers (**Figure S2.3**).

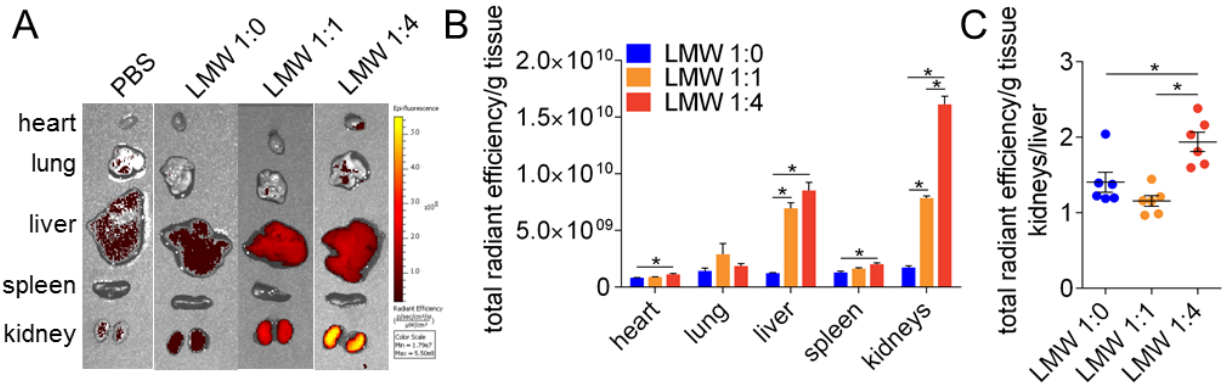

Figure 2.2 Organ distribution of low molecular weight (23-27 kDa) polymers in normal mice. **A.** Representative fluorescent images of major organs 7 days after intravenous administration of PBS or fluorescent polymers. **B.** Region of interest quantification of tissue fluorescence normalized by tissue weight. All treatments were n = 6. **C.** Kidney/liver normalized fluorescent signal ratio. Statistical analysis was performed using a one-way ANOVA with post-hoc Tukey's multiple comparisons test, and a post-hoc linear trend test. Bars represent means ± SEM. *p-value < 0.05.

2.3.3 Biodistribution of HMW and LMW polymers in normal and experimental FSGS mice

We hypothesized that glomerular kidney disease may alter the polymer accumulation in this organ due to loss of filtration selectivity. As highly anionic LMW 1:4 (80% MAA content) copolymers exhibited the most fluorescence in the kidneys, HMW 1:4 (M_n = 47 kDa) and LMW 1:4 (M_n = 25 kDa) copolymers were tested to determine the effect of molecular weight on biodistribution in normal mice and mice with experimental FSGS. To induce FSGS, a cytotoxic anti-podocyte antibody that causes podocyte loss was administered to mice.[21] Damage to glomeruli and disruption of the glomerular filtration barrier was confirmed histologically

(**Figure S2.4**) and by proteinuria, which peaked on day 7 (**Figure 2.4A**) and persisted up to day 14. Polymers were injected on day 7 at peak proteinuria, and polymer distribution assessed 7 days post-polymer administration (**Figure 2.4A**).

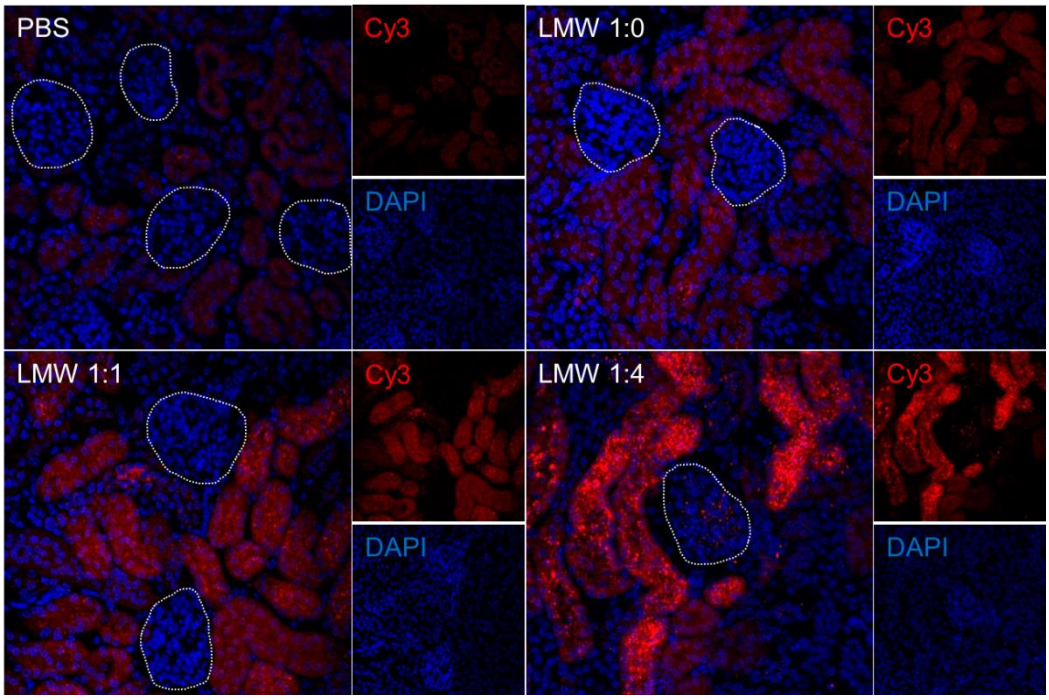

Figure 2.3 Kidney distribution of low molecular weight (23-27 kDa) polymers in normal mice. Representative fluorescent images of kidneys 7 days after intravenous administration of PBS or fluorescent polymers obtained by confocal microscopy. Kidney glomeruli are denoted by dashed white lines. Blue, DAPI; red, Cy3-labeled polymers. Individual DAPI and Cy3 channels are shown to the right of their respective images.

In normal animals, LMW 1:4 copolymers exhibited greater fluorescence in the kidneys than HMW 1:4 copolymers (**Figure 2.4B** and 2.**4C**). Experimental FSGS increased kidney and liver fluorescence of LMW 1:4 copolymers, but not HMW 1:4 copolymers (**Figure 2.4C**). Generally, LMW 1:4 copolymers exhibited greater kidney/liver fluorescence ratios compared to HMW 1:4 polymers in normal and experimental FSGS conditions (**Figure 2.4D**). Kidney tissue distribution patterns were similar to the initial LMW polymer panel, with no remarkable differences noted in mice with experimental FSGS (data not shown).

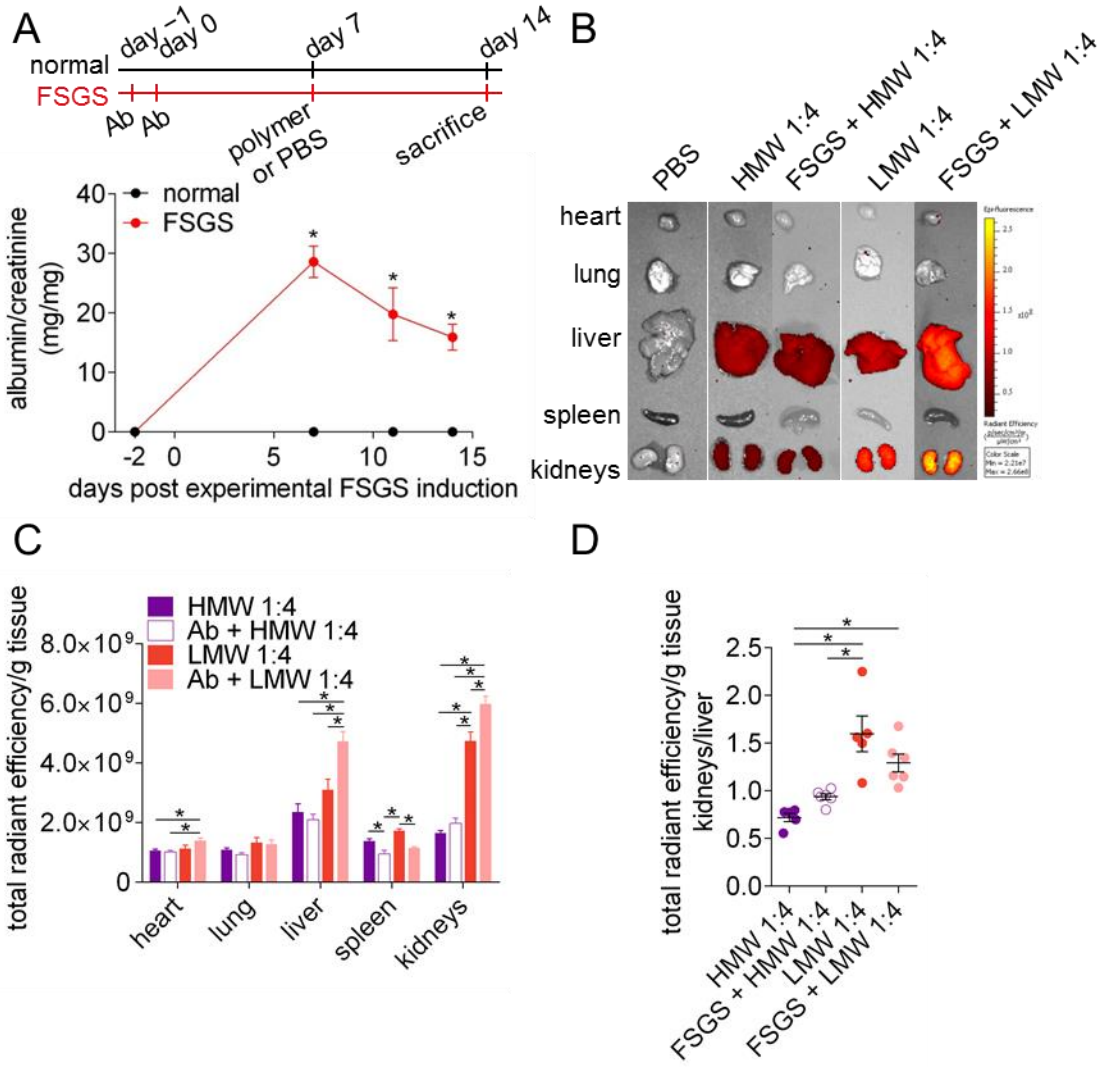

Figure 2.4 Organ distribution of polymers in normal and experimental FSGS mice. **A.** Top: treatment schedule of normal and experimental FSGS mice. FSGS mice were administered a cytotoxic anti-podocyte antibody on days −1 and 0. Both normal and FSGS mice were administered PBS or fluorescent polymers on day 7 and sacrificed on day 14 for analysis. Bottom: urine albumin/creatinine ratios of animals administered the cytotoxic anti-podocyte antibody (red, FSGS, n = 5) or not (black, normal, n = 4). All mice were administered PBS on day 7. Statistical analysis was performed using a two-tailed Student's t-test compared to normal animals. **B.** Representative fluorescent images of major organs analyzed on day 14. **C.** Region of interest quantification of tissue fluorescence normalized by tissue weight. All antibody treatments were n = 6; otherwise n = 5. **D.** Kidney/liver normalized fluorescent signal ratio. Statistical analysis was performed using a one-way ANOVA with post-hoc Tukey's multiple comparisons test. Bars represent means ± SEM. *p-value < 0.05.

2.3.4 *In vitro* characterization of polymers in proximal tubule cells

The LMW 1:4 polymer was then characterized for internalization, cytotoxicity, and uptake mechanism using an immortalized human proximal tubule cell line, HK-2, which exhibits key features of primary proximal tubule cells.[36] By confocal microscopy, polymer-treated cells exhibited punctate polymer fluorescence within the cell body (**Figure 2.5A**). Treatment of HK-2

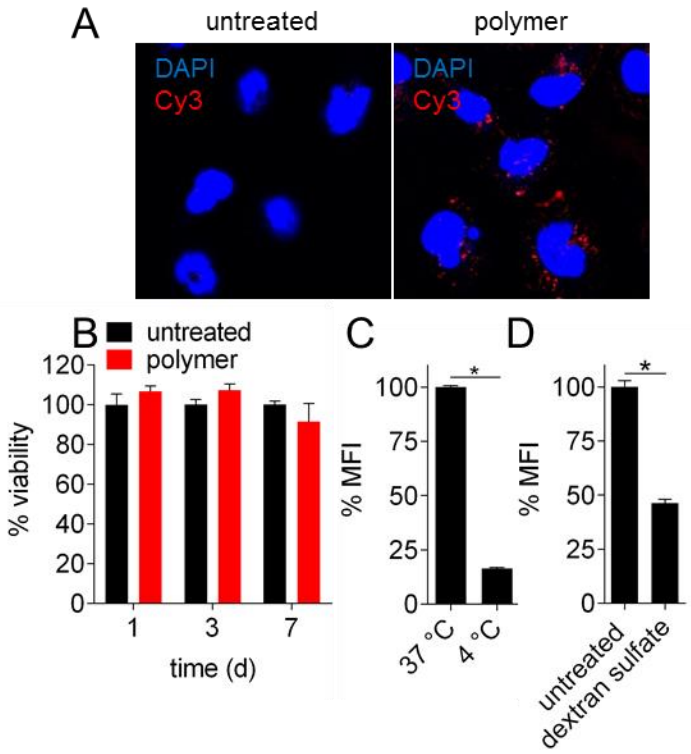

Figure 2.5 *In vitro* LMW 1:4 polymer characterization. **A.** Representative fluorescent images of HK-2 cells after incubation with fluorescent polymer. Cells were incubated with polymers for 2 h prior to imaging. Blue, DAPI; red, Cy3-labeled polymers. **B.** HK-2 cell viability after polymer treatment at various days (n = 5). **C.** Polymer uptake, measured by mean fluorescence intensity (MFI), after 1 h incubation with polymer at 37 or 4 °C (n = 4). **D.** Polymer uptake, measured by mean fluorescence intensity (MFI), after 1 h incubation with polymer in media or in the presence of dextran sulfate (n = 3). Bars represent means ± SEM. Statistical analysis was performed using a two-tailed Student's t-test. *p-value < 0.05.

cells with 1 μM polymer for up to 7 days did not cause significant differences in viability compared to untreated cells, as determined by MTS/PMS assay (**Figure 2.5B**). To investigate the mechanism of polymer internalization, polymer uptake was measured after incubation in either 37 °C or 4 °C using flow cytometry, as reduced temperature is known to effectively inhibit active endocytosis.[17,37] Incubation of cells on ice (4 °C) significantly reduced polymer fluorescence (*p*-value < 0.0001) compared to cells maintained at 37 °C (**Figure 2.5C**). Moreover, in a competition uptake experiment with anionic dextran sulfate (500 kDa), incubation of polymer in an excess of dextran sulfate significantly reduced polymer fluorescence intensity to ~46% compared to control (*p*-value < 0.0001, **Figure 2.5D**).

2.4 Discussion

In engineering intravenous polymeric drug carriers for targeted drug delivery applications, careful consideration of polymer properties must be taken to understand and control "passive targeting" effects, inadvertent or intentional.[20] Ideally, materials are designed with properties that enhance accumulation at target tissue, and avoid properties that enhance accumulation in off-target tissues. This is especially true when considering the kidneys, which filter up to 180 L of blood per day, and are a major clearance organ with intimate contact with the circulatory system. However, polymer design guidelines to either enhance or avoid kidney targeting have been limited.

Here, we systematically interrogated the effect of polymer anionic charge density and molecular weight, as well as glomerular filtration barrier integrity, on polymer accumulation in the kidneys. Polymers were synthesized by living radical polymerization to control composition and molecular weight. By using a pyridyl disulfide-terminated initiator, polymer chains were fluorescently labeled with a single Cy3-maleimide resulting in ~1:1 dye:polymer ratio, enabling direct comparison of fluorescent signals for the polymers tested. Thioether linkages have been reported in a variety of *in vivo* applications, including cellular nanoparticle "backpack" conjugation[38] and antibody-drug conjugates.[39] Whole-organ fluorescence imaging was selected due to ease of fluorophore conjugation and throughput. While this method presents limitations to accurate quantification due to tissue light-scattering,[40,41] it still provides a semi-quantitative means of evaluating biodistribution.

In an initial panel, polymers with fixed molecular weights (23-27 kDa), but varying anionic charge, were examined in normal mice. Cationic polymers were not tested due to the toxicity of these materials.[42] The molecular weights were well below the renal filtration cutoff of 50 kDa, allowing passage of these polymers through the glomerular filtration barrier via filtration. A polymer with M_n 25 kDa and high (80%) anionic monomer content was found to localize the most in the kidneys, and taken up specifically in proximal tubule cells. This was a surprising result, as both the glomerular endothelial cells and the glomerular basement membrane of the filtration barrier are highly negatively charged due to a glycocalyx and anionic heparan sulfate proteoglycans, respectively, and presumably repel the polymers.[43] Other uptake mechanisms, such as secretion and reabsorption, may also result in polymer uptake. Moreover, HPMA polymers containing anionic DTPA also exhibited kidney-specific accumulation, indicating that

the observed biodistribution is not unique to MAA monomer and likely generalizable to other anionic monomers.

We utilized a cytotoxic anti-podocyte antibody to induce experimental FSGS. This antibody method is well-reported and specifically causes apoptosis of glomerular podocytes,[21,27,44-53] leading to albuminuria, a clinical signature of a dysfunctional glomerular filtration barrier and loss of size-selective filtration.[54] This model was used to test the effects of polymer molecular weight with fixed anionic charge density (80%). Experimental FSGS increased the kidney fluorescence of LMW 1:4 polymer (25 kDa) but not HMW 1:4 polymer (47 kDa), providing some evidence that LMW 1:4 polymer kidney distribution is driven partly by filtration while HMW 1:4 is not. Moreover, these findings suggest that there is an optimal molecular weight for kidney delivery applications. Our observation that experimental FSGS enhanced LMW 1:4 polymer distribution suggests that disease conditions resulting in loss of filtration size-selectivity may be exploited to enhance material targeting to the kidneys, similar to the enhanced permeability and retention effect observed in animal models of tumors.[20]

These two size regimes, low-molecular weight (~25 kDa) and high-molecular weight (~50 kDa), were selected to test the kidney distribution behavior of polymers below and near the filtration cutoff for linear polymers (~50 kDa). Many reports have shown that circulation half-life increases significantly for linear polymers of size ~50 kDa compared to those of size 20 kDa,[55,56] indicating that the filtration cutoff is near 50 kDa. Our study seems to corroborate these findings. Given that the polymer backbones studied here are non-degradable and the clinical importance of

eliminating nondegradable materials,[57] we therefore studied these molecular weights as an intrinsic mechanism to eliminate these materials, but at different rates.

The immortalized human proximal tubule cell line, HK-2, was used to study polymer features *in vitro*, as these cells exhibit similar phenotype, function, and toxicity responses compared to primary cells.[36] LMW 1:4 polymers were internalized into punctate structures as early as 2 h after polymer treatment, and polymer treatment (1 μM) did not inflict significant toxicity, even at extended exposure times (7 d). Notably, this concentration and timescale is significantly higher and longer than what would be encountered *in vivo*, as the injected polymer concentration (40 μM) should be rapidly diluted and cleared after intravenous injection and tissue distribution. In subsequent experiments, polymer internalization was found to be significantly reduced at 4 °C and in the presence of excess anionic dextran sulfate, a known competitor of scavenger receptors, indicating that uptake is driven primarily by active endocytosis and/or non-specific scavenger receptors.[17,58] Proximal tubule reabsorption of macromolecules such as albumin and IgG is well-reported, with multi-ligand scavenger receptors megalin and cubilin responsible for uptake.[59,60] Indeed, various studies have shown that knockdown of megalin and/or cubilin results in reduced kidney uptake of synthetic peptides,[61] albumin,[62] and nanoparticles.[63] These receptors may mediate uptake of the polymers in the kidneys. Polymer uptake correlating with increasing anionic charge was also observed for the liver, albeit to a lesser degree compared to the kidneys. Liver endothelial and Kupffer cells express scavenger receptors SR-AI and SR-AII that broadly recognize polyanionic ligands.[64-66] These non-specific scavenger receptors may mediate liver uptake of the polymers studied in this work.

While the polymers studied here did not exhibit significant podocyte uptake in the context of glomerular disease, these findings may still be useful for glomerular disease applications. As these polymers seem to be filtered, functionalization of these polymers with ligands that recognize podocyte receptors may enable cellular binding and internalization as these polymers travel through the glomerular filtration barrier. Moreover, targeted drug delivery to proximal tubule cells during glomerular disease may improve renal health. Proteinuria causes tubular cell atrophy and fibrosis due to protein overload, which contributes to worsening chronic kidney disease.[67] Therefore, delivery of pro-survival molecules may be a strategic method of halting tubular necrosis.

2.5 Conclusions

By examining a panel of synthetic polymers, we have determined that polymers with molecular weight ~25 kDa and high anionic monomer content are taken up in kidney proximal tubule cells up to 1 week after injection, with enhanced accumulation observed in conditions of loss of glomerular filtration barrier integrity. These guidelines may inform the development of improved polymeric materials for a variety of applications. For chemotherapeutics such as cisplatin that inflict serious renal toxicity,[68] polymeric drug carriers should potentially avoid high anionic monomer content to mitigate uptake into proximal tubule cells. In kidney diseases such as polycystic kidney disease where tubule cells are principally afflicted,[69] anionic polymeric drug carriers may be considered to improve the therapeutic profile of drugs.

2.6 Acknowledgments

This work was supported by the Office of the Assistant Secretary of Defense for Health Affairs through the Peer Reviewed Medical Research Program under Award Numbers PR151175 and PR151965, National Institutes of Health Grants 1R01DK097598 and R01AG046231, a National Science Foundation Graduate Research Fellowship Program under Grant No. DGE-1256082 to GWL, and a National Cancer Institute NRSA award 1F31CA213901 to NS. Opinions, interpretations, conclusions, and recommendations are those of the authors and are not necessarily endorsed by the Department of Defense, National Institutes of Health, or National Science Foundation. We would like to thank Heather Gustafson, Meilyn Sylvestre, Soren Johnson, Ritika Jain, and George Sun for their help with experiments, and Michele Shaffer for consultation on statistical analysis.

References

1. Duncan, R. The dawning era of polymer therapeutics. *Nat Rev Drug Discov* **2**, 347-360 (2003).
2. Larson, N. & Ghandehari, H. Polymeric conjugates for drug delivery. *Chem Mater* **24**, 840-853 (2012).
3. Tong, R. & Cheng, J. Anticancer Polymeric Nanomedicines. *Polymer Reviews* **47**, 345-381 (2007).
4. Pack, D.W., Hoffman, A.S., Pun, S. & Stayton, P.S. Design and development of polymers for gene delivery. *Nat Rev Drug Discov* **4**, 581-593 (2005).
5. Davis, M.E., Chen, Z.G. & Shin, D.M. Nanoparticle therapeutics: an emerging treatment modality for cancer. *Nat Rev Drug Discov* **7**, 771-782 (2008).
6. Veronese, F.M., *et al.* PEG-doxorubicin conjugates: influence of polymer structure on drug release, in vitro cytotoxicity, biodistribution, and antitumor activity. *Bioconjug Chem* **16**, 775-784 (2005).
7. Alexis, F., Pridgen, E., Molnar, L.K. & Farokhzad, O.C. Factors affecting the clearance and biodistribution of polymeric nanoparticles. *Mol Pharm* **5**, 505-515 (2008).

8. He, C., Hu, Y., Yin, L., Tang, C. & Yin, C. Effects of particle size and surface charge on cellular uptake and biodistribution of polymeric nanoparticles. *Biomaterials* **31**, 3657-3666 (2010).
9. Imran ul-haq, M., Lai, B.F., Chapanian, R. & Kizhakkedathu, J.N. Influence of architecture of high molecular weight linear and branched polyglycerols on their biocompatibility and biodistribution. *Biomaterials* **33**, 9135-9147 (2012).
10. Thanou, M. & Duncan, R. Polymer-protein and polymer-drug conjugates in cancer therapy. *Curr Opin Investig Drugs* **4**, 701-709 (2003).
11. Matsumura, Y. & Maeda, H. A new concept for macromolecular therapeutics in cancer chemotherapy: mechanism of tumoritropic accumulation of proteins and the antitumor agent smancs. *Cancer Res* **46**, 6387-6392 (1986).
12. Fox, M.E., Szoka, F.C. & Frechet, J.M. Soluble polymer carriers for the treatment of cancer: the importance of molecular architecture. *Acc Chem Res* **42**, 1141-1151 (2009).
13. Williams, R.M., Jaimes, E.A. & Heller, D.A. Nanomedicines for kidney diseases. *Kidney Int* **90**, 740-745 (2016).
14. Kamaly, N., He, J.C., Ausiello, D.A. & Farokhzad, O.C. Nanomedicines for renal disease: current status and future applications. *Nat Rev Nephrol* **12**, 738-753 (2016).
15. Choi, C.H., Zuckerman, J.E., Webster, P. & Davis, M.E. Targeting kidney mesangium by nanoparticles of defined size. *Proc Natl Acad Sci U S A* **108**, 6656-6661 (2011).
16. Zuckerman, J.E., Choi, C.H., Han, H. & Davis, M.E. Polycation-siRNA nanoparticles can disassemble at the kidney glomerular basement membrane. *Proc Natl Acad Sci U S A* **109**, 3137-3142 (2012).
17. Kamada, H., *et al.* Synthesis of a poly(vinylpyrrolidone-co-dimethyl maleic anhydride) co-polymer and its application for renal drug targeting. *Nat Biotechnol* **21**, 399-404 (2003).
18. Borgman, M.P., *et al.* Tumor-targeted HPMA copolymer-(RGDfK)-(CHX-A"-DTPA) conjugates show increased kidney accumulation. *J Control Release* **132**, 193-199 (2008).
19. Bruni, R., *et al.* Ultrasmall polymeric nanocarriers for drug delivery to podocytes in kidney glomerulus. *J Control Release* **255**, 94-107 (2017).
20. Wang, C.E., Stayton, P.S., Pun, S.H. & Convertine, A.J. Polymer nanostructures synthesized by controlled living polymerization for tumor-targeted drug delivery. *J Control Release* **219**, 345-354 (2015).
21. Eng, D.G., *et al.* Glomerular parietal epithelial cells contribute to adult podocyte regeneration in experimental focal segmental glomerulosclerosis. *Kidney Int* **88**, 999-1012 (2015).
22. Jia, L., *et al.* Reduction-responsive cholesterol-based block copolymer vesicles for drug delivery. *Biomacromolecules* **15**, 2206-2217 (2014).
23. Lamm, R.J., *et al.* Peptide valency plays an important role in the activity of a synthetic fibrin-crosslinking polymer. *Biomaterials* **132**, 96-104 (2017).
24. Strohalm, J. & Kopeček, J. Poly[N-(2-hydroxypropyl)methacrylamide]. IV. Heterogeneous polymerization. *Die Angewandte Makromolekulare Chemie* **70**, 109-118 (1978).
25. Mitra, A., Nan, A., Papadimitriou, J.C., Ghandehari, H. & Line, B.R. Polymer-peptide conjugates for angiogenesis targeted tumor radiotherapy. *Nucl Med Biol* **33**, 43-52 (2006).

26. Omelyanenko, V., Kopeckova, P., Gentry, C. & Kopecek, J. Targetable HPMA copolymer-adriamycin conjugates. Recognition, internalization, and subcellular fate. *J Control Release* **53**, 25-37 (1998).
27. Eng, D.G., *et al.* Detection of renin lineage cell transdifferentiation to podocytes in the kidney glomerulus with dual lineage tracing. *Kidney Int* (2018).
28. Marshall, C.B., Krofft, R.D., Pippin, J.W. & Shankland, S.J. CDK inhibitor p21 is prosurvival in adriamycin-induced podocyte injury, in vitro and in vivo. *Am J Physiol Renal Physiol* **298**, F1140-1151 (2010).
29. Ma, H., Hyun, J., Stiller, P. & Chilkoti, A. "Non-Fouling" Oligo(ethylene glycol)-Functionalized Polymer Brushes Synthesized by Surface-Initiated Atom Transfer Radical Polymerization. *Advanced Materials* **16**, 338-341 (2004).
30. Bhattacharjee, S., *et al.* Site-Specific Zwitterionic Polymer Conjugates of a Protein Have Long Plasma Circulation. *Chembiochem* **16**, 2451-2455 (2015).
31. Lutz, J.-F. Polymerization of oligo(ethylene glycol) (meth)acrylates: Toward new generations of smart biocompatible materials. *Journal of Polymer Science Part A: Polymer Chemistry* **46**, 3459-3470 (2008).
32. Qi, Y., *et al.* A brush-polymer conjugate of exendin-4 reduces blood glucose for up to five days and eliminates poly(ethylene glycol) antigenicity. *Nat Biomed Eng* **1**(2016).
33. Ruggiero, A., *et al.* Paradoxical glomerular filtration of carbon nanotubes. *Proc Natl Acad Sci U S A* **107**, 12369-12374 (2010).
34. Nasongkla, N., *et al.* Dependence of pharmacokinetics and biodistribution on polymer architecture: effect of cyclic versus linear polymers. *J Am Chem Soc* **131**, 3842-3843 (2009).
35. Lewis, A., Tang, Y., Brocchini, S., Choi, J.W. & Godwin, A. Poly(2-methacryloyloxyethyl phosphorylcholine) for protein conjugation. *Bioconjug Chem* **19**, 2144-2155 (2008).
36. Ryan, M.J., *et al.* HK-2: an immortalized proximal tubule epithelial cell line from normal adult human kidney. *Kidney Int* **45**, 48-57 (1994).
37. Goldenthal, K.L., Pastan, I. & Willingham, M.C. Initial steps in receptor-mediated endocytosis. The influence of temperature on the shape and distribution of plasma membrane clathrin-coated pits in cultured mammalian cells. *Exp Cell Res* **152**, 558-564 (1984).
38. Stephan, M.T., Moon, J.J., Um, S.H., Bershteyn, A. & Irvine, D.J. Therapeutic cell engineering with surface-conjugated synthetic nanoparticles. *Nat Med* **16**, 1035-1041 (2010).
39. Lyon, R.P., Meyer, D.L., Setter, J.R. & Senter, P.D. Conjugation of anticancer drugs through endogenous monoclonal antibody cysteine residues. *Methods Enzymol* **502**, 123-138 (2012).
40. Liu, Y., Tseng, Y.-c. & Huang, L. Biodistribution Studies of Nanoparticles Using Fluorescence Imaging: A Qualitative or Quantitative Method? *Pharmaceutical Research* **29**, 3273-3277 (2012).
41. Tasciotti, E., *et al.* Near-Infrared Imaging Method for the In Vivo Assessment of the Biodistribution of Nanoporous Silicon Particles. *Molecular Imaging* **10**, 7290.2011.00011 (2011).
42. Lv, H., Zhang, S., Wang, B., Cui, S. & Yan, J. Toxicity of cationic lipids and cationic polymers in gene delivery. *J Control Release* **114**, 100-109 (2006).

43. Miner, J.H. The glomerular basement membrane. *Exp Cell Res* **318**, 973-978 (2012).
44. Kaverina, N.V., *et al.* WT1 Is Necessary for the Proliferation and Migration of Cells of Renin Lineage Following Kidney Podocyte Depletion. *Stem Cell Reports* **9**, 1152-1166 (2017).
45. Kaverina, N.V., Eng, D.G., Schneider, R.R., Pippin, J.W. & Shankland, S.J. Partial podocyte replenishment in experimental FSGS derives from nonpodocyte sources. *Am J Physiol Renal Physiol* **310**, F1397-1413 (2016).
46. Kaverina, N.V., *et al.* Tracking the stochastic fate of cells of the renin lineage after podocyte depletion using multicolor reporters and intravital imaging. *PLoS One* **12**, e0173891 (2017).
47. Lichtnekert, J., *et al.* Renin-Angiotensin-Aldosterone System Inhibition Increases Podocyte Derivation from Cells of Renin Lineage. *J Am Soc Nephrol* **27**, 3611-3627 (2016).
48. Ohse, T., *et al.* De novo expression of podocyte proteins in parietal epithelial cells during experimental glomerular disease. *Am J Physiol Renal Physiol* **298**, F702-711 (2010).
49. Pippin, J.W., *et al.* Cells of renin lineage are adult pluripotent progenitors in experimental glomerular disease. *Am J Physiol Renal Physiol* **309**, F341-358 (2015).
50. Schneider, R.R., *et al.* Compound effects of aging and experimental FSGS on glomerular epithelial cells. *Aging (Albany NY)* **9**, 524-546 (2017).
51. Zhang, J., *et al.* Podocyte repopulation by renal progenitor cells following glucocorticoids treatment in experimental FSGS. *Am J Physiol Renal Physiol* **304**, F1375-1389 (2013).
52. Zhang, J., *et al.* Retinoids augment the expression of podocyte proteins by glomerular parietal epithelial cells in experimental glomerular disease. *Nephron Exp Nephrol* **121**, e23-37 (2012).
53. Roeder, S.S., *et al.* Activated ERK1/2 increases CD44 in glomerular parietal epithelial cells leading to matrix expansion. *Kidney Int* **91**, 896-913 (2017).
54. Jefferson, J.A., Alpers, C.E. & Shankland, S.J. Podocyte biology for the bedside. *Am J Kidney Dis* **58**, 835-845 (2011).
55. Caliceti, P. & Veronese, F.M. Pharmacokinetic and biodistribution properties of poly(ethylene glycol)-protein conjugates. *Adv Drug Deliv Rev* **55**, 1261-1277 (2003).
56. Seymour, L.W., Duncan, R., Strohalm, J. & Kopecek, J. Effect of molecular weight (Mw) of N-(2-hydroxypropyl)methacrylamide copolymers on body distribution and rate of excretion after subcutaneous, intraperitoneal, and intravenous administration to rats. *J Biomed Mater Res* **21**, 1341-1358 (1987).
57. Gustafson, H.H., Holt-Casper, D., Grainger, D.W. & Ghandehari, H. Nanoparticle Uptake: The Phagocyte Problem. *Nano Today* **10**, 487-510 (2015).
58. Tsubamoto, Y., *et al.* Dextran sulfate, a competitive inhibitor for scavenger receptor, prevents the progression of atherosclerosis in Watanabe heritable hyperlipidemic rabbits. *Atherosclerosis* **106**, 43-50 (1994).
59. Christensen, E.I. & Birn, H. Megalin and cubilin: synergistic endocytic receptors in renal proximal tubule. *Am J Physiol Renal Physiol* **280**, F562-573 (2001).
60. Christensen, E.I., Birn, H., Verroust, P. & Moestrup, S.K. Membrane receptors for endocytosis in the renal proximal tubule. *Int Rev Cytol* **180**, 237-284 (1998).
61. Wischnjow, A., *et al.* Renal Targeting: Peptide-Based Drug Delivery to Proximal Tubule Cells. *Bioconjug Chem* **27**, 1050-1057 (2016).

62. Zhai, X.Y., *et al.* Cubilin- and megalin-mediated uptake of albumin in cultured proximal tubule cells of opossum kidney. *Kidney Int* **58**, 1523-1533 (2000).
63. Gao, S., *et al.* Megalin-mediated specific uptake of chitosan/siRNA nanoparticles in mouse kidney proximal tubule epithelial cells enables AQP1 gene silencing. *Theranostics* **4**, 1039-1051 (2014).
64. Platt, N. & Gordon, S. Scavenger receptors: diverse activities and promiscuous binding of polyanionic ligands. *Chem Biol* **5**, R193-203 (1998).
65. Kawabata, K., Takakura, Y. & Hashida, M. The fate of plasmid DNA after intravenous injection in mice: involvement of scavenger receptors in its hepatic uptake. *Pharm Res* **12**, 825-830 (1995).
66. van Oosten, M., van de Bilt, E., van Berkel, T.J. & Kuiper, J. New scavenger receptor-like receptors for the binding of lipopolysaccharide to liver endothelial and Kupffer cells. *Infect Immun* **66**, 5107-5112 (1998).
67. Abbate, M., Zoja, C. & Remuzzi, G. *How Does Proteinuria Cause Progressive Renal Damage?*, (2006).
68. Miller, R.P., Tadagavadi, R.K., Ramesh, G. & Reeves, W.B. Mechanisms of Cisplatin nephrotoxicity. *Toxins (Basel)* **2**, 2490-2518 (2010).
69. Grantham, J.J. Polycystic kidney disease: a predominance of giant nephrons. *Am J Physiol* **244**, F3-10 (1983).

Supporting information

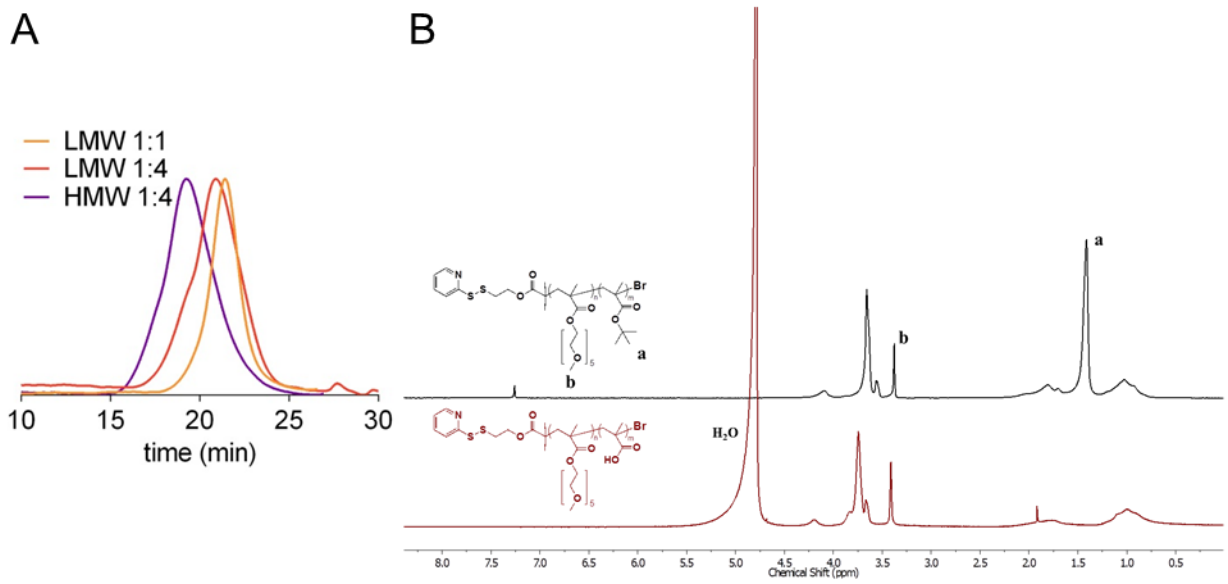

Figure S2.1 Polymer characterization. **A.** GPC differential refractive index traces of LMW 1:1, LMW 1:4, and HMW 1:4 copolymers prior to deprotection. Molecular weight of LMW 1:0 polymer was characterized by NMR. **B.** Representative ^{1}H NMR spectra of protected p(OEGMA-*co*-tBuMA)-PDS (top) and deprotected p(OEGMA-*co*-MAA)-PDS (bottom) LMW 1:4 copolymer. Removal of the *tert*-Butyl group was confirmed by disappearance of proton signal at ~1.4 ppm. The ratio of tBuMA to OEGMA was determined by comparing the integrations of peak **a** (9 protons) to peak **b** (3 protons). The combination of monomer ratios and M_n obtained by GPC was used to approximate the total monomer composition of each polymer. Due to solubility changes, the final polymer was only soluble in D_2O, which contains a large H_2O signal due to proton exchange.

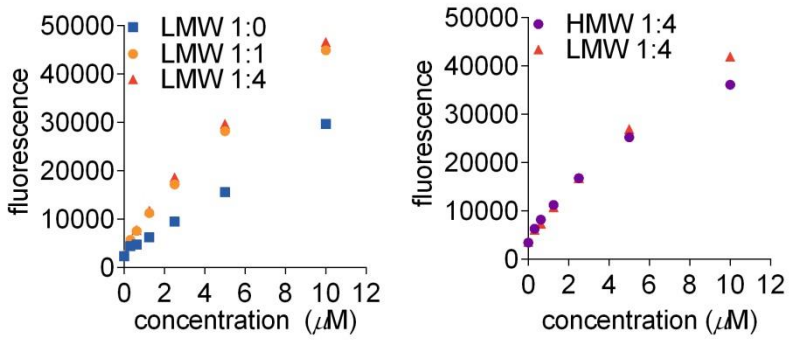

Figure S2.2 Polymer fluorescence. Polymers were diluted in PBS and fluorescence quantified.

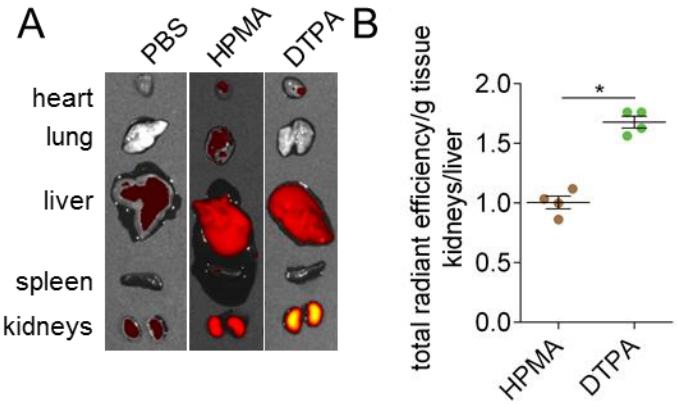

Figure S2.3 Kidney distribution of HPMA polymers. **A.** Representative fluorescent images of major organs 7 days after intravenous administration of PBS, HPMA control copolymer, p(HPMA-*co*-APMA-rhodamine) (M_n = 24 kDa, $Đ$ = 1.58), or p(HPMA-*co*-APMA-CHX-A"-DTPA-*co*-APMA-rhodamine) anionic copolymer (M_n = 27 kDa, $Đ$ = 1.94). DTPA is a functional group attached to the side chains that contains 5 carboxylic acids. All polymer treatments were n = 4. **B.** Kidney/liver normalized fluorescent ratio. Statistical analysis was performed using a two-tailed Student's *t*-test. Bars represent means ± SEM. **p*-value < 0.05.

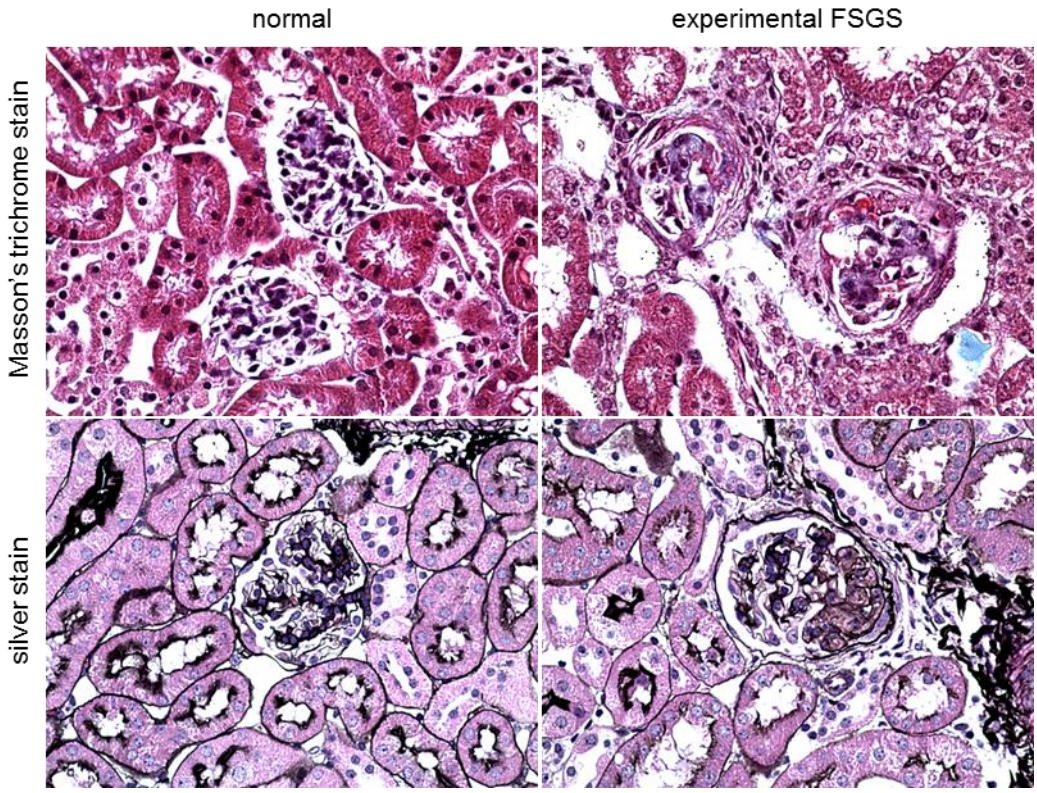

Figure S2.4 Histology of kidney sections from normal and experimental FSGS animals. Sections (day 14) from normal (left) and experimental FSGS (right) animals were stained with Masson's trichrome (top panels) and silver (bottom panels). In animals with experimental FSGS, Masson's trichrome staining revealed thickening and scarring of the Bowman's capsule, dilated glomerular capillary loops, and reduced nuclear staining on the glomerular tuft indicative of podocyte loss that is segmental in pattern. In animals with experimental FSGS, silver staining of kidney sections revealed segmental scarring as well as characteristics of synechial attachments between the glomerular tuft and the Bowman's capsule. All images were captured at 600× magnification.

Chapter 3

Boronic acid copolymers for direct loading and acid-triggered release of Bis-T-23 in cultured podocytes

Gary Liu, Yilong Cheng, Ritika Jain, Jeffrey W. Pippin,
Stuart J. Shankland, and Suzie H. Pun

Abstract

We report an acid-reversible linker for triggered release of Bis-T-23, an experimental small molecule drug for kidney disease treatment that restores podocyte morphology during disease. Bis-T-23 contains catechols, which form an acid-reversible, covalent boronate ester bond with boronic acids. We synthesized phenylboronic acid-containing polymers using reversible addition-fragmentation chain transfer polymerization that were able to directly load and solubilize Bis-T-23. Due to the reversibility of the boronic ester bond, drug was released in its native form in a pH-dependent manner. The polymers rapidly trafficked into acidic compartments and did not exhibit cytotoxicity, and polymer-drug conjugates successfully delivered Bis-T-23 into cultured podocytes.

[1]Adapted with permission from Y Cheng, GW Liu, *et al*. Boronic acid copolymers for direct loading and acid-triggered release of Bis-T-23 in cultured podocytes. *ACS Biomater. Sci. Eng.* 4, 3968-3973 (2018).

3.1 Introduction

Over 850 million people worldwide are afflicted with kidney disease.[1] Due to limited therapies to halt disease advancement, many patients progress to chronic kidney failure and ultimately require dialysis or kidney transplantation. However, kidney disease patients continue to face high morbidity and poor five-year survival rates.[2] Human and experimental studies have shown that loss and dysfunction of podocytes, highly specialized and terminally differentiated epithelial cells within the kidney glomerulus essential to filtration, directly underlies scarring of kidney filtration units that leads to deteriorating kidney function and proteinuria.[3] However, current therapies do not specifically modulate podocyte dysfunction, and burden the patient with significant side effects that further complicate the disease.[4-6]

A common response to injury in podocytes is actin cytoskeleton derangement, which precedes morphological changes that lead to disruption of the filtration barrier.[7] Therefore, drugs that modulate the actin cytoskeleton could have widespread clinical impact in treating chronic kidney disease. Schiffer *et al.* recently reported on the therapeutic efficacy of a small molecule, Bis-T-23, which promotes actin polymerization via dynamin oligomerization.[7] In various rodent models of podocyte injury, Bis-T-23 restored overall podocyte morphology and reduced proteinuria, a clinical signature of podocyte injury. However, low drug solubility and the ubiquitous expression of dynamin preclude systemic administration of Bis-T-23 in the clinic due to off-target toxicity.[8,9] Therefore, targeted Bis-T-23 delivery to glomerular podocytes could significantly expedite clinical translation of this experimental drug.

A critical component of targeted drug delivery is spatiotemporal control of drug release. Ideally, drugs are conjugated or loaded onto carriers in a manner that minimizes drug release during circulation to mitigate drug loss and reduce side effects, and releases drug after target cell binding and uptake. Drug linkers have been engineered to be sensitive to a variety of local cues (pH, enzymes, or reduction/oxidation) for programmed drug release within the target tissue or cell.[10,11] For example, the antibody-drug conjugate Adcetris contains cathepsin-sensitive linkers for drug release after cellular internalization and trafficking into lysosomes,[12] enabling targeted delivery of the highly potent drug monomethyl auristatin E. These advances in linker chemistry have subsequently improved the safety and efficacy of chemotherapeutics, and similar technologies could improve the standard of treatment for kidney diseases.

Here, we report on an acid-labile, boronate ester linkage for programmed release of Bis-T-23. We exploited the fact that Bis-T-23 contains catechol groups, which bind tightly to boronic acids to form a reversible covalent boronate ester bond.[13] Importantly, no drug modification is required for conjugation to boronic acid-functionalized carriers, and drugs are released in original form. Boronic acids bind tightly to diols, and reactions with catechols such as Bis-T-23 are especially favored due to the aromatic hydroxyl groups (association constant K_a ~830 M^{-1} and 4.6 M^{-1} for catechols and D-glucose, respectively).[13] The conjugated Bis-T-23 can be released by bond-breaking triggered by acidic pH conditions.[14,15] Therefore, the drug remains in a pro-drug form during circulation, but is released in active form after cellular binding and internalization into acidic, intracellular vesicles (**Figure 3.1**). In this work, we developed boronic acid-containing copolymers for loading and pH-sensitive release of the catechol-containing drug Bis-T-23. We characterize these materials for drug loading, release kinetics, cellular trafficking, and

cytotoxicity, and demonstrate polymer-drug conjugate delivery in cultured podocytes. Moreover, we report a new method of evaluating Bis-T-23 delivery to podocytes.

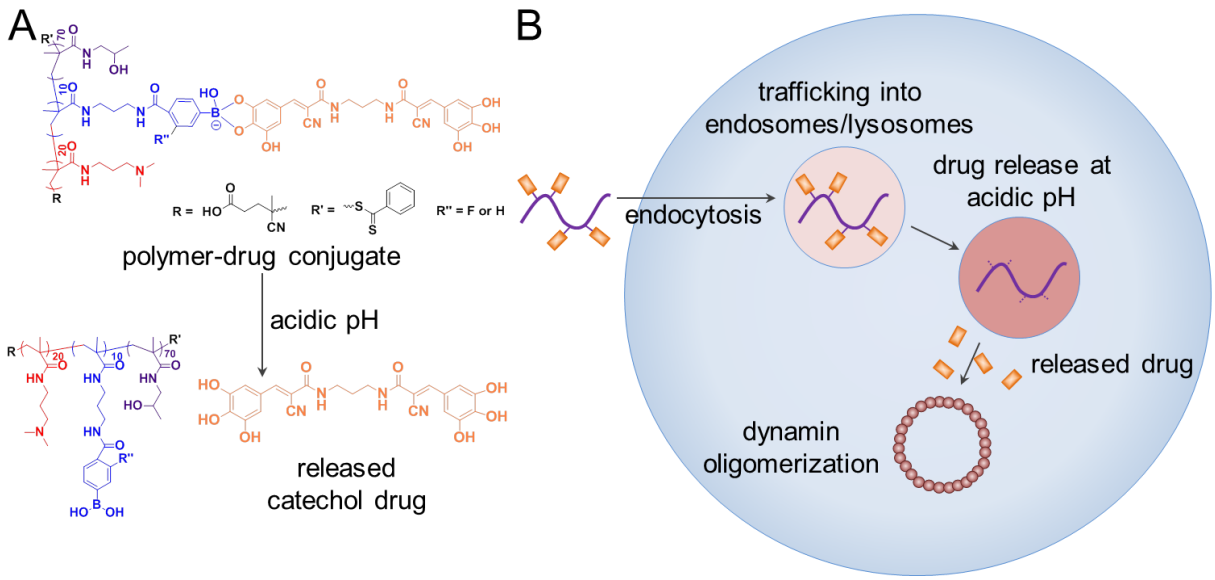

Figure 3.1 Schematic of polymer-drug conjugates and release mechanism. **A.** Phenylboronic acid (PBA) copolymers load Bis-T-23 through boronate ester formation between boronic acids on copolymer side chains and catechols on Bis-T-23. At acidic pH conditions, the boronate ester bond reverses, and Bis-T-23 is released in its native form. **B.** Copolymers are rapidly endocytosed due to cationic side chains and are trafficked into acidic endosomes and lysosomes, which trigger bond reversal. Bis-T-23 is then released, catalyzing dynamin oligomerization.

3.2 Materials and methods

3.2.1 Materials

N-(3-dimethylaminopropyl)-*N*′-ethylcarbodiimide hydrochloride (EDC) and *N*-hydroxysuccinimide (NHS) were purchased from Sigma-Aldrich. *N*-(2-hydroxypropyl) methacrylamide (HPMA), *N*-[3-(dimethylamino)propyl]methacrylamide (DMAPMA), and *N*-(3-

aminopropyl)methacrylamide (APMA) monomers were purchased from Polysciences, and 4-carboxyphenylboronic acid and 4-carboxy-3-fluorophenylboronic acid were purchased from Combi-Blocks. The chain-transfer agent 4-cyano-4-(ethylsulfanylthiocarbonyl) sulfanylvpentanoic acid (ECT) was a generous gift from Anthony Convertine. VA-044 was purchased from Wako Chemicals. Bis-T-23 was purchased from Aberjona Laboratories and dissolved to 30 mM stocks in DMSO. NHS-fluorescein was purchased from Thermo Fisher Scientific.

3.2.2 p(HPMA-*co*-DMAPMA-*co*-(APMA-*g*-PBA)) copolymer synthesis

p($HPMA_{70}$-*co*-$DMAPMA_{20}$-*co*-$APMA_{10}$) was synthesized by reversible addition-fragmentation chain transfer polymerization (RAFT). In a typical reaction, HPMA (381 mg, 2.66 mmol), DMAPMA (130 mg, 0.76 mmol), and APMA (68 mg, 0.38 mmol) were dissolved in 5.4 mL acetate buffer (1 M, pH 5.1) with ECT (10 mg, 0.038 mmol) and VA-044 (1.23 mg, 0.0038 mmol). After purging with argon for 10 min, polymerization was initiated by placing the reaction in a 44 °C oil bath. After 24 h, polymerization was stopped and the polymer was purified by dialysis against dH_2O followed by lyophilization. Polymer was characterized by ^1H NMR and GPC. Yield: 78%.

To functionalize copolymers with phenylboronic acid, 4-carboxyphenylboronic acid (PBA) (55 mg, 0.33 mmol), EDC (95 mg, 0.495 mmol), and NHS (57 mg, 0.495 mmol) were dissolved in a solution of DMSO (4 mL) and dH_2O (0.1 mL), then stirred at room temperature for 30 min. p(HPMA-*co*-DMAPMA-*co*-APMA) (100 mg) dissolved in 1 mL DMSO was added to the above

solution, and the reaction was allowed to proceed for 24 h. The final product, p(HPMA$_{70}$-*co*-DMAPMA$_{20}$-*co*-(APMA-*g*-PBA)$_{10}$), was obtained by sequential dialysis against methanol and dH_2O followed by lyophilization. Polymers were characterized by ^{1}H NMR. Yield: 90%. A phenylboronic acid derivative, 4-carboxy-3-fluorophenylboronic acid (FPBA), was also conjugated onto p(HPMA$_{70}$-*co*-DMAPMA$_{20}$-*co*-APMA$_{10}$) to produce p(HPMA$_{70}$-*co*-DMAPMA$_{20}$-*co*-(APMA-*g*-FPB)$_{10}$) with the same procedure.

In order to investigate the intracellular distribution of the polymer, p(HPMA-*co*-DMAPMA-*co*-APMA) was labeled with fluorescein followed by functionalization with PBA. p(HPMA-*co*-DMAPMA-*co*-APMA) (100 mg) was first dissolved in DMSO (4 mL) and dH_2O (0.1 mL), and the solution was purged with argon for 10 min followed by the addition of 38 μL NHS-fluorescein solution in DMF (1 mg/mL). After 2 h, PBA pre-activated with EDC and NHS was added, and the reaction was conducted for an additional 24 h. Afterwards, the mixture was dialyzed against dH_2O for 2 days and purified using a PD-10 column (GE). The labeled polymer, p(HPMA$_{70}$-*co*-DMAPMA$_{20}$-*co*-((APMA-*g*-fluorescein)$_1$-co-(APMA-*g*-PBA)$_9$)), was obtained after lyophilization. Yield: 75%.

3.2.3 Polymer characterization

^{1}H NMR spectra were recorded on a Bruker AV 300 (Bruker Corporation, Billerica, MA) nuclear magnetic resonance (NMR) instrument in deuteroxide (D_2O). The molecular weight and molecular weight dispersity ($Đ$) of the polymers were determined by size exclusion chromatography. To prepare materials for analysis, the purified polymer was dissolved at 5

mg/mL in running buffer (0.15 M sodium acetate buffered to pH 4.4 with acetic acid) for analysis by SEC. Samples were then applied to an OHpak SB-804 HQ column (Shodex) in line with a miniDAWN TREOS light scattering detector (Wyatt) and a OptiLab rEX refractive index detector (Wyatt). Absolute molecular weight averages (M_w and M_n) was calculated using ASTRA software (Wyatt). To test if aggregates were formed in the process of drug loading, the mixed solutions were analyzed by dynamic light scattering using a ZetaPLUS (Brookhaven Instruments Corporation, Holtsvile, NY) by preparing samples as described in polymer-drug conjugate drug delivery studies. UV absorption was tested by NanoDrop (Thermo Fisher Scientific).

3.2.4 Drug loading

Bis-T-23 was dissolved in DMSO (100 mg/mL), and a series of polymer was dissolved in 1 mL H_2O at various polymer:drug mass ratios (0:1-20:1). Drug (1 μL) was added to the polymer solution and then vortexed, and loading was tested after 2 h. The UV spectra of all samples was measured using λ = 410 nm and compared. Drug was considered completely loaded when no apparent increase in UV spectra was observed with increasing polymer:drug ratio.

3.2.5 Drug release

To investigate the copolymer-drug conjugate release behavior under different pH conditions, 1 mL of polymer-drug conjugate solution (100 μg Bis-T-23 at polymer:drug mass ratio = 14) was dissolved in 1 mL buffer, transferred inside dialysis tubing (MWCO 7 kDa), and placed within a

250-mL beaker containing 50 mL buffer. The following citric acid/sodium phosphate pH buffers were prepared: pH 4.6, 5.6, 6.8, and 7.4. Samples were incubated at 37 °C with rotation at 125 RPM. At each time point, 5 mL dialysate sample was collected and replaced with fresh buffer. Samples were then lyophilized, dissolved in 1 mL 10% DMSO, and quantified for drug content by absorbance spectroscopy using λ = 357 nm. In further experiments, PBA copolymer-drug conjugate release was tested in glucose (1.0 or 1.5 mg/mL) or mannitol (1.5 mg/mL) as described above.

3.2.6 Immortalized murine podocyte culture

Immortalized murine podocytes were cultured as previously described.[16] Briefly, cells were maintained in growth-permissive conditions (33 °C, mIFN-γ, bovine collagen I-coated plates) and then passaged into 24- or 96-well plates at 37 °C overnight prior to experiments. Jurkat cells were cultured according to supplier instructions (ATCC).

3.2.7 Cytotoxicity

Immortalized podocytes (1×10^4 per well in a 96-well plate) were washed twice with PBS and then incubated with various concentrations of polymer (0-200 μg/mL) dissolved in PBS for 20 min at 37 °C. After, cells were washed with PBS, and fresh PBS was added. Cells were allowed to incubate for 10 min at 37 °C. Viability was determined by CellTiter-Glo 2.0 (Promega).

3.2.8 Polymer uptake

Immortalized podocytes (2×10^5) were cultured on bovine collagen I (Corning)-coated 12-mm glass coverslips overnight, and then incubated with 50 nM LysoTracker Deep Red (Thermo Fisher Scientific) for 30 min according to manufacturer instructions. Fluorescently labeled polymers dissolved in PBS (200 μg/mL) were added, and cells were incubated for 20 min in the presence of 50 nM LysoTracker. After, the treatments were replaced with fresh PBS to emulate treatment conditions. For flow cytometry analysis, cells were washed with PBS and then lifted with trypsin; LysoTracker was not used for flow cytometry experiments. For microscopy analysis, cells were washed with PBS, fixed with 4% PFA, washed, and stained with DAPI according to manufacturer instructions. Images were collected with a confocal microscope (Leica).

3.2.9 Bis-T-23 drug efficacy by image analysis

Immortalized podocytes cultured on glass coverslips were treated with DMSO (0.2% v/v) or 60 μM Bis-T-23 for 4 h. After, cells were processed as above and stained with rhodamine-phalloidin (Cytoskeleton, Inc.) and DAPI for F-actin and nuclei, respectively, according to manufacturer instructions. Images were taken using an EVOS fluorescence microscope and F-actin was quantified by ImageJ analysis. First, 100 individual cells across all treatments were analyzed for size, and the middle 50% of cell sizes was used to determine the size range inclusion criteria for F-actin analysis. For each individual cell, F-actin was thresholded using the "Moments" method, and this area was recorded as the F-actin area and divided by the total cell area. Both image capture and analysis were performed in a blind manner.

3.2.10 Protein labeling

Bovine serum albumin (BSA, Thermo Fisher Scientific) and human holo-transferrin (R&D Biosystems) were dissolved in 0.1 M sodium bicarbonate buffer, pH 8.56 (20 mg/mL) and then labeled with NHS-fluorescein at an 8-fold molar excess for 1 h at room temperature. Afterwards, proteins were purified by Zeba column (Thermo Fisher Scientific) twice into water.

3.2.11 Polymer-drug conjugate drug delivery

Polymer-drug conjugates were prepared as follows: in a total volume of 100 μL in molecular-grade H_2O, PBA copolymer (at a 14-fold mass excess to drug, typically 67.3 μg/mL final concentration) was added, and then Bis-T-23 (typically 10 μM or 4.8 μg/mL final concentration) was added. The solution was then vortexed and allowed to incubate at room temperature for at least 2 h. After, PBS was added to achieve the final drug concentration (typically 10 μM). DMSO and free drug treatments were prepared immediately before treatment.

For drug delivery studies, podocytes (5-6×10^4 cells per well in a 24-well plate) were washed twice with PBS, incubated with treatments in PBS for 20 min at 37 °C, and then incubated with 50-100 μg/mL fluorescein-BSA in PBS for 10 min at 37 °C. After, cells were washed twice with ice-cold PBS, lifted with trypsin, resuspended in PBS+0.5% BSA, and then analyzed for FITC fluorescence using an Attune NxT flow cytometer (Thermo Fisher Scientific). Two independent experiments were performed.

For Jurkat studies, cells (1×10^5 cells per well in a round-bottom 96-well plate) were washed twice with PBS, incubated with treatments as above, and then incubated with 10 μg/mL fluorescein-transferrin as above. After, cells were washed, resuspended in PBS+0.5% BSA, and analyzed by flow cytometry as above. Three independent experiments were performed.

3.2.12 Data analysis

Data analysis was performed using GraphPad Prism software. Statistical analysis was performed using a one-way ANOVA with post-hoc Dunnett's multiple comparisons test to untreated cells, or a Student's *t*-test for single comparisons.

3.3 Results and discussion

3.3.1 Synthesis and characterization of p(HPMA-*co*-DMAPMA-*co*-(APMA-*g*-PBA)) copolymers

Phenylboronic acid-grafted copolymers (PBA copolymers) were synthesized by reversible addition-fragmentation chain transfer (RAFT) polymerization (**Scheme S3.1**) of the monomers *N*-(2-hydroxypropyl) methacrylamide (HPMA), *N*-[3-(dimethylamino)propyl]methacrylamide (DMAPMA), and *N*-(3-aminopropyl)methacrylamide (APMA). HPMA was selected due to its biocompatibility and water solubility;[17] DMAPMA, which contains a tertiary amine and is positively charged at physiologic pH, was selected to facilitate cellular internalization in lieu of a

targeting ligand;[18] and APMA was selected for facile functionalization with 4-carboxyphenylboronic acid by EDC/NHS conjugation post-polymerization. Notably, cationic polymers containing similar tertiary amines were observed to be rapidly internalized and trafficked into acidic endosomes and lysosomes.[19,20] This internalization route is an important requirement for the polymers studied here to reverse the boronate ester bond and trigger intracellular drug release.

Monomer conversion and copolymer composition was monitored by ^{1}H NMR during polymerization. Monomer conversion was nearly 100% after 18 h, and polymer composition was determined to be 70:20:10 for HPMA:DMAPMA:APMA (**Figure S3.1**). The copolymers exhibited a number average molecular weight (M_n) of 22 kDa and low dispersity ($Đ$ = 1.05) by GPC analysis, indicating good control of polymerization (**Figure S3.2** and **Table 3.1**). Functionalization of the copolymers with 4-carboxyphenylboronic acid was confirmed by ^{1}H NMR via emergence of new peaks at 7.9 and 7.6 ppm, indicating successful and complete reaction of primary amine side chains with PBA (**Figure S3.1**). Based on comparison of the integrals of the protons in PBA at 7.6 and 7.9 ppm with that of the protons in HPMA at 3.8 ppm, the final PBA copolymer was confirmed as p(HPMA$_{70}$-*co*-DMAPMA$_{20}$-*co*-(APMA-*g*-PBA)$_{10}$).

Table 3.1 Summary of p(HPMA-*co*-DMAPMA-*co*-APMA) polymers

Polymer	M_n [a] **(Da)**	M_n [b] **(Da)**	$Đ$
p(HPMA$_{70}$-*co*-DMAPMA$_{20}$-*co*-APMA$_{10}$)	15,200	22,000	1.05
p(HPMA$_{70}$-*co*-DMAPMA$_{20}$-*co*-(APMA-*g*-PBA)$_{10}$)	16,300	N/A	N/A

[a] ^{1}H NMR, [b]GPC

3.3.2 Drug loading optimization

When conjugated to PBA copolymers, Bis-T-23 gained a new absorbance at λ = 410 nm, which was used to monitor polymer drug loading. In the absence of polymer, Bis-T-23 exhibited low water solubility and formed a yellow precipitate in aqueous solutions (**Figure 3.2A**). At increasing polymer:drug mass ratios, precipitation decreased, and drug absorbance increased until at 14:1 ratio, after which the observed drug absorbance plateaued (**Figure 3.2A** and **B**). Therefore, a polymer:drug ratio of 14:1 was used for subsequent drug loading and studies. In these conditions, 24.2% of the available PBA are loaded with drug (see **Supporting Information** for calculations). Dynamic light scattering analysis was also performed to test if aggregation occurred during drug loading, as Bis-T-23 is symmetrical and may crosslink polymers. No differences in size distribution were observed between polymer only and polymer-drug conjugates, suggesting that these loading conditions do not result in crosslinking and aggregation (**Figure S3.3**). This may be due to steric hindrance of the benzyl in both the polymer and Bis-T-23.

3.3.3 pH-sensitive drug release

Polymer-drug conjugates were then tested for pH-dependent drug release in buffers at pH 7.4, 6.8, 5.6, and 4.6, with the latter two values within the late endosomal and lysosomal pH spanning 6.5-4.5.[21,22] While polymer-conjugates at pH 4.6 and 5.6 exhibited rapid and nearly complete drug release, conjugates at pH 6.8 and 7.4 exhibited minimal drug release within the same timeframe (**Figure 3.2C**). After 48 h, PBA copolymers exhibited 14.5%, 19.3%, 80.4%, and

98.1% cumulative Bis-T-23 release in pH 7.4, 6.8, 5.6, and 4.6, respectively. These observations demonstrate that the copolymers exhibit pH-sensitive drug release, and that the PBA copolymers could release Bis-T-23 in pH ranges relevant to acidic endosomes and lysosomes.

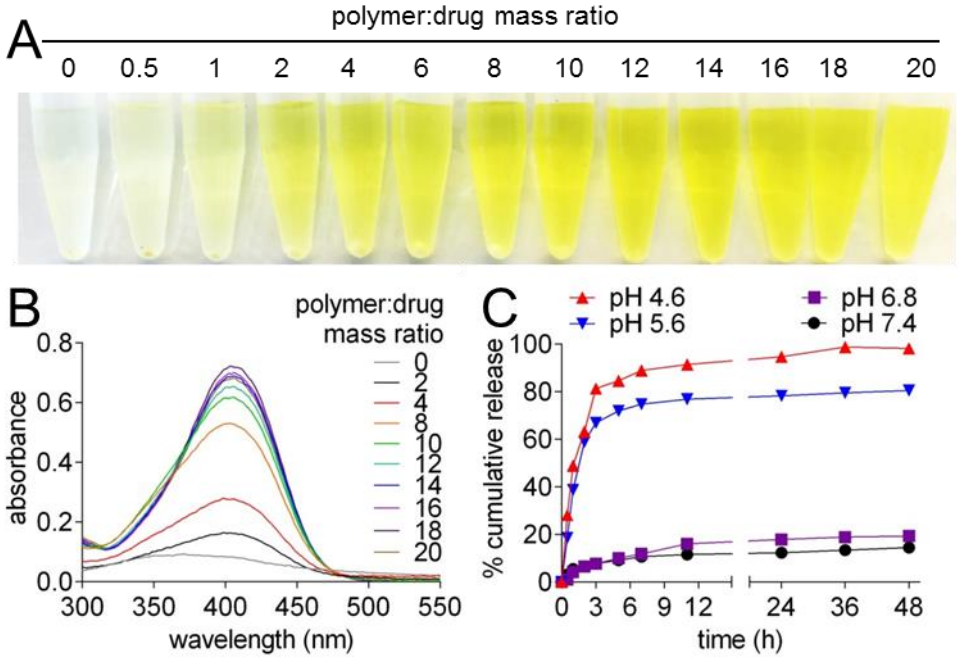

Figure 3.2 Characterization of PBA copolymer behavior. **A.** Image of polymer-drug conjugates loaded at increasing polymer:drug mass ratios. **B.** Absorbance quantification of polymer-drug conjugates. When loaded onto PBA copolymers, Bis-T-23 exhibits a new absorbance at λ = 410. **C.** Bis-T-23 release from polymer-drug conjugates at various pH.

Despite the pK_a of the PBA studied here being greater than 8.0,[23,24] Bis-T-23 was retained on the PBA copolymer at pH 7.4, likely due to the high binding affinity between PBA and catechols. As the pK_a of the boronic acid may affect drug loading and release, polymers containing fluoroPBA (FPBA), which exhibits a lower pK_a around 7.2-7.8 due to an electronegative fluorine,[25,26] were similarly synthesized and characterized (**Figure S3.1**). FPBA copolymers exhibited optimal drug loading at polymer:drug ratio 12:1 with similar trends of pH-dependent drug release as PBA

copolymers (**Figure S3.4**). As no major differences in drug loading and release were observed between PBA and FPBA copolymers, PBA copolymers were selected for further study due to greater aqueous solubility. Therefore, polymer-drug conjugates may be formed at pH 7 without the need to modulate the pK_a of the phenylboronic acid.

Drug release was also tested in the presence of glucose, as vicinal diols might prematurely displace conjugated Bis-T-23. Physiologically, blood glucose concentrations range from 0.63-0.99 mg/mL in normal children and adults.[27] Glucose at concentrations up to 1.5 mg/mL did not cause significant drug release from the PBA copolymers (**Figure S3.5**). Moreover, mannitol, which contains multiple hydroxyls and exhibits a higher K_a with boronic acid than glucose (K_a = 120 M^{-1} and 4.6 M^{-1}, respectively),[13] did not cause any significant Bis-T-23 release at the same concentration (**Figure S3.5**). The stability of the boronate ester is likely due to the 180-fold higher K_a of catechols and boronic acids compared to diols. Therefore, diols at physiological concentrations do not displace Bis-T-23, indicating that boronate ester reversal is more sensitive to pH than diols (**Figure S3.5**).

3.3.4 Polymer endocytosis and trafficking

Bis-T-23-loaded polymers were then tested for drug delivery in cultured podocytes. First, the trafficking of PBA copolymers in podocytes was examined by flow cytometry and confocal microscopy. As early as 20-30 min, fluorescently labeled PBA copolymers were mostly internalized (**Figure 3.3A**) and colocalized with LysoTracker, a marker of lysosomes (**Figure 3.3B**). This is consistent with other studies reporting that polycationic materials rapidly traffic

into acidic compartments as early as 5 min, with greater trafficking into more acidic late endosomes and lysosomes observed 10-20 min later.[28,29]

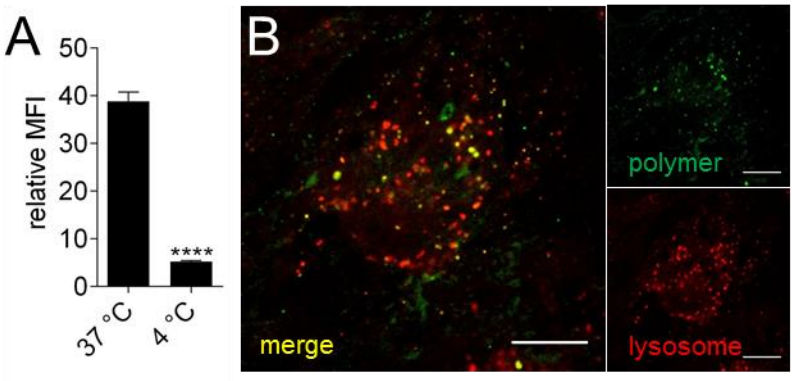

Figure 3.3 *In vitro* polymer uptake. **A.** Polymer uptake by podocytes, measured by mean fluorescence intensity (MFI), after 20 min incubation at 37 or 4 °C. **B.** Fluorescent images of podocytes treated with fluorescein-PBA copolymers obtained by confocal microscopy. Green, polymer; red, lysosomes; yellow, merge. Pearson's correlation coefficient = 0.5. Scale bars, 10 μm.

3.3.5 Drug delivery and cytotoxicity *in vitro*

Bis-T-23 promotes dynamin oligomerization, which causes actin polymerization and crosslinking and focal adhesion maturation.[7,30-32] By image analysis, while Bis-T-23 significantly increased F-actin content in cultured podocytes, polymer-drug conjugates did not (**Figure S3.6**), likely due to the low dynamic range of this method. Therefore, we sought to develop a more high-throughput method of evaluating Bis-T-23 delivery in cultured podocytes. Given that podocytes endocytose albumin[33] and the importance of dynamin in this process,[34] we hypothesized that Bis-T-23 would modulate uptake of albumin. Indeed, in initial studies, Bis-T-23 inhibited albumin uptake up to 27% (**Figure S3.7**). Therefore, flow cytometry analysis of fluorescein-albumin uptake was used to quantify polymer-drug delivery. In podocytes, free Bis-

T-23 and polymer-Bis-T-23 significantly inhibited albumin uptake (**Figure 3.4A**). Notably, cells were incubated with treatments for 20 min in PBS; due to minimal drug release within this time in pH 7.4 (<5%), polymer-Bis-T-23 effects was more likely due to acid-triggered release rather than basal release. Additionally, free Bis-T-23 and polymer-Bis-T-23 significantly inhibited transferrin uptake in a human T cell line (**Figure 3.4B**), consistent with previous studies showing Bis-T-23 inhibition of transferrin uptake,[35] and did not exhibit significant toxicity towards cultured podocytes (**Figure 3.4C**). These findings indicate that polymer-Bis-T-23 conjugates are internalized into acidic compartments, Bis-T-23 is being released intracellularly, and the polymers are not significantly toxic in the conditions tested.

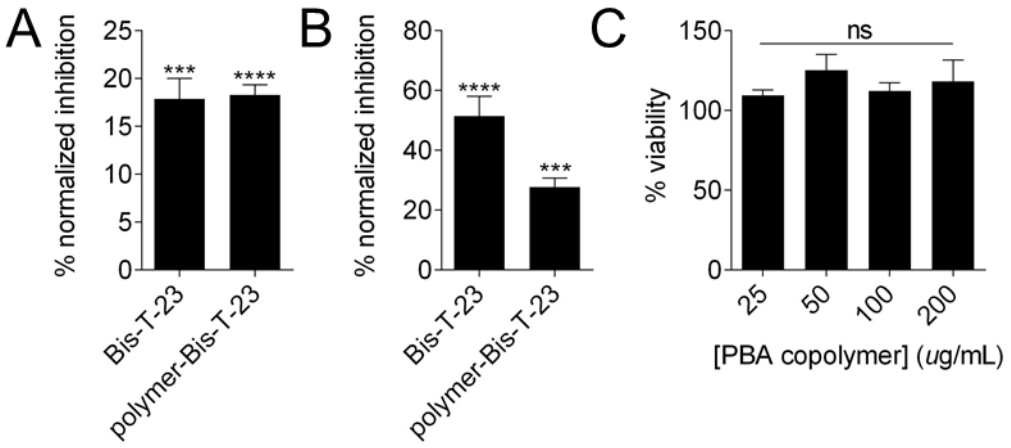

Figure 3.4 *In vitro* drug delivery and cytotoxicity of polymer-drug conjugates. **A.** Normalized inhibition of fluorescein-BSA uptake in podocytes. **B.** Normalized inhibition of fluorescein-transferrin in Jurkat cells. Treatments were normalized by respective vehicle (DMSO or polymer only) controls. **C.** Percent viability of treatments relative to untreated podocytes. Bars represent means ± SEM. ****p*-value < 0.001; *****p*-value < 0.0001; ns, not significant.

While recent high-throughput screening campaigns have identified new small molecule drug candidates for treating kidney disease,[36,37] solubility and off-target side effects remain major obstacles to clinical translation of experimental drugs such as Bis-T-23. Polymeric drug carriers

have emerged as an answer to some of these challenges by altering drug properties and pharmacokinetics. An important aspect of these carriers is the drug linker that controls drug release under specific conditions. Phenylboronic acid-containing polymers have been recently reported in applications in drug delivery due to their various stimuli-sensitive properties.[14,15,38] In this work, we developed PBA copolymers for acid-triggered release of the catechol-containing drug Bis-T-23, taking advantage of the fact that catechols form an acid-reversible boronate ester with boronic acids. This chemistry has been utilized in a number of drug delivery applications for stimulus-triggered drug release from polymer systems. Su *et al* reported on polymer-drug conjugates comprising the boronic acid-containing chemotherapeutic, bortezomib, and catechol-containing polymers.[15] The materials exhibited acidic pH-selective drug release and maintained *in vitro* cancer cell killing. Aguirre-Chagala *et* al and Ma *et al* reported on boronic acid-containing polymers for loading the diol-containing chemotherapeutic, capecitabine. These materials self-assembled into micelles and exhibited pH-sensitive drug release.[39,40] Li *et al* developed drug-loaded, polymeric micelles through crosslinking of adjacent boronic acid- and catechol-containing polymers. These micelles also exhibited acidic pH- and mannitol-triggered drug release, as well as improved particle stability *in vivo*.[14] Moreover, boronate esters have broad utility in other applications, including isolation of catechol-containing compounds from plasma for quantification,[41] and saccharide-triggered release of catechol-containing model drugs from boronic acid-functionalized nanoparticles.[42]

3.4 Conclusions

This work reports PBA copolymers that reversibly load the catechol-containing drug Bis-T-23 without any further drug modification and release active drug after cell internalization. Polymer-drug conjugates were stable at physiological pH and in the presence of sugars, indicating potential stability of the conjugates during circulation *in vivo*. *In vitro*, PBA copolymers distributed into acidic endosomes, and through a flow cytometry assay to evaluate Bis-T-23 delivery, polymer-drug conjugates were able to deliver drug intracellularly. Collectively, these findings suggest that boronate ester chemistry may be an attractive strategy for releasing Bis-T-23 after cellular uptake. The copolymers reported here included the tertiary amine-containing monomer DMAPMA, which mediates cellular internalization for proof-of-concept *in vitro* studies. Future work includes functionalizing uncharged versions of these polymers for targeted podocyte delivery of Bis-T-23 in the kidney. This strategy could also be readily applied to other catechol-containing drugs such as quercetin or EGCG.[43,44]

3.5 Acknowledgments

This work was supported by the Office of the Assistant Secretary of Defense for Health Affairs through the Peer Reviewed Medical Research Program under Award No. W81XWH-16-1-0167 and by the National Science Foundation Graduate Research Fellowship Program under Grant No. DGE-1256082 to G. W. L. Y.L.C. gratefully acknowledges support from the "Young Talent Support Plan" of Xi'an Jiaotong University and the Fundamental Research Funds for the Central

Universities. S. J. S. and J. W. P. were supported by the NIDDK (R01 DK09759801A1 and UH2 DK107343-01) and the NIA (R01 AG046231-01A1). We thank Changkyu Gu and Sanja Sever for important discussion about Bis-T-23. Opinions, interpretations, conclusions, and recommendations are those of the authors and are not necessarily endorsed by the Department of Defense or the National Science Foundation. We also acknowledge support from the NIH (S10 OD016240) to the W. M. Keck Center for Advanced Studies in Neural Signaling and the assistance of Keck Center manager Dr. Nathaniel Peters, as well as thank Shijie Cao for his expertise and guidance on dynamic light scattering experiments.

References

1. Hill, N.R., *et al.* Global Prevalence of Chronic Kidney Disease - A Systematic Review and Meta-Analysis. *PLoS One* **11**, e0158765 (2016).
2. Collins, A.J., Foley, R.N., Gilbertson, D.T. & Chen, S.C. The state of chronic kidney disease, ESRD, and morbidity and mortality in the first year of dialysis. *Clin J Am Soc Nephrol* **4 Suppl 1**, S5-11 (2009).
3. Kriz, W. & Lemley, K.V. A potential role for mechanical forces in the detachment of podocytes and the progression of CKD. *J Am Soc Nephrol* **26**, 258-269 (2015).
4. Ruggenenti, P., *et al.* Rituximab in steroid-dependent or frequently relapsing idiopathic nephrotic syndrome. *J Am Soc Nephrol* **25**, 850-863 (2014).
5. Greenbaum, L.A., Benndorf, R. & Smoyer, W.E. Childhood nephrotic syndrome--current and future therapies. *Nat Rev Nephrol* **8**, 445-458 (2012).
6. Gipson, D.S., *et al.* Management of childhood onset nephrotic syndrome. *Pediatrics* **124**, 747-757 (2009).
7. Schiffer, M., *et al.* Pharmacological targeting of actin-dependent dynamin oligomerization ameliorates chronic kidney disease in diverse animal models. *Nat Med* (2015).
8. Sontag, J.M., *et al.* Differential expression and regulation of multiple dynamins. *J Biol Chem* **269**, 4547-4554 (1994).
9. Allison, S.J. Chronic kidney disease: Actin cytoskeleton alterations in podocytes: a therapeutic target for chronic kidney disease. *Nat Rev Nephrol* **11**, 385 (2015).
10. Chu, D.S., *et al.* MMP9-sensitive polymers mediate environmentally-responsive bivalirudin release and thrombin inhibition. *Biomater Sci* **3**, 41-45 (2015).

11. Aryal, S., Hu, C.M. & Zhang, L. Polymer--cisplatin conjugate nanoparticles for acid-responsive drug delivery. *ACS Nano* **4**, 251-258 (2010).
12. Vaklavas, C. & Forero-Torres, A. Safety and efficacy of brentuximab vedotin in patients with Hodgkin lymphoma or systemic anaplastic large cell lymphoma. *Ther Adv Hematol* **3**, 209-225 (2012).
13. Springsteen, G. & Wang, B. A detailed examination of boronic acid–diol complexation. *Tetrahedron* **58**, 5291-5300 (2002).
14. Li, Y., *et al.* Well-defined, reversible boronate crosslinked nanocarriers for targeted drug delivery in response to acidic pH values and cis-diols. *Angew Chem Int Ed Engl* **51**, 2864-2869 (2012).
15. Su, J., Chen, F., Cryns, V.L. & Messersmith, P.B. Catechol polymers for pH-responsive, targeted drug delivery to cancer cells. *J Am Chem Soc* **133**, 11850-11853 (2011).
16. Shankland, S.J., Pippin, J.W., Reiser, J. & Mundel, P. Podocytes in culture: past, present, and future. *Kidney Int* **72**, 26-36 (2007).
17. Kopecek, J. & Kopeckova, P. HPMA copolymers: origins, early developments, present, and future. *Adv Drug Deliv Rev* **62**, 122-149 (2010).
18. Agarwal, S., Zhang, Y., Maji, S. & Greiner, A. PDMAEMA based gene delivery materials. *Materials Today* **15**, 388-393 (2012).
19. Cheng, Y., Yumul, R.C. & Pun, S.H. Virus-Inspired Polymer for Efficient In Vitro and In Vivo Gene Delivery. *Angew Chem Int Ed Engl* **55**, 12013-12017 (2016).
20. Jones, R.A., Poniris, M.H. & Wilson, M.R. pDMAEMA is internalised by endocytosis but does not physically disrupt endosomes. *Journal of Controlled Release* **96**, 379-391 (2004).
21. Hu, Y.B., Dammer, E.B., Ren, R.J. & Wang, G. The endosomal-lysosomal system: from acidification and cargo sorting to neurodegeneration. *Transl Neurodegener* **4**, 18 (2015).
22. Huotari, J. & Helenius, A. Endosome maturation. *EMBO J* **30**, 3481-3500 (2011).
23. Kubo, Y., Nishiyabu, R. & James, T.D. Hierarchical supramolecules and organization using boronic acid building blocks. *Chem Commun (Camb)* **51**, 2005-2020 (2015).
24. Roy, D. & Sumerlin, B.S. Glucose-Sensitivity of Boronic Acid Block Copolymers at Physiological pH. *ACS Macro Letters* **1**, 529-532 (2012).
25. Matsumoto, A., *et al.* A synthetic approach toward a self-regulated insulin delivery system. *Angew Chem Int Ed Engl* **51**, 2124-2128 (2012).
26. Sharma, B., *et al.* Bisboronic Acids for Selective, Physiologically Relevant Direct Glucose Sensing with Surface-Enhanced Raman Spectroscopy. *J Am Chem Soc* (2016).
27. Güemes, M., Rahman, S.A. & Hussain, K. What is a normal blood glucose? *Archives of Disease in Childhood* **101**, 569-574 (2016).
28. Lazebnik, M. & Pack, D.W. Rapid and facile quantitation of polyplex endocytic trafficking. *J Control Release* **247**, 19-27 (2017).
29. Canton, I. & Battaglia, G. Endocytosis at the nanoscale. *Chemical Society Reviews* **41**, 2718-2739 (2012).
30. Sever, S. & Schiffer, M. Actin dynamics at focal adhesions: a common endpoint and putative therapeutic target for proteinuric kidney diseases. *Kidney International* **93**, 1298-1307 (2018).
31. Gu, C., *et al.* Regulation of dynamin oligomerization in cells: the role of dynamin-actin interactions and its GTPase activity. *Traffic* **15**, 819-838 (2014).

32. Gu, C., *et al.* Dynamin Autonomously Regulates Podocyte Focal Adhesion Maturation. *J Am Soc Nephrol* **28**, 446-451 (2017).
33. Dobrinskikh, E., Okamura, K., Kopp, J.B., Doctor, R.B. & Blaine, J. Human podocytes perform polarized, caveolae-dependent albumin endocytosis. *Am J Physiol Renal Physiol* **306**, F941-951 (2014).
34. Inoue, K. & Ishibe, S. Podocyte endocytosis in the regulation of the glomerular filtration barrier. *Am J Physiol Renal Physiol* **309**, F398-405 (2015).
35. Sandgren, K.J., *et al.* A differential role for macropinocytosis in mediating entry of the two forms of vaccinia virus into dendritic cells. *PLoS Pathog* **6**, e1000866 (2010).
36. Sieber, J., *et al.* GDC-0879, a BRAF(V600E) Inhibitor, Protects Kidney Podocytes from Death. *Cell Chem Biol* **25**, 175-184 e174 (2018).
37. Lee, H.W., *et al.* A Podocyte-Based Automated Screening Assay Identifies Protective Small Molecules. *J Am Soc Nephrol* (2015).
38. Lv, S., *et al.* High Drug Loading and Sub-Quantitative Loading Efficiency of Polymeric Micelles Driven by Donor-Receptor Coordination Interactions. *J Am Chem Soc* **140**, 1235-1238 (2018).
39. Aguirre-Chagala, Y.E., Santos, J.L., Huang, Y. & Herrera-Alonso, M. Phenylboronic Acid-Installed Polycarbonates for the pH-Dependent Release of Diol-Containing Molecules. *ACS Macro Letters* **3**, 1249-1253 (2014).
40. Ma, R., *et al.* Iminoboronate-based dual-responsive micelles via subcomponent self-assembly for hydrophilic 1,2-diol-containing drug delivery. *RSC Advances* **7**, 21328-21335 (2017).
41. Huang, T., *et al.* Highly selective enrichment of baicalin in rat plasma by boronic acid-functionalized core-shell magnetic microspheres: Validation and application to a pharmacokinetic study. *Talanta* **147**, 501-509 (2016).
42. Liu, H.-B., *et al.* Saccharide- and temperature-responsive polymer brushes grown on gold nanoshells for controlled release of diols. *Colloids and Surfaces A: Physicochemical and Engineering Aspects* **386**, 131-134 (2011).
43. Jung, J.H., *et al.* Quercetin suppresses HeLa cell viability via AMPK-induced HSP70 and EGFR down-regulation. *J Cell Physiol* **223**, 408-414 (2010).
44. Chakrabarty, S., Ganguli, A., Das, A., Nag, D. & Chakrabarti, G. Epigallocatechin-3-gallate shows anti-proliferative activity in HeLa cells targeting tubulin-microtubule equilibrium. *Chemico-Biological Interactions* **242**, 380-389 (2015).

Supporting information

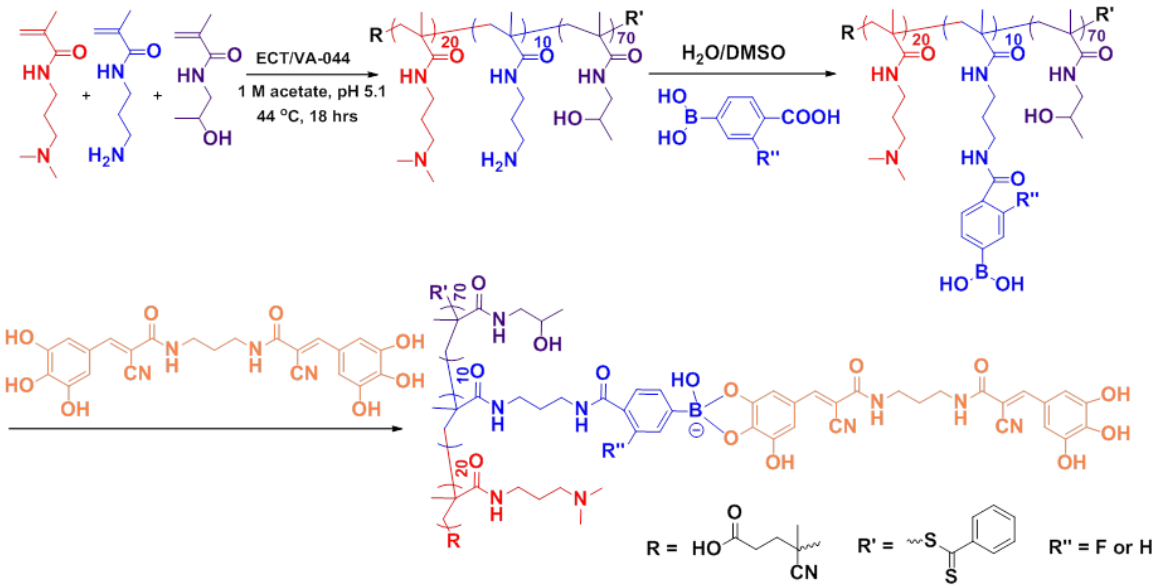

Scheme S3.1 Synthetic route of boronic acid-containing copolymers and Bis-T-23 loading.

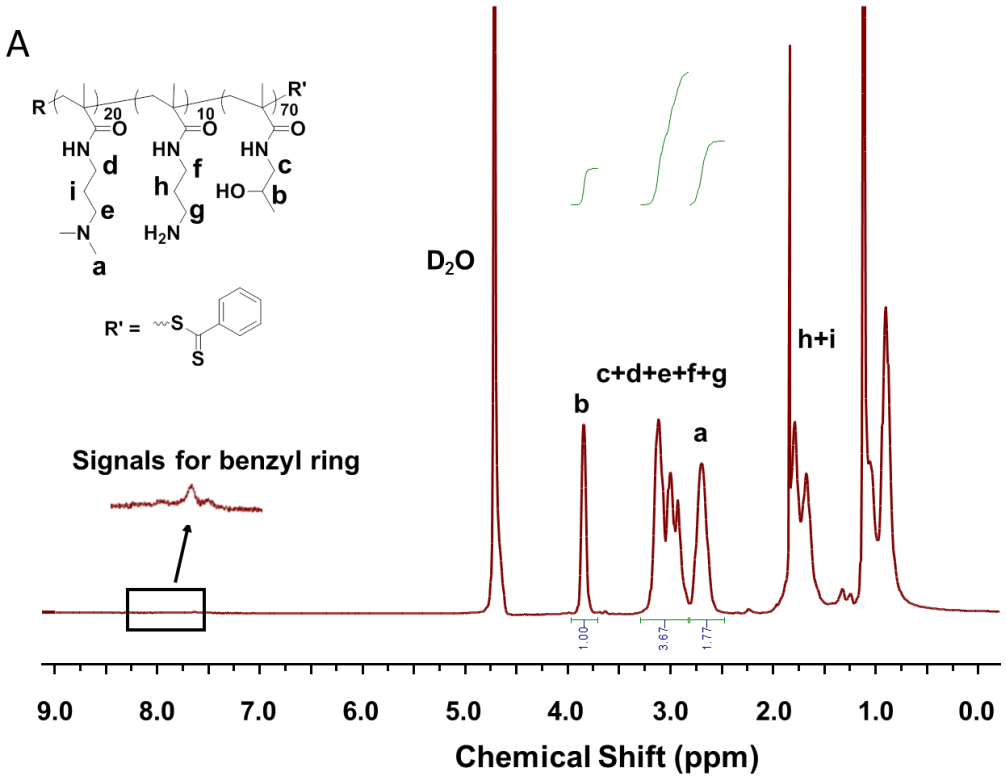
A
R
R'
20
10
70
HN
HO
H_2N
a
b
c
d
e
f
g
h
i
R' =
S
S
Signals for benzyl ring
D_2O
b
c+d+e+f+g
a
h+i
1.00
3.67
1.77
9.0
8.0
7.0
6.0
5.0
4.0
3.0
2.0
1.0
0.0
Chemical Shift (ppm)

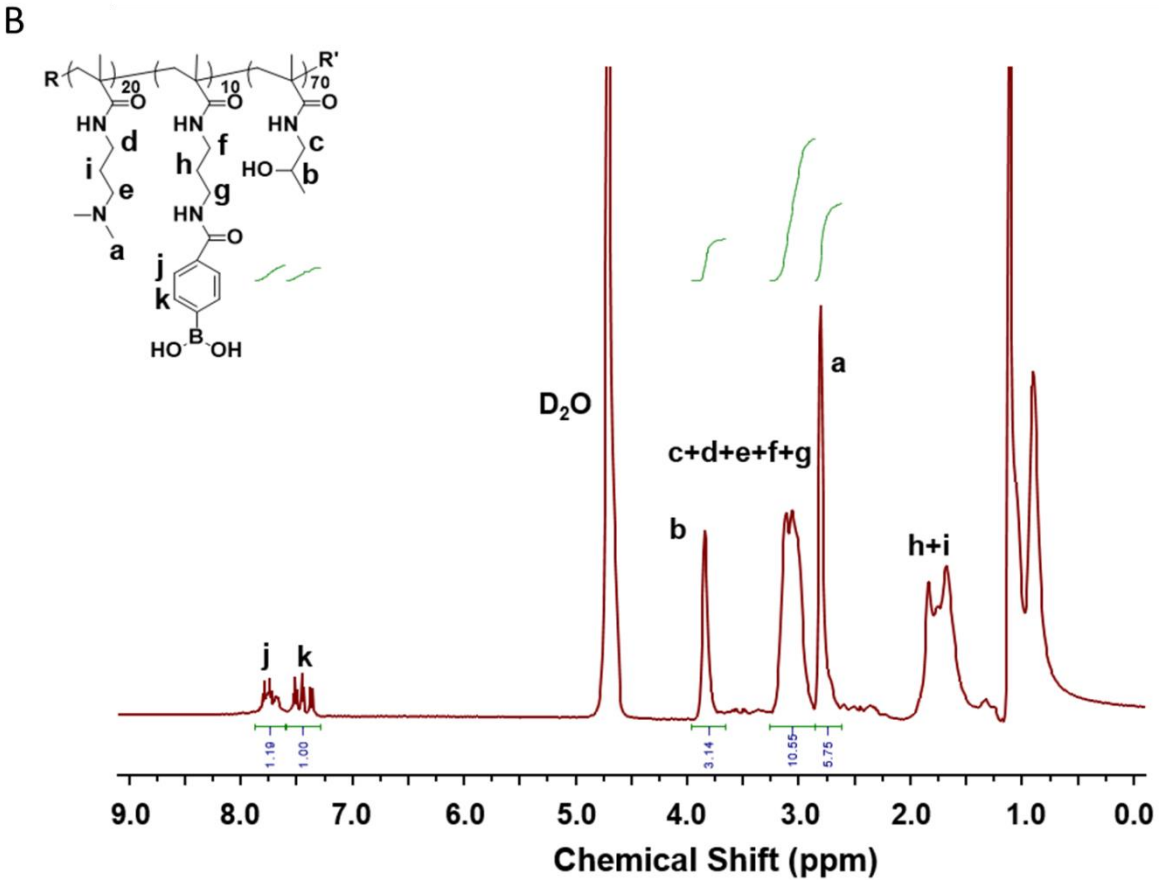
B
R
R'
20
10
70
HN
HO
a
b
c
d
e
f
g
h
i
j
k
HO
B
OH
D_2O
a
c+d+e+f+g
b
h+i
j
k
1.19
1.00
3.14
10.55
5.75
9.0
8.0
7.0
6.0
5.0
4.0
3.0
2.0
1.0
0.0
Chemical Shift (ppm)

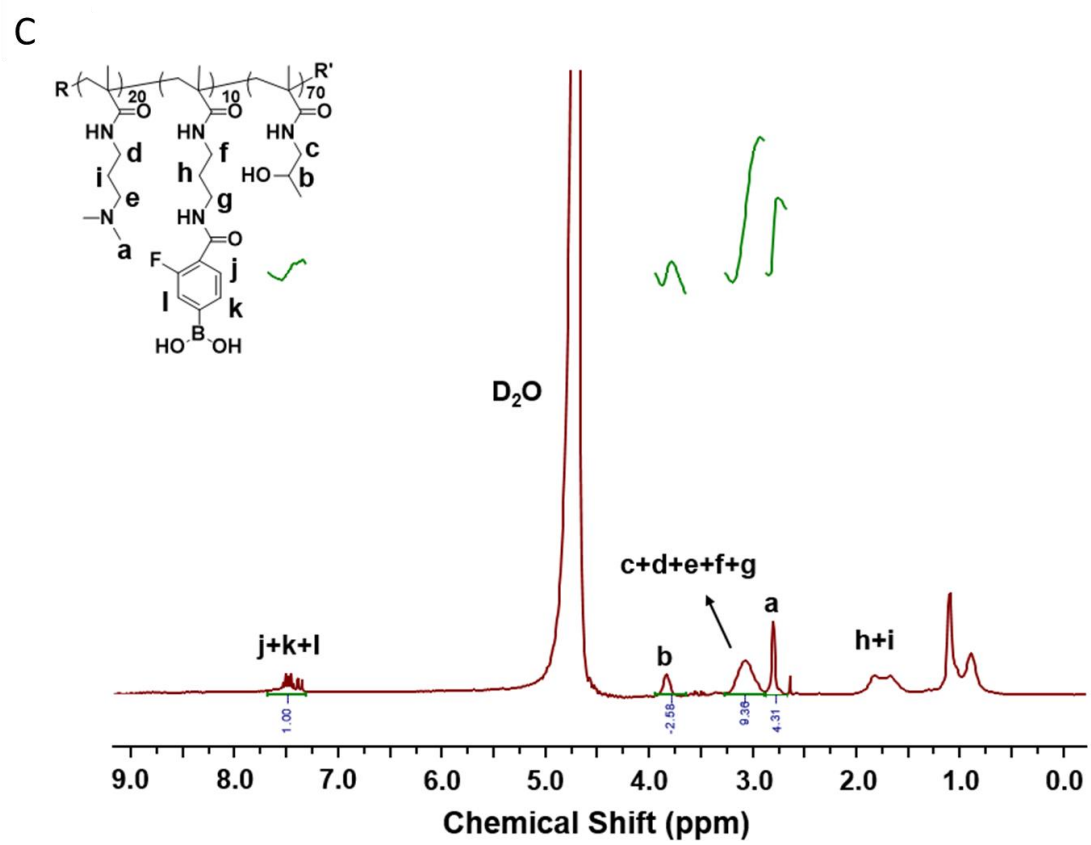

Figure S3.1 ^{1}H NMR spectra of **A.** p(HPMA$_{70}$-DMAPMA$_{20}$-APMA$_{10}$), **B.** p(HPMA$_{70}$-*co*-DMAPMA$_{20}$-*co*-(APMA-*g*-PBA)$_{10}$), and **C.** p(HPMA$_{70}$-DMAPMA$_{20}$-(APMA-*g*-FPBA$_{10}$)).

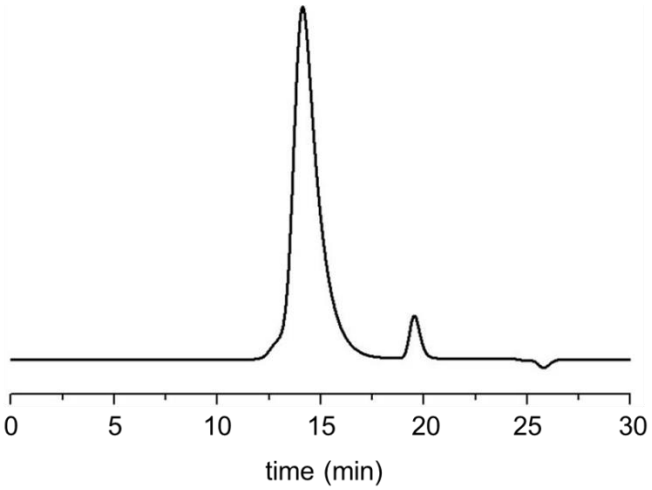

Figure S3.2 GPC trace of p(HPMA$_{70}$-DMAPMA$_{20}$-APMA$_{10}$).

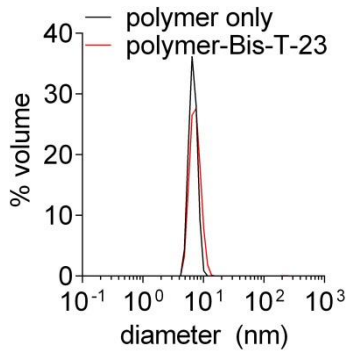

Figure S3.3 Characterization of polymer and polymer-Bis-T-23 conjugates by dynamic light scattering. A representative spectra of three independent reads is shown.

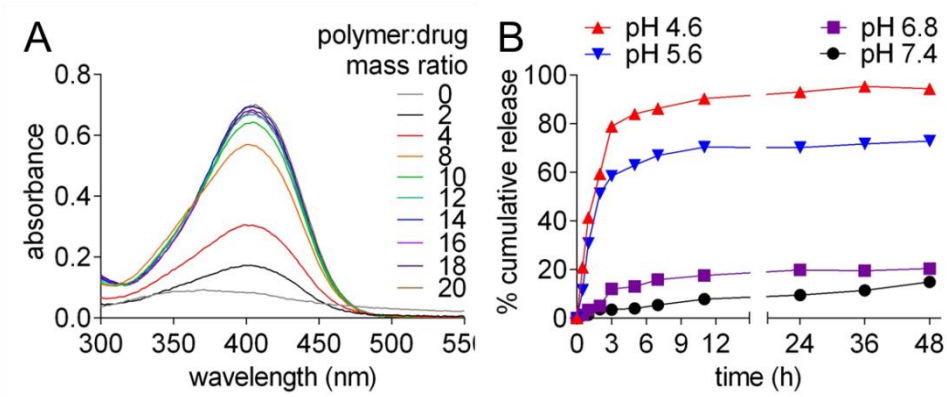

Figure S3.4 Characterization of FPBA copolymer behavior. **A.** Absorbance quantification of polymer-drug conjugates. **B.** Release profile of Bis-T-23 from polymer-drug conjugates at various pH.

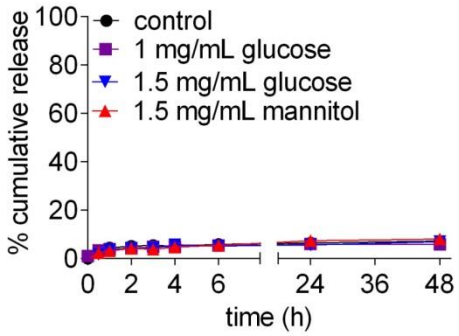

Figure S3.5 Bis-T-23 release from PBA copolymers in the presence of diols.

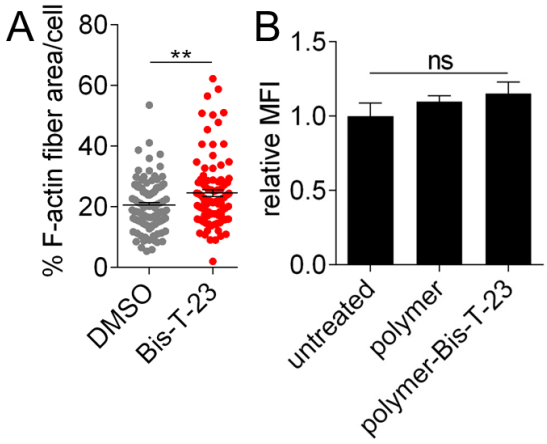

Figure S3.6 **A.** F-actin quantification of Bis-T-23-treated podocytes, expressed as percentage of area per cell. At least $n = 98$ individual cells were analyzed for each treatment. **B.** F-actin intensity quantification of treated podocytes, expressed relative to untreated cells. Bars represent means ± SEM. $^{**}p$-value < 0.01.

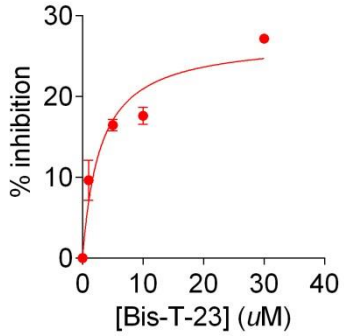

Figure S3.7 Bis-T-23 inhibition of albumin uptake in cultured podocytes.

Calculations

Given that a polymer:drug mass ratio of 14 is required to load all drug, the following calculation was used to determine the percent of boronic acids loaded with Bis-T-23:

Bis-T-23 MW = 480.43 g/mol
p(HPMA$_{70}$-*co*-DMAPMA$_{20}$-*co*-(APMA-*g*-PBA)$_{10}$) MW = 16,300 g/mol
per polymer, there are ~10 PBA groups
polymer:drug mass ratio = 14

$$\frac{1\ \mu g\ drug}{14\ \mu g\ polymer} \times \frac{mol\ drug}{480.43\ g\ drug} \times \frac{16300\ g\ polymer}{mol\ polymer} = 2.42\ \frac{mol\ drug}{mol\ polymer}$$

each mol of polymer contains 10 PBA groups:

$$2.42\ \frac{mol\ drug}{mol\ polymer} \times \frac{1\ mol\ polymer}{10\ mol\ PBA} = 0.242\ \frac{mol\ drug}{mol\ polymer} = 24.2\%$$

Chapter 4

Engineered nanoparticles for targeted drug delivery to glomerular podocytes

Gary W. Liu, Shixian Lyu, Diana G. Eng, Jeffrey W. Pippin,
Stuart J. Shankland, and Suzie H. Pun

Abstract

Loss and dysfunction of glomerular podocytes is a leading cause of kidney failure. While glucocorticoids can be effective in maintaining disease remission, these therapies cause many serious side effects that complicate the initial kidney disease. Recent studies have revealed that glucocorticoids have direct therapeutic effects on podocytes, motivating targeted glucocorticoid delivery to these cells as a clinical strategy to achieve disease remission while mitigating side effects. Towards this goal, we developed block copolymer nanoparticles (NPs) conjugated with antibodies that recognize podocytes for targeted drug delivery, using dexamethasone (DEX) as a model glucocorticoid. The polymers comprised a hydrophilic block for solubility and antibody conjugation and a hydrophobic DEX-containing block, and self-assembled into NPs in aqueous solution. DEX was linked to the NPs via a pH-sensitive hydrazone bond such that DEX remains bound to NPs in prodrug form during circulation but is released in its active form after internalization into acidic vesicles in podocytes. Targeted NPs exhibited greater uptake into cultured podocytes compared to control NPs, but did not rescue podocytes during an *in vitro* injury model. In a preliminary *in vivo* study, targeted NPs exhibited greater binding to glomerular podocytes compared to control NPs.

[1]Manuscript in preparation.

4.1 Introduction

Chronic kidney disease (CKD) is a public health problem and afflicts nearly 15% of Americans,[1] often progressing to kidney failure due to a lack of effective interventions. The leading glomerular cause of CKD is focal segmental glomerulosclerosis (FSGS), characterized by progressive scarring of kidney glomeruli, the site of renal filtration.[2,3] Glucocorticoid steroids have been the frontline FSGS therapy for the past five decades;[4] however, long-term glucocorticoid therapy results in serious side effects such as diabetes, cardiovascular disease, and osteoporosis that complicate the disease,[5] and 60-70% of patients are glucocorticoid-dependent and frequently relapse after steroid cessation.[6,7] These patients will require many cycles of high-dose steroids to achieve remission, and face chronic complications relapse after relapse. New treatment strategies with improved safety profiles are urgently needed to induce and maintain disease remission in these patients.

As glucocorticoids are classically known to induce T-cell apoptosis,[8] its efficacy in glomerular disease has been attributed to systemic immunosuppression. New findings challenge this notion and suggest that glomerular podocytes are a therapeutic target of glucocorticoids. Podocytes are highly specialized and differentiated epithelial cells that form an essential component of the tripartite glomerular filtration barrier. These cells are highly dendritic, with multiple foot processes that interdigitate to form the filtration slit diaphragm.[9] Glucocorticoids are now known to have various direct effects on podocytes: *in vitro*, glucocorticoids increase nephrin (slit diaphragm protein) expression,[10,11] modulate cell motility,[12,13] and maintain cellular viability and actin filament stability during cell injury models;[14-16] *in vivo*, glucocorticoids mitigate podocyte

apoptosis, maintain podocyte foot process structure, and reduce proteinuria, a clinical signature of glomerular filtration barrier dysfunction, in animal models of podocyte injury and loss.[17,18] Notably, podocyte-specific knockout of glucocorticoid receptor or the transcription factor KLF15 in mice aggravates kidney disease after glomerular injury and abrogates glucocorticoid-induced reduction of proteinuria, respectively,[18,19] emphasizing the importance of direct glucocorticoid effects in glomerular podocytes during disease. These data collectively support that the therapeutic efficacy of glucocorticoids in glomerular disease may be independent of systemic immunosuppression.[20] Moreover, given the direct correlation between reduced podocyte number during disease and CKD progression,[21,22] focused glucocorticoid delivery to podocytes could be clinically strategic in achieving remission while mitigating side effects.

Nanoparticle (NP) drug carriers can substantially alter the pharmacokinetics of drug cargo through tuning of NP physicochemical properties such as size, surface charge, chemical composition, and functionalization with targeting ligands (e.g., antibodies, peptides, aptamers) that facilitate molecular recognition and NP accumulation in target cells.[23,24] For example, administration of the clinically approved pegylated liposomal doxorubicin formulation, Doxil, results in an 87-fold higher tumor drug concentration and 6-fold higher circulation half-life than free doxorubicin in preclinical models,[25] which may be contributing factors to the reduced cardiotoxicity and alopecia observed in humans.[26] Multiple lines of evidence support glucocorticoid delivery to podocytes as a clinically viable approach. Podocytes are actively endocytotic and increase macropinocytosis in disease,[27-30] which provide several avenues of NP internalization into these cells. Previous work has shown that targeted delivery of a CaMK4 inhibitor using NPs to podocytes reduces proteinuria in animal models of nephrosis.[31]

In this work, we developed block copolymer NPs for targeted delivery of dexamethasone (DEX), a model glucocorticoid well-studied in *in vitro* and animal models of podocyte injury,[14,18] to glomerular podocytes. Nanoparticles were targeted to glomerular podocytes by conjugation with polyclonal podocyte-binding antibodies (podocyte IgG) that we have previously generated.[32] We characterized these antibodies *in vitro* and *in vivo* to inform NP design, and show that podocyte IgG is internalized by cultured podocytes into acidic compartments and recognize glomerular podocytes *in vivo*. In normal mice, targeted NPs exhibited increased binding to glomerular podocytes compared to untargeted NPs.

4.2 Materials and methods

4.2.1 Antibody purification and labeling

Polyclonal podocyte-binding antibodies were generated as previously reported,[32] by immunizing sheep with cultured mouse podocytes. Control antibodies were isolated from sheep prior to immunization. After, IgG antibodies were purified via protein G chromatography (ThermoFisher Scientific) and concentrated using an Amicon centrifugal spin filter (MWCO 50 kDa, Millipore).

For fluorescein labeling, control and podocyte IgG antibodies (1 mL, 1 mg/mL in 50 mM borate buffer pH 8.51) were reacted with NHS-fluorescein (4.7 μL, 10 mg/mL in DMSO) for 1 h at room temperature. After, antibodies were desalted by Zeba desalting columns (ThermoFisher Scientific). For sulfo-cyanine7 labeling, antibodies (0.7 mL, 4.96 mg/mL in 100 mM sodium

bicarbonate buffer pH 8.56) were reacted with sulfo-cyanine7-NHS ester (14.49 uL, 10 mg/mL in water) for 4 h at room temperature, and purified as described above.

4.2.2 Cell culture

Immortalized murine podocytes were cultured as previously described.[33] Briefly, cells were maintained in growth-permissive conditions (33 °C, mIFN-γ, bovine collagen I-coated plates) and then passaged into growth-restrictive conditions (37 °C) to promote differentiation. After 3 d, cells were then passaged into 24-well plates (2.5-5.0×10^4 cells/well) and maintained in growth-restrictive conditions for a total of 11 d before experiments. For microscopy studies, podocytes were cultured as described above on bovine collagen I-coated glass coverslips.

4.2.3 Antibody characterization *in vitro*

For antibody binding characterization, podocytes were incubated with control or podocyte IgG diluted in complete media at 0-250 nM for 1 h at 37 °C. After, cells were washed with PBS, lifted with trypsin, resuspended in 1% BSA/PBS, and then analyzed for fluorescein fluorescence using an Attune NxT flow cytometer (Thermo Fisher Scientific).

To assess antibody toxicity, podocytes were incubated with control or podocyte IgG diluted in complete media at 100-500 nM for 48 h at 37 °C. After, cells were washed with PBS, and viability assessed by MTS/PMS assay (Promega).

To examine intracellular antibody trafficking, podocytes were incubated with control or podocyte IgG diluted in complete media at 100 nM for 29 h, stained with LysoTracker Deep Red (Thermo Fisher Scientific) according to manufacturer instructions, washed, and fixed with 4% PFA/PBS. Images were collected with a Leica SP8X confocal microscope.

4.2.4 Antibody biodistribution

Fluorescently labeled (sulfo-Cy7) antibodies (1 nmol) dissolved in PBS were injected in 8-week old male BALB/c mice (Jackson Laboratory) via retro-orbital route. After 48 h, animals were sacrificed, perfused with PBS, and major organs (heart, lungs, liver, spleen, and kidneys) were harvested. Organ fluorescence was quantified by a Xenogen IVIS using ex/em = 710/780 nm. Regions of interest were drawn across each organ for quantification, and total radiant efficiencies were normalized by organ weight. Statistical analyses were performed using GraphPad Prism.

Kidney tissues were fixed in 4% PFA, washed with PBS, and incubated overnight with 30% sucrose/PBS at 4 °C. Tissues were then embedded in OCT and snap frozen in an ethanol/dry ice bath. After cryosectioning, tissues were permeabilized with 0.1% Triton X-100/PBS for 10 min and blocked with 1% BSA/PBS for 1 h. Tissues were then stained for control or podocyte IgG using RRX-donkey anti-sheep IgG (Jackson ImmunoResearch Laboratories, 1:100). Images were collected using a fluorescent microscope (Nikon).

4.2.5 Polymer synthesis

N-(2-hydroxypropyl)methacrylamide (HPMA), methacryloyl chloride, glycyl glycine, hydrazine, *N*-(3-dimethylaminopropyl)-*N′*-ethylcarbodiimide hydrochloride (EDC), 4-((((2-carboxyethyl)thio)carbonothioyl)thio)-4-cyanopentanoic acid (CCC), azobisisobutyronitrile (AIBN), dexamethasone (DEX), and *N*-hydroxysuccinimide (NHS) were purchased from Sigma-Aldrich. The monomers methacryloylglycylglycine (MAGG) and *N*-methacryloylglycylglycyl hydrazone DEX (MAGG-H-DEX) were synthesized as previously described,[34,35] but with less acetic acid (1-2 drops) when conjugating DEX to *N*-methacryloylglycylglycyl hydrazine.

Block copolymers were synthesized by reversible addition-fragmentation chain-transfer polymerization using CCC as the chain-transfer agent. The first block, p(HPMA-*co*-MAGG), was synthesized using the following reaction conditions: HPMA (3.0 g, 21.0 mmol) and MAGG (420 mg, 2.1 mmol) were dissolved in 0.1 M acetate buffer (pH 5.0) with CCC (99.3 mg, 0.32 mmol) and VA-044 (8.74 mg, 0.032 mmol). The reaction was then purged with argon for 30 min and carried out at 44 °C for 48 h. After, polymers were dialyzed, lyophilized, and then characterized for size and dispersity by gel permeation chromatography (GPC). Polymers were fluorescently labeled by conjugation of a small number of carboxylic acids to Cy5-amine via EDC/NHS chemistry.

A second block of p(MAGG-H-DEX) was extended off of the first block using the following reaction conditions: p(HPMA-*co*-MAGG) (200 mg, 0.02 mmol) and MAGG-H-DEX (176 mg, 0.30 mmol) were dissolved in dimethylacetamide and AIBN (0.6 mg, 0.004 mmol). The reaction

was purged for 30 min and carried out at 70 °C for 48 h. The polymers were purified first by dialysis against methanol for 24 h and then dH_2O for 3 d before lyophilization. Purified polymers were characterized by GPC, for composition by ^1H NMR, and for nanoparticle (NP) formation by dynamic light scattering.

For antibody conjugation, polymer (100 μg) was dissolved to 1 mg/mL in PBS pH 6.5 to form NPs, and then activated with EDC (10.64 μmol) and NHS (2.66 μmol) for 30 min at room temperature. Non-specific (control) or podocyte IgG was then added at various masses and allowed to react for 3.5 h, resulting in control or podocyte NPs, respectively. After, antibody-conjugated NPs were washed extensively with PBS pH 7.4 using Amicon centrifugal spin filters (MWCO 30 kDa, Millipore) and resuspended in PBS to a final volume of 500 μL.

4.2.6 *In vitro* efficacy model

DEX delivery efficacy was evaluated *in vitro* using a model of puromycin aminonucleoside (PAN)-induced podocyte injury as previously described.[14,15] Briefly, podocytes were incubated with free DEX and DEX-containing control or podocyte NPs (at an equivalent DEX concentration of 3 μM) for various times, and then PAN was directly added to a final concentration of 5 μg/mL. Cells were then incubated for 72 h, and viability was assessed by MTS/PMS assay.

4.2.7 Nanoparticle biodistribution and efficacy *in vivo*

For preliminary biodistribution analysis of nanoparticles, fluorescently labeled DEX-NPs (30 μg in PBS), functionalized with either control or podocyte IgG, were injected into mice retro-orbitally. After 4 d, tissues were harvested and organ fluorescence was quantified as described above. Kidney tissues were processed and stained as above. Images were collected using a confocal microscope (Leica). For glomerular fluorescence quantification, 10 glomeruli were randomly selected and analyzed by ImageJ. Fluorescence intensity was normalized by glomerular surface area to generate mean fluorescence/glomerular cross section.

4.3 Results and discussion

4.3.1 Antibody characterization *in vitro*

A major challenge in designing targeted drug delivery systems for glomerular podocytes has been the lack of targeting ligands (antibodies, peptides, aptamers) that facilitate molecular recognition and internalization of drug carriers by these cells. To address this limitation, we have previously developed targeting antibodies by immunizing sheep with immortalized podocytes, generating polyclonal IgG that bind to glomerular podocytes (podocyte IgG).[32,33] Antibodies harvested from sheep prior to immunization were used as non-specific controls (control IgG). These antibodies were first examined for binding kinetics, cytotoxicity, subcellular localization, and biodistribution to inform the design of the nanoparticle (NP) drug carrier. Antibodies were

fluorescently labeled and exhibited equivalent labeling efficiencies (data not shown), enabling direct comparisons of fluorescence in subsequent experiments. In preliminary experiments (n = 1), podocyte IgG bound to cultured podocytes greater than control IgG (**Figure 4.1A**), and antibody concentrations up to 500 nM did not cause significant toxicity (**Figure 4.1B**).

Antibody sub-cellular localization in podocytes was then studied to inform nanoparticle design, as specific DEX linker strategies would need to be employed depending on if the antibodies are membrane-bound or internalized. Podocyte IgG exhibited punctate staining and colocalized extensively with lysosomes in podocytes, indicating that the antibody is internalized and trafficked through the endolysosomal pathway (**Figure 4.1C**). Control IgG exhibited minimal internalization under the same conditions (data not shown).

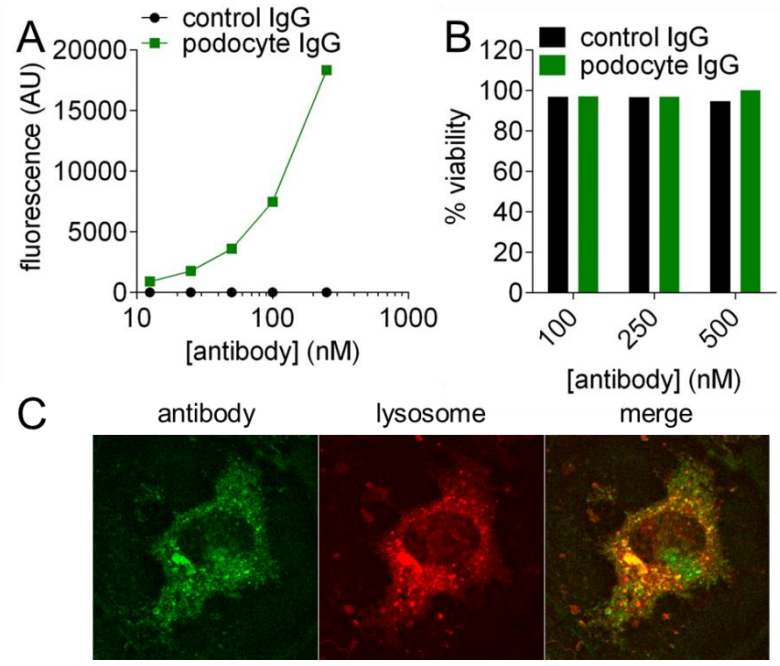

Figure 4.1 Binding and cytotoxicity of antibodies to podocytes. **A.** Binding of control or podocyte IgG to podocytes after 1 h incubation at 37 °C. **B.** Viability of podocytes incubated with various concentrations of control or podocyte IgG after 48 h, normalized to untreated cells. **C.** Subcellular trafficking of podocyte IgG in cultured podocytes. Images were acquired after 29 h incubation with 100 nM IgG by confocal microscopy. Green, podocyte IgG; red, lysosomes; yellow, merge.

4.3.2 Antibody binding to glomerular podocytes

The biodistribution and kidney tissue distribution of fluorescently labeled antibodies were examined for binding to podocytes *in vivo*. At 48 h after intravenous injection, podocyte IgG exhibited significantly greater kidney fluorescence than control IgG (*p*-value = 0.0124, **Figures 4.2A** and **4.2B**) by whole-organ imaging. In kidney tissue, podocyte IgG exhibited glomeruli-specific staining while control IgG did not (**Figure 4.2C**). These observations confirm that podocyte IgG bind to glomerular podocytes, and are a potential ligand for targeted drug delivery.

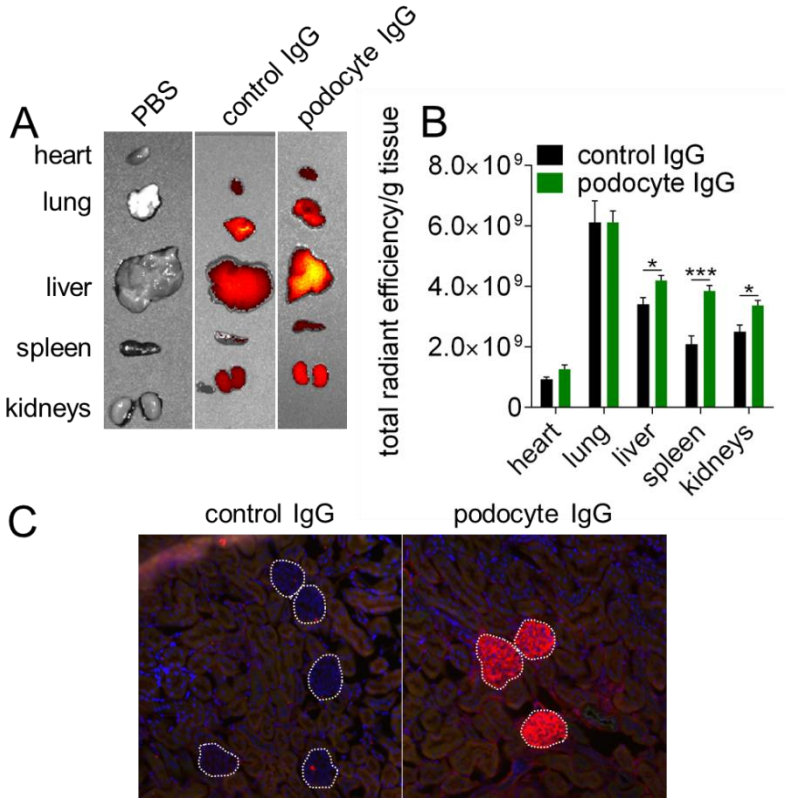

Figure 4.2 Antibody binding *in vivo*. **A.** Representative fluorescence images of major organs 48 h after intravenous administration of PBS (n = 4) or fluorescent control or podocyte IgG (n = 5 each). **B.** Region of interest quantification of tissue fluorescence normalized by tissue weight. Bars represent means ± SEM. **p*-value < 0.05; ****p*-value < 0.001. **C.** Representative fluorescent images of kidneys 48 h after intravenous injection of fluorescent control or podocyte IgG. Kidney glomeruli are denoted by dashed white lines. Blue, DAPI; red, antibody staining.

4.3.3 Polymer synthesis and nanoparticle formulation

Polymeric block copolymer NPs were synthesized by reversible addition-fragmentation chain transfer, utilizing a hydrophilic block and a hydrophobic DEX-containing block to drive NP self-assembly into micelles and mask loaded DEX during circulation. The hydrophilic block, poly(*N*-(2-hydroxypropyl)methacrylamide-*co*-*N*-methacryloylglycylglycine) (p(HPMA-*co*-MAGG)), comprises HPMA, a hydrophilic monomer that imparts biocompatibility and stability,[36] and MAGG, another hydrophilic monomer that contains carboxylic acids for antibody conjugation via EDC/NHS chemistry. As podocyte IgG is rapidly internalized into the endolysosomal pathway, we engineered a DEX release mechanism that exploits the shift in pH from circulation (pH 7.4) to intracellular endosomes and lysosomes after internalization (pH spanning 6.5-4.5).[37,38] DEX contains ketones, which can be reacted with hydrazines to form pH-sensitive and covalent hydrazone bonds that exhibit high stability at pH 7.4 but release drug in physiologically relevant acidic pH ranges.[35,39-41] To control drug loading and NP self-assembly, the hydrazone-DEX-containing monomer, *N*-methacryloylglycylglycyl hydrazone DEX (MAGG-H-DEX), was synthesized as previously reported[35] and polymerized as the second block (**Figure 4.3**).

The final block copolymer composition was determined to be p($HPMA_{60}$-*co*-$MAGG_6$)-*b*-p(MAGG-H-DEX_{10}) by ^{1}H NMR. By gel permeation chromatography (GPC), polymers exhibited a number average molecular weight (M_n) of 14.2 kDa and low dispersity ($Đ$ = 1.114), indicating good control over polymerization. DEX loading content was determined to be 26-28% w/w by GPC and spectroscopy. Given their amphiphilic nature, these block copolymers are expected to self-assemble into nanoparticle structures. To test this, polymers were dissolved in

aqueous buffer at 1 mg/mL and analyzed by dynamic light scattering, which revealed nanoparticles of size ~22 nm, *PDI* = 0.019, and a ζ-potential of −20 mV, confirming the self-assembly and presence of carboxylic acids of NPs (data not shown).

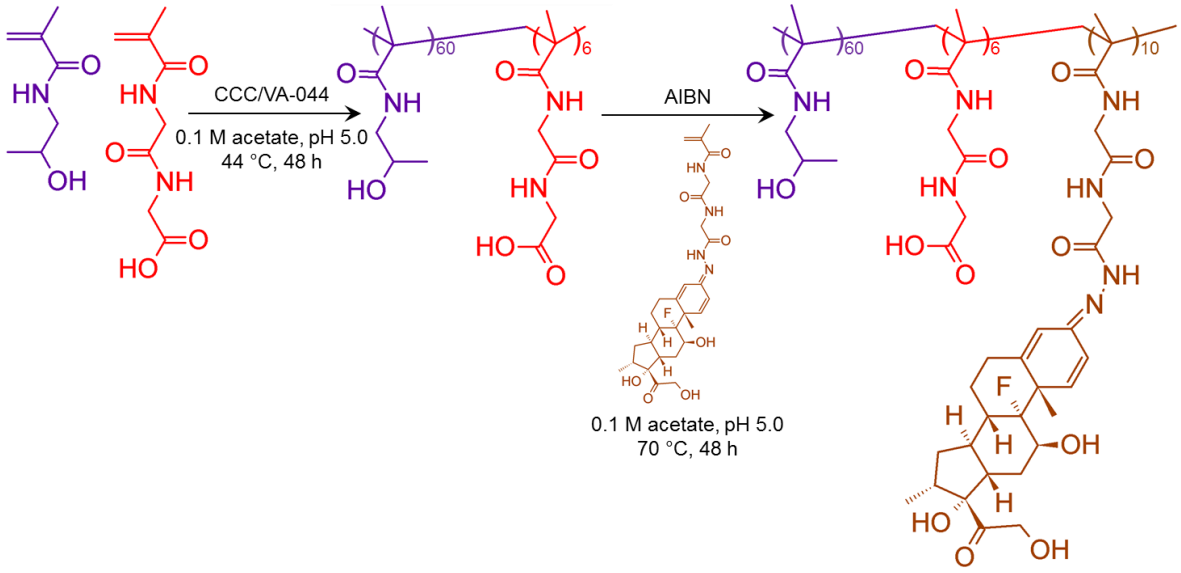

Figure 4.3 Synthetic route of block copolymer nanoparticles.

NPs were then conjugated with control or podocyte IgG by reaction of NP carboxylic acids to antibody primary amines by EDC/NHS chemistry. A panel of NPs with different antibody conjugation densities was formulated, as antibody density may affect podocyte behavior and migration. Indeed, multivalent display of binding ligands can be cytotoxic compared to monovalent ligands due to receptor crosslinking.[42,43] In these preliminary reactions, NP mass was fixed at 100 μg, and either control IgG (forming control NP) or podocyte IgG (forming podocyte NP) was added at an NP:Ab mass ratio of 2.5, 5, 10, or 25 (antibody mass ranging 40-4 μg).

4.3.4 *In vitro* DEX-NP efficacy

To test antibody-mediated binding and internalization of NPs, cultured podocytes were incubated with fluorescently labeled control or podocyte NPs at NP:Ab mass ratios of 2.5, 5, or 10 for 48 h at a DEX-equivalent dose of 3 μM, and then analyzed for uptake by flow cytometry. At each of the tested NP:Ab conjugation ratios, podocyte NPs exhibited 1.40-1.63-fold greater uptake than the respective control NPs. Overall NP uptake decreased with decreasing NP antibody density (**Figure 4.4A**).

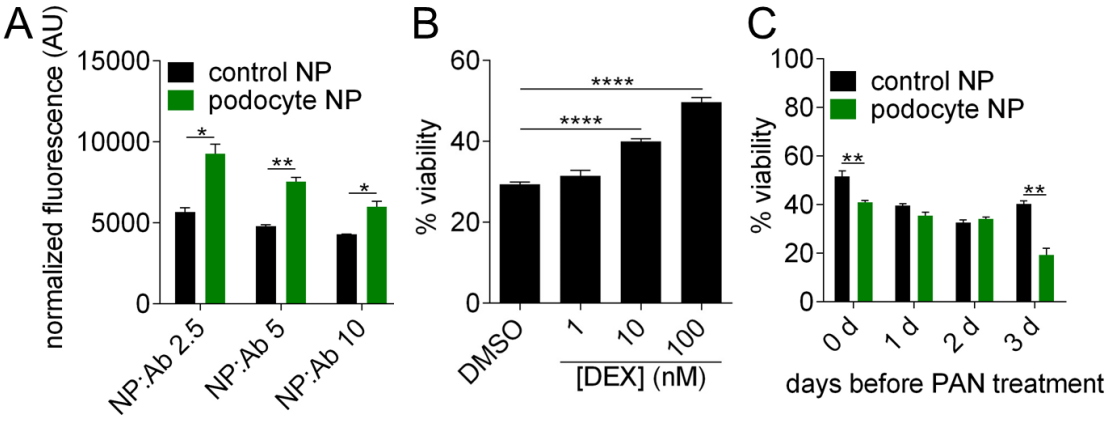

Figure 4.4 Nanoparticle characterization *in vitro*. **A.** Flow cytometry analysis of control and podocyte NP uptake by cultured podocytes after 48 h incubation. **B.** Viability of cultured podocytes treated with DEX (1-100 nM) and then challenged with puromycin aminonucleoside (PAN, 5 μg/mL, 72 h). **C.** Viability of cultured podocytes pre-treated with control or podocyte NPs at an NP:Ab mass ratio 2.5 for various days before PAN treatment. Bars represent means ± SEM. **p*-value < 0.05; ***p*-value < 0.01; *****p*-value < 0.0001.

NP efficacy *in vitro* was then evaluated in the puromycin aminonucleoside (PAN)-induced injury model, which causes oxidant-mediated DNA damage and apoptosis in cultured and glomerular podocytes.[14,44] In this model, treatment with DEX prevents apoptosis by upregulating pro-survival pathways,[14] and mitigates podocyte death at concentrations as low as 100 nM (**Figure**

4.4B). As the availability and drug release by NPs is lower and slower than that of free drug treatment *in vitro*, cultured podocytes were pre-treated with NPs (at the highest antibody density, NP:Ab = 2.5) at a DEX-equivalent concentration of 3 μM for various days (1-3 d) prior to PAN addition. Podocyte NPs did not significantly rescue viability compared to control NPs, and in most conditions reduced viability, suggesting that higher podocyte IgG densities or longer incubation times causes cytotoxicity (**Figure 4.4C**). These observations indicate that at least *in vitro*, both NP incubation time and antibody density are important experimental parameters and need to be optimized to evaluate DEX release and efficacy. Studies are currently ongoing to evaluate the *in vitro* efficacy of control and podocyte NPs conjugated at NP:Ab mass ratios 5, 10, and 25 with various incubation times.

4.3.5 Biodistribution of DEX-NP in normal mice

After confirming antibody-mediated NP binding *in vitro*, fluorescently labeled DEX-NPs (NP:Ab 5) were evaluated for biodistribution and binding to glomerular podocytes in normal mice. In a preliminary study (n = 1 animal each), mice were injected with PBS, control NPs, or podocyte NPs, and analyzed 4 days after injection. This time point is beyond the circulation half-life of similarly sized NPs (4-32 h),[45] and enables differentiation between tissue accumulation due to binding and internalization or transient accumulation due to clearance. At the organ scale, no major differences were observed in NP fluorescence between control and podocyte NPs (**Figure 4.5A**). This observation may be due to the fact that podocytes compose a small minority of total kidney cells, resulting in poor signal. Indeed, a recent single-cell profiling study of the kidneys observed that <1% of analyzed cells were podocytes, with the vast majority (~79%) of

cells being proximal or distal convoluted tubule cells.[46] While the podocyte antibody exhibited greater fluorescence within the kidneys compared to control antibody, NPs exhibit different pharmacokinetics that may alter biodistribution at the organ scale. NPs were instead evaluated for binding to glomerular podocytes through microscopic analysis of kidney sections. For each treatment, 10 glomeruli were randomly imaged and analyzed for mean fluorescence (fluorescence intensity normalized by glomerular area). Glomeruli of the podocyte NP-treated mouse exhibited greater fluorescence than those of the control NP-treated mouse, indicating greater NP binding and internalization (**Figure 4.5B** and **4.5C**, *p*-value = 0.0273). Baseline fluorescence of both control and podocyte NPs before injection were comparable (**Table S4.1**). Moreover, punctate NP fluorescence was observed, suggesting cellular internalization. While these studies are preliminary, this data along with the *in vitro* binding studies (**Figure 4.4A**) provide evidence that the podocyte NPs bind to and are internalized by glomerular podocytes.

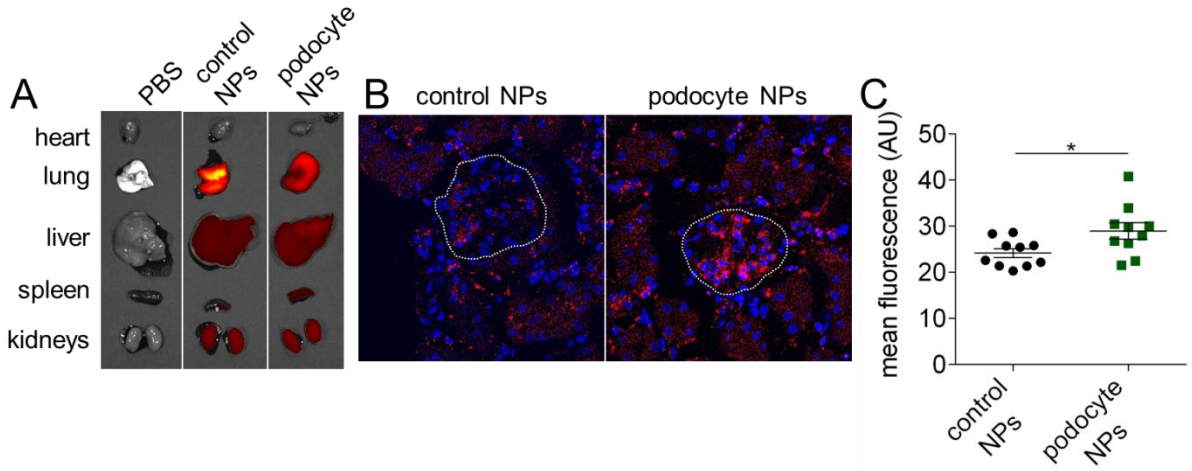

Figure 4.5 Organ and kidney distribution of NPs in normal mice. **A.** Fluorescent images of major organs 4 days after intravenous administration of PBS or fluorescent NPs. **B.** Representative fluorescent images of kidneys 4 days after intravenous administration of control NPs (left) or podocyte NPs (right). Kidney glomeruli are denoted by dashed white lines. Blue, DAPI; red, Cy5-labeled NPs. **C.** Cy5 fluorescence intensity of individual glomeruli normalized by glomerular surface area. Bars represent means ± SEM. **p*-value < 0.05.

The clinical efficacy of many classical immunosuppressants such as glucocorticoids, cyclosporine A, and rituximab in treating glomerular disease all seem to point to the immune system as the cause, and therefore the therapeutic target, of these diseases.[6,47,48] Recent studies have revealed that many of these drugs have direct effects on podocytes themselves by modulating the actin cytoskeleton and upregulating survival pathways, raising hypotheses that the clinical efficacy of these drugs is due to podocyte-centric effects, and that targeting therapeutics to these cells can be efficacious while mitigating side effects.[49-51] However, a lack of methods to deliver drugs to glomerular podocytes has made answering these questions technically challenging.

In this work, we engineered nanoparticle (NPs) carriers for targeted DEX delivery to glomerular podocytes. This is significant because glucocorticoids such as DEX are the frontline therapy in glomerular disease treatment, but cause severe complications.[5,17] Targeted DEX delivery to glomerular podocytes using NP drug carriers could be efficacious while avoiding systemic toxicity. To formulate NPs, the block copolymer p(HPMA-*co*-MAGG)-*b*-p(MAGG-H-DEX) was synthesized by reversible addition-fragmentation chain-transfer polymerization, and polymers were conjugated with podocyte-targeting antibodies that we have previously reported[32] after self-assembly into NP micelles. The pH-sensitive hydrazone bond was selected as the DEX linker, as it is well-established in the literature and exhibits a sharp difference in drug release behavior between neutral and acidic pH.[52] This linker enables spatiotemporal control of drug release: DEX would remain detained on NPs during circulation, and is released after antibody-mediated podocyte uptake into acidic endosomes and lysosomes.

Polyclonal podocyte IgG, generated by immunizing sheep with cultured mouse podocytes, was utilized to facilitate molecular recognition and internalization of nanoparticles by podocytes. While podocyte IgG did bind to glomerular podocytes, non-specific antibody accumulation in the lungs, liver, and spleen was also observed. The antigen(s) of podocyte IgG remain to be identified, and protein antigens highly expressed by podocytes are very likely expressed by other cell types. Indeed, the podocyte markers podoplanin is expressed on lymphatic endothelium and type I alveolar cells;[53] nephrin is expressed in heart, spleen, pancreas, and brain tissue;[54] and Neph1 is expressed in kidney, brain, heart, lung, liver, and pancreas tissue.[55] The wide expression of classically "podocyte-specific" proteins may contribute to greater accumulation of podocyte IgG in the liver and spleen compared to control IgG. Moreover, Hauser *et al.* have previously shown that no significant podocyte IgG accumulation was noted in the lungs and liver,[32] while significant lung and liver accumulation was observed in this study. This may be due to differences in antibody detection methods: here, whole-organ imaging was used to detect fluorophore-labeled antibodies, whereas Hauser *et al.* utilized tissue imaging to detect fluorescent secondary antibodies against podocyte IgG. The fluorophore structure and degree of labeling can substantially alter antibody pharmacokinetics compared to native antibody,[56] and may also contribute to non-specific antibody accumulation in other organs.

Podocyte NPs were observed to bind to cultured podocytes more than control NPs at various antibody densities, indicating successful conjugation of targeting antibodies to the NPs. However, podocyte NPs did not exhibit significant rescue of podocyte viability in an *in vitro* PAN challenge assay, which may be due to several factors. First, previous reports have observed slow *in vitro* DEX release kinetics (~5% drug release over 5 d) even in acidic pH

conditions.[35,39,40] We attempted to overcome this limitation by treating podocytes with NPs at a DEX-equivalent concentration 30-fold greater than therapeutic concentrations (3 μM v. 100 nM) and for up to 3 days before PAN challenge. DEX contains two potential hydrazone-forming ketones, and slow DEX release kinetics may be due to the favorable reaction of the highly stable hydrazone bond formed with the aromatic ketone.[40,57] Second, multivalent display of podocyte IgG on NPs may be cytotoxic to podocytes: at most time points, podocytes treated with podocytes NPs (at the highest antibody conjugation density) exhibited lower viability than those treated with control. We recognize that given the nature of the PAN challenge assay, cultured podocytes are continuously treated with NPs at concentrations and durations significantly greater than what would occur *in vivo*. Ongoing work seeks to identify an optimal point between NP treatment time, antibody density, and DEX dose. Alternatively, linker chemistries with faster release profiles, such as a dual hydrazone-ester linker,[40] may be pursued.

In a preliminary *in vivo* study, podocyte NPs bound to glomerular podocytes greater than control NPs. Interestingly, even control NPs were uptaken by podocytes. This may be due to the fact that podocytes express FcRn, a receptor that recognizes and transports IgG,[58] causing high baseline internalization of antibody-functionalized NPs and entrapping NPs intracellularly. While the overall objective is to test these NPs in an animal model of podocyte injury, these preliminary results provide strong feasibility data for targeted NP delivery to podocytes. Future work will quantify targeted NP binding to glomeruli in a larger cohort of animals.

Other reports have provided some important insight into NP design for targeting the kidneys and more specifically, glomerular podocytes. Bruni *et al.* studied a panel of polymeric NPs that

encapsulated DEX for passive targeting to the kidneys, and observed that NPs of size 5-28 nm were excreted as soon as 24 h after injection.[59] While NPs mitigated podocyte apoptosis *in vitro*, they did not accumulate in the kidneys and bind to glomerular podocytes, likely due to the lack of targeting ligands. Work by Maeda *et al.* developed CaMK4 inhibitor-loaded nanolipogels of size ~200 nm and functionalized with antibodies that recognize podocin, a podocyte protein. The nanolipogels exhibited preferential podocyte binding *in vivo* and reduced proteinuria in several animal models of podocyte injury, and importantly did not elicit an immune response.[31] Collectively these reports indicate that a wide range of NP sizes (5-200 nm) might be useful for targeting the kidneys by passive targeting, and that targeting ligands are critical to promote cell-specific NP accumulation.

4.4 Conclusions

Here, we engineered DEX-containing NPs for targeted drug delivery to glomerular podocytes, towards the overall goal of maintaining DEX therapy for steroid-dependent patients and mitigating side effects. While NPs did not exhibit efficacy *in vitro*, they did preferentially bind to cultured and glomerular podocytes. Refinements in drug linker chemistry are likely needed for therapeutically relevant levels of DEX release. Development of such targeted drug carriers are needed to answer important clinical and scientific questions: whether the therapeutic effects of glucocorticoids are due to systemic immunosuppression or podocyte-centric effects, and how podocytes interact with nanoscale materials during health and in disease.

4.5 Acknowledgments

This work was supported by the Office of the Assistant Secretary of Defense for Health Affairs through the Peer Reviewed Medical Research Program under Award Numbers PR151175 and PR151965, and by the National Science Foundation Graduate Research Fellowship Program under Grant No. DGE-1256082 to GWL. Opinions, interpretations, conclusions, and recommendations are those of the authors and are not necessarily endorsed by the Department of Defense or the National Science Foundation. We would also like to thank Robert Lamm for insightful discussion about antibody labeling, and acknowledge support from the NIH (S10 OD016240) to the W. M. Keck Center for Advanced Studies in Neural Signaling and the assistance of Keck Center manager Dr. Nathaniel Peters.

References

1. Saran, R., *et al.* US Renal Data System 2018 Annual Data Report: Epidemiology of Kidney Disease in the United States. *American Journal of Kidney Diseases* **73**, A7-A8 (2019).
2. D'Agati, V.D., Kaskel, F.J. & Falk, R.J. Focal Segmental Glomerulosclerosis. *New England Journal of Medicine* **365**, 2398-2411 (2011).
3. Korbet, S.M. Treatment of primary FSGS in adults. *J Am Soc Nephrol* **23**, 1769-1776 (2012).
4. Schwarz, A. New aspects of the treatment of nephrotic syndrome. *J Am Soc Nephrol* **12 Suppl 17**, S44-47 (2001).
5. Ponticelli, C. & Locatelli, F. Glucocorticoids in the Treatment of Glomerular Diseases: Pitfalls and Pearls. *Clin J Am Soc Nephrol* **13**, 815-822 (2018).
6. Ruggenenti, P., *et al.* Rituximab in steroid-dependent or frequently relapsing idiopathic nephrotic syndrome. *J Am Soc Nephrol* **25**, 850-863 (2014).
7. Iijima, K., Sako, M., Kamei, K. & Nozu, K. Rituximab in steroid-sensitive nephrotic syndrome: lessons from clinical trials. *Pediatr Nephrol* **33**, 1449-1455 (2018).
8. Herold, M.J., McPherson, K.G. & Reichardt, H.M. Glucocorticoids in T cell apoptosis and function. *Cell Mol Life Sci* **63**, 60-72 (2006).

9. Grahammer, F., Schell, C. & Huber, T.B. The podocyte slit diaphragm--from a thin grey line to a complex signalling hub. *Nat Rev Nephrol* **9**, 587-598 (2013).
10. Xing, C.Y., *et al.* Direct effects of dexamethasone on human podocytes. *Kidney Int* **70**, 1038-1045 (2006).
11. Yamauchi, K., *et al.* Screening and identification of substances that regulate nephrin gene expression using engineered reporter podocytes. *Kidney International* **70**, 892-900 (2006).
12. McCaffrey, J.C., *et al.* Glucocorticoid therapy regulates podocyte motility by inhibition of Rac1. *Sci Rep* **7**, 6725 (2017).
13. Lewko, B., *et al.* Dexamethasone-dependent modulation of cyclic GMP synthesis in podocytes. *Mol Cell Biochem* **409**, 243-253 (2015).
14. Wada, T., Pippin, J.W., Marshall, C.B., Griffin, S.V. & Shankland, S.J. Dexamethasone prevents podocyte apoptosis induced by puromycin aminonucleoside: role of p53 and Bcl-2-related family proteins. *J Am Soc Nephrol* **16**, 2615-2625 (2005).
15. Agrawal, S., Guess, A.J., Benndorf, R. & Smoyer, W.E. Comparison of direct action of thiazolidinediones and glucocorticoids on renal podocytes: protection from injury and molecular effects. *Mol Pharmacol* **80**, 389-399 (2011).
16. Ransom, R.F., Lam, N.G., Hallett, M.A., Atkinson, S.J. & Smoyer, W.E. Glucocorticoids protect and enhance recovery of cultured murine podocytes via actin filament stabilization. *Kidney Int* **68**, 2473-2483 (2005).
17. Zhang, J., *et al.* Podocyte repopulation by renal progenitor cells following glucocorticoids treatment in experimental FSGS. *Am J Physiol Renal Physiol* **304**, F1375-1389 (2013).
18. Mallipattu, S.K., *et al.* Krüppel–Like Factor 15 Mediates Glucocorticoid-Induced Restoration of Podocyte Differentiation Markers. *Journal of the American Society of Nephrology* **28**, 166-184 (2017).
19. Zhou, H., *et al.* Loss of the podocyte glucocorticoid receptor exacerbates proteinuria after injury. *Sci Rep* **7**, 9833 (2017).
20. Mathieson, P.W. Proteinuria and immunity--an overstated relationship? *N Engl J Med* **359**, 2492-2494 (2008).
21. Wharram, B.L., *et al.* Podocyte depletion causes glomerulosclerosis: diphtheria toxin-induced podocyte depletion in rats expressing human diphtheria toxin receptor transgene. *J Am Soc Nephrol* **16**, 2941-2952 (2005).
22. Kriz, W. & Lemley, K.V. A potential role for mechanical forces in the detachment of podocytes and the progression of CKD. *J Am Soc Nephrol* **26**, 258-269 (2015).
23. Blanco, E., Shen, H. & Ferrari, M. Principles of nanoparticle design for overcoming biological barriers to drug delivery. *Nat Biotechnol* **33**, 941-951 (2015).
24. Rosenblum, D., Joshi, N., Tao, W., Karp, J.M. & Peer, D. Progress and challenges towards targeted delivery of cancer therapeutics. *Nat Commun* **9**, 1410 (2018).
25. Laginha, K.M., Verwoert, S., Charrois, G.J. & Allen, T.M. Determination of doxorubicin levels in whole tumor and tumor nuclei in murine breast cancer tumors. *Clin Cancer Res* **11**, 6944-6949 (2005).
26. Gabizon, A., Shmeeda, H. & Barenholz, Y. Pharmacokinetics of pegylated liposomal Doxorubicin: review of animal and human studies. *Clin Pharmacokinet* **42**, 419-436 (2003).

27. Yoshikawa, N., *et al.* Glomerular podocyte vacuolation in focal segmental glomerulosclerosis. *Arch Pathol Lab Med* **110**, 394-398 (1986).
28. Eyre, J., *et al.* Statin-sensitive endocytosis of albumin by glomerular podocytes. *Am J Physiol Renal Physiol* **292**, F674-681 (2007).
29. Chung, J.J., *et al.* Albumin-associated free fatty acids induce macropinocytosis in podocytes. *J Clin Invest* (2015).
30. Inoue, K. & Ishibe, S. Podocyte endocytosis in the regulation of the glomerular filtration barrier. *Am J Physiol Renal Physiol* **309**, F398-405 (2015).
31. Maeda, K., *et al.* CaMK4 compromises podocyte function in autoimmune and nonautoimmune kidney disease. *J Clin Invest* **128**, 3445-3459 (2018).
32. Hauser, P.V., *et al.* Novel siRNA delivery system to target podocytes in vivo. *PLoS One* **5**, e9463 (2010).
33. Shankland, S.J., Pippin, J.W., Reiser, J. & Mundel, P. Podocytes in culture: past, present, and future. *Kidney Int* **72**, 26-36 (2007).
34. Borgman, M.P., *et al.* Tumor-targeted HPMA copolymer-(RGDfK)-(CHX-A"-DTPA) conjugates show increased kidney accumulation. *J Control Release* **132**, 193-199 (2008).
35. Liu, X.M., *et al.* Synthesis and evaluation of a well-defined HPMA copolymer-dexamethasone conjugate for effective treatment of rheumatoid arthritis. *Pharm Res* **25**, 2910-2919 (2008).
36. Kopecek, J. & Kopeckova, P. HPMA copolymers: origins, early developments, present, and future. *Adv Drug Deliv Rev* **62**, 122-149 (2010).
37. Hu, Y.B., Dammer, E.B., Ren, R.J. & Wang, G. The endosomal-lysosomal system: from acidification and cargo sorting to neurodegeneration. *Transl Neurodegener* **4**, 18 (2015).
38. Huotari, J. & Helenius, A. Endosome maturation. *EMBO J* **30**, 3481-3500 (2011).
39. Wang, D., *et al.* Novel dexamethasone-HPMA copolymer conjugate and its potential application in treatment of rheumatoid arthritis. *Arthritis Res Ther* **9**, R2 (2007).
40. Howard, M.D., Ponta, A., Eckman, A., Jay, M. & Bae, Y. Polymer micelles with hydrazone-ester dual linkers for tunable release of dexamethasone. *Pharm Res* **28**, 2435-2446 (2011).
41. Wang, C.E., Wei, H., Tan, N., Boydston, A.J. & Pun, S.H. Sunflower Polymers for Folate-Mediated Drug Delivery. *Biomacromolecules* **17**, 69-75 (2016).
42. Ngambenjawong, C. & Pun, S.H. Multivalent polymers displaying M2 macrophage-targeting peptides improve target binding avidity and serum stability. *ACS Biomater Sci Eng* **3**, 2050-2053 (2017).
43. Wu, K., Liu, J., Johnson, R.N., Yang, J. & Kopecek, J. Drug-free macromolecular therapeutics: induction of apoptosis by coiled-coil-mediated cross-linking of antigens on the cell surface. *Angew Chem Int Ed Engl* **49**, 1451-1455 (2010).
44. Marshall, C.B., Pippin, J.W., Krofft, R.D. & Shankland, S.J. Puromycin aminonucleoside induces oxidant-dependent DNA damage in podocytes in vitro and in vivo. *Kidney Int* **70**, 1962-1973 (2006).
45. Hoshyar, N., Gray, S., Han, H. & Bao, G. The effect of nanoparticle size on in vivo pharmacokinetics and cellular interaction. *Nanomedicine (Lond)* **11**, 673-692 (2016).
46. Park, J., *et al.* Single-cell transcriptomics of the mouse kidney reveals potential cellular targets of kidney disease. *Science* **360**, 758-763 (2018).
47. Gipson, D.S., *et al.* Management of childhood onset nephrotic syndrome. *Pediatrics* **124**, 747-757 (2009).

48. Waldman, M., *et al.* Adult minimal-change disease: clinical characteristics, treatment, and outcomes. *Clin J Am Soc Nephrol* **2**, 445-453 (2007).
49. Faul, C., *et al.* The actin cytoskeleton of kidney podocytes is a direct target of the antiproteinuric effect of cyclosporine A. *Nat Med* **14**, 931-938 (2008).
50. Fornoni, A., *et al.* Rituximab targets podocytes in recurrent focal segmental glomerulosclerosis. *Sci Transl Med* **3**, 85ra46 (2011).
51. Schonenberger, E., Ehrich, J.H., Haller, H. & Schiffer, M. The podocyte as a direct target of immunosuppressive agents. *Nephrol Dial Transpl* **26**, 18-24 (2011).
52. Sonawane, S.J., Kalhapure, R.S. & Govender, T. Hydrazone linkages in pH responsive drug delivery systems. *Eur J Pharm Sci* **99**, 45-65 (2017).
53. Ugorski, M., Dziegiel, P. & Suchanski, J. Podoplanin - a small glycoprotein with many faces. *Am J Cancer Res* **6**, 370-386 (2016).
54. Li, X., *et al.* Nephrin Preserves Podocyte Viability and Glomerular Structure and Function in Adult Kidneys. *J Am Soc Nephrol* **26**, 2361-2377 (2015).
55. Grahammer, F., *et al.* A flexible, multilayered protein scaffold maintains the slit in between glomerular podocytes. *JCI Insight* **1**(2016).
56. Cilliers, C., Nessler, I., Christodolu, N. & Thurber, G.M. Tracking Antibody Distribution with Near-Infrared Fluorescent Dyes: Impact of Dye Structure and Degree of Labeling on Plasma Clearance. *Mol Pharm* **14**, 1623-1633 (2017).
57. Kale, A.A. & Torchilin, V.P. Design, Synthesis, and Characterization of pH-Sensitive PEG−PE Conjugates for Stimuli-Sensitive Pharmaceutical Nanocarriers: The Effect of Substitutes at the Hydrazone Linkage on the pH Stability of PEG−PE Conjugates. *Bioconjugate Chemistry* **18**, 363-370 (2007).
58. Akilesh, S., *et al.* Podocytes use FcRn to clear IgG from the glomerular basement membrane. *Proc Natl Acad Sci U S A* **105**, 967-972 (2008).
59. Bruni, R., *et al.* Ultrasmall polymeric nanocarriers for drug delivery to podocytes in kidney glomerulus. *J Control Release* **255**, 94-107 (2017).

Supporting information

Table S4.1 Baseline NP fluorescence. NPs were diluted from a 0.2 mg/mL stock 1:100 in PBS, and fluorescence was determined using a plate reader (ex/em = 630/670 nm). Fluorescence was normalized by subtracting background PBS signal.

NP	Fluorescence (AU)
C5	45536
T5	45332

.

Chapter 5

Major findings and future perspectives

Abstract

In this chapter, major findings from Chapters 2-4 are summarized, and future work is proposed that builds off of the platforms developed in these works. Proposed are a new polymer-drug conjugate intervention for acute kidney injury, evaluation of drug-loaded nanoparticle efficacy in an animal model of podocyte injury, and interrogation of nanoparticle physicochemical properties that lead to increased uptake in glomerular podocytes.

5.1 Summary of major findings

The following work sought to engineer new drug carrier and linker technologies that enable pharmacokinetic control over current and experimental drugs used in the nephrology clinic.

5.1.1 Proximal tubule delivery technologies

In Chapter 2, we evaluated the effects of polymer molecular weight and anion density on accumulation in the kidneys. Highly anionic ~25 kDa polymers accumulated in kidney proximal tubule cells, and these polymers exhibited greater kidney accumulation during conditions of podocyte loss compared to normal conditions. Therefore, low-molecular weight anionic polymers may be interesting drug carriers for targeted drug delivery to proximal tubule cells, and disruption of the glomerular filtration barrier can be leveraged to augment tubular cell accumulation.

5.1.2 Podocyte delivery technologies

Bis-T-23 is an interesting experimental drug to modulate the podocyte cytoskeleton, but is challenging to administer due to its poor solubility and side effects. Work in Chapter 3 developed a pH-sensitive drug linker for programmable release of Bis-T-23 from drug carriers. Boronic acid copolymers were able to load Bis-T-23 and release drug at acidic, but not neutral pH, and delivered bioactive Bis-T-23 to cultured podocytes. Boronic acids may therefore be useful for programmed release of Bis-T-23 and other catechol-containing drugs under acidic conditions.

Glucocorticoids are a cornerstone of glomerular disease treatment, but cause many serious side effects that complicate the initial disease. Nanoparticle drug carriers for targeted dexamethasone drug delivery to glomerular podocytes were described in Chapter 4. Block copolymers were synthesized and self-assembled into nanoparticles, and targeted nanoparticles exhibited selective binding to podocytes *in vitro* and *in vivo*. This platform could enable long-term and low-dose glucocorticoid therapy that maintains disease remission and mitigates side effects.

5.2 Future perspectives

The proposed future work applies the anionic polymer and podocyte-targeting nanoparticle delivery platforms in animal models of kidney injury, and examines fundamental NP design parameters to target glomerular podocytes.

5.2.1 Anionic polymers for delivery to proximal tubule cells

Rationale. The anionic polymers developed in Chapter 2 exhibit highly selective accumulation in kidney proximal tubules. A potential application of these materials is to deliver autophagy activators to proximal tubules to mitigate acute kidney injury (AKI) and proximal tubule cell apoptosis during ischemia/reperfusion injury (IRI).[1] IRI is defined as the tissue injury caused by an initial ischemia as well as the additional injury after restoration of flow (reperfusion).[2] In the kidneys, IRI is a leading cause of AKI and induces apoptosis and necrosis of renal tissue,[1] in particular proximal tubule cell death given their abundance in the kidneys.[3] Guan *et al*. reported

that autophagy levels increase in kidney tissue after reperfusion injury and is important in promoting cell survival.[1] Administration of rapamycin, a small molecule that induces autophagy, prior to IRI reduces apoptosis of proximal tubule cell. However, rapamycin exhibits multisystem and toxic side effects.[4,5] As AKI is a frequent occurrence peri-operatively and in the hospital,[6] we propose a pre-surgical intervention of rapamycin-polymer conjugates to reduce the risk and extent of acute kidney injury in high-risk patients.

Polymer design. Ideally, rapamycin remains conjugated to the carrier throughout circulation and is released after internalization into proximal tubule cells. Given the intervention timeframe in the clinic, polymer-drug conjugates are ideally delivered and release drug on the scale of hours before surgical anesthesia or other procedures with a high-risk of AKI. Anionic polymers are internalized into proximal tubules (Chapter 2), which motivates designing pH-sensitivity as a drug release mechanism. Rapamycin contains ketones and hydroxyls, which are amenable to reaction with polymer carboxylic acid side chains to form pH-sensitive hydrazone bonds (as discussed in Chapter 4) or esterase-sensitive ester bonds, respectively. The hydrazone bond will be highly stable and likely exhibit slower release kinetics than the highly labile ester bond. Both can be evaluated to determine the optimal variant *in vitro* before testing in an efficacy model.

Anionic polymers will be synthesized as we have previously described.[7] Rapamycin-polymer conjugates containing hydrazone bonds will be synthesized by reaction of a small number of carboxylic side chains with hydrazine and then rapamycin, as described in Chapter 4; conjugates containing ester bonds will be synthesized by direct conjugation of rapamycin to carboxylic acid side chains via EDC/DMAP chemistry.

In vitro tests. Polymer-drug conjugates will be characterized for molecular weight and drug release. To test conjugate drug release and efficacy, HK-2 proximal tubule cells or the tubule-on-a-chip system (Ying Zheng, Jonathan Himmelfarb)[8,9] will be incubated with polymer-drug conjugates and quantified for autophagosome number as previously described.[10]

Therapeutic animal model. Polymer-conjugate efficacy will be tested in an animal model of IRI-induced AKI as previously described.[1] First, animals will be pre-treated with the following: (*i*) PBS, (*ii*) free rapamycin, (*iii*) polymer only, and (*iv*) polymer-rapamycin. Rapamycin dose will be equivalent at 1 mg/kg (per prior work[1]) across all relevant treatments, and polymer content will be normalized between treatments *iii* and *iv*. Sham-operated controls will be included. To induce IRI, the bilateral renal arteries will be clamped for 35 min before reperfusion. Various time points of pre-treatment will be evaluated to determine the optimal dosing schedule. Blood will be collected throughout the study for analysis.

Metrics. Elevated blood urea nitrogen and serum creatinine are indicative of acute kidney injury.[1] These metrics will be compared across treatments to determine treatment efficacy and the optimal dosing schedule window. Kidney tissue will be examined for injury.

Significance. The growing epidemic of cardiovascular disease in the United States greatly increases the risk and incidence of IRI and acute kidney injury,[11] and interventions are needed to preserve the renal health of these patients. The technology developed in Chapter 2 may be applied to enable rapamycin delivery to proximal tubule cells pre-anesthesia, to reduce the risk of renal cell injury and apoptosis. Moreover, nephrotic range proteinuria causes tubule cell death

and dysfunction, with inhibition of autophagy being a contributing factor.[10] Treatment with rapamycin-polymer conjugates during diseases of podocyte injury or loss may help to mitigate overall kidney injury. Another potential application is pre-treatment of donor kidneys, which can present with AKI that limits the lifespan of the graft.[12] Preloading of donor kidneys with polymer-drug conjugates could potentially mitigate the extent of AKI and improve graft survival.

5.2.2 Evaluation of podocyte nanoparticles in a mouse model of nephropathy

Rationale. Chapter 4 described the development of podocyte-targeting nanoparticles (NPs) loaded with dexamethasone (DEX). While further optimization is needed, ideally the NPs are evaluated in an animal model to test the hypothesis that targeted glucocorticoid delivery to glomerular podocytes can improve renal heath during podocyte injury. To enable this study, first an animal model of nephropathy that is responsive to free DEX should be developed and validated.

Animal model development. Therapeutic DEX models have been reported in doxorubicin (DOX)- and anti-glomerular antibody-induced nephropathy, both of which cause podocyte injury and proteinuria in mice.[13-15] Clinical dosing regimens of DEX (1-2 mg/kg) significantly reduces proteinuria in these animals. Current work has not yet been able to recapitulate these findings (summarized in **Table 5.1**).

Studies 1 and 3 were performed in accordance with published reports, which observed robust reduction in proteinuria with DEX treatment. In our hands, these models resulted in significant

mortality (at least 50%). While no reduction in proteinuria was observed in Study 1 with DEX treatment, there was a trend of decreased proteinuria in Study 3 that was not statistically significant due to animal mortality. Study 2 was a repeat of Study 1, but at a reduced anti-glomerular antibody dose to reduce toxicity. While nearly all animals survived to the study endpoint (11/12), no reduction in proteinuria was observed with DEX treatment. Serum was also collected in this study to quantify serum creatinine as an alternative readout, as untreated, diseased animals are expected to exhibit greater serum creatinine than DEX-treated animals.[15] No differences were observed in serum creatinine in this study (data not shown). Given the lack of DEX efficacy in the anti-glomerular model of nephropathy, this model is no longer being pursued. Study 4 is a repeat of Study 3, but with reduced DOX to reduce mortality (8-8.5 mg/kg v. 10 mg/kg). While animals exhibited greater survival (11/12), no significant reduction in proteinuria was observed with DEX treatment. These animals exhibited a lesser degree of disease than those in Study 3, suggesting that the initial disease state is important for observing reductions in proteinuria. A DOX dose of 9 mg/kg may be optimal in inducing disease while maintaining animal survival.

If DEX does not appear to reduce proteinuria in the DOX-induced nephropathy model, the mouse lipopolysaccharide model may be validated,[14] although the short time course of this model (24-48 h) may be challenging to handle in terms of urine collection and assessing the efficacy of slow-releasing NPs. This model is also not without controversy in the field.[16,17] If free DEX does not reduce proteinuria in any of these models, then NP studies could potentially shift focus towards biodistribution and kidney distribution, optimizing antibody density and/or NP

size for glomerular podocyte targeting. Alternate readouts may be required, such as glomerular podocyte density or podocyte foot process width.

Table 5.1 Summary of therapeutic DEX model outcomes. Ab, antiglomerular antibody; DOX, doxorubicin; DEX, dexamethasone.

Study Number and Model		Strain	Literature Summary	Outcome
1	5 mg/kg Ab on days -1 and 0 2 mg/kg DEX on day 1 and every other day after	8 week-old FVB/NJ male	complete reduction in proteinuria after 14 days of treatment[14]	significant mortality no proteinuria reduction with DEX treatment
2	4 mg/kg Ab on days -1 and 0 2 mg/kg DEX on day 1 and every other day after	8 week-old FVB/NJ male	N/A	improved survival no proteinuria reduction with DEX treatment no differences in serum creatinine
3	10 mg/kg DOX on day 0 1 mg/kg DEX on day 1 and every other day after	8-week old BALB/c male	50% reduction in proteinuria after 14 days of treatment[15]	significant mortality trend in proteinuria reduction with DEX treatment but not statistically significant no differences in serum creatinine
4	8-8.5 mg/kg DOX on day 0 1 mg/kg DEX on day 1 and every other day after	8-week old BALB/c male	N/A	improved survival no proteinuria reduction with DEX treatment

Therapeutic animal model. After validating a DEX-responsive model, DEX-NPs developed in Chapter 4 can then be evaluated for *in vivo* efficacy. The validated model (DOX, LPS) will be treated with the following: (*i*) PBS, (*ii*) free DEX, (*iii*) podocyte IgG, (*iv*) control NPs, and (*v*) podocyte NPs. DEX dose will be equivalent at 1 mg/kg (per prior work[13-15]) across all relevant treatments, and the podocyte IgG dose will be equivalent to the antibodies on podocyte NPs. Urines will be collected regularly, and serum will be collected at the study endpoint.

Metrics. Urinary proteinuria (albumin/creatinine ratio), serum creatinine, and glomerular podocyte density will be quantified to evaluate treatment efficacy. Glomeruli will also be quantified for fluorescent NP density as described in Chapter 4 to validate podocyte NP targeting. We expect free DEX and podocyte NPs to exhibit similar degrees of proteinuria and serum creatinine reduction compared to controls, and to mitigate podocyte loss by glomerular podocyte density quantification. As DEX induces T-cell apoptosis, spleen weights can be used as a metric for side effects.[18] Indeed, animals treated with DEX exhibited significantly reduced spleen weights compared to DMSO-treated animals (Study 2, **Figure 5.1**). In this proposed efficacy study, we expect spleen weights to decrease the most with free DEX-treated animals, and an attenuated reduction with podocyte NP treatment due to differences in drug pharmacokinetics.

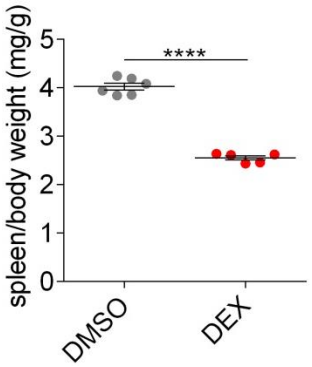

Figure 5.1 Normalized spleen weights of DMSO- or DEX-treated animals. Bars represent means ± SEM. ****p-value < 0.0001.

Significance. As discussed in Chapter 4, glucocorticoids are the frontline therapy in glomerular disease treatment, but burden the patient with significant side effects that complicate the disease. Development of NP drug carriers for targeted drug delivery to podocytes could be important in achieving disease remission while mitigating side effects, as well as establishing an important

proof-of-principle that the clinical efficacy of glucocorticoids can be due to podocyte-centric effects rather than systemic immunosuppression.

5.2.3 Fundamental understanding of NP parameters that promote podocyte accumulation

Rationale. The findings in Chapter 2 concluded that size (molecular weight) and charge are important physicochemical parameters that drive polymer accumulation in the kidneys. Another, perhaps more important parameter that emerged from the study was disease state: podocyte loss increases the permeability of the glomerular filtration barrier and subsequently augments the accumulation of polymers, similar to the enhanced permeation and retention effect hypothesized for tumors.[19] As the development of targeted nanoscale drug carriers to glomerular podocytes is still in its early stages, design of such carriers could substantially benefit from a thorough interrogation of the NP design space. Specifically, what are the effects of NP size and disease state on NP accumulation in the kidneys? The latter question is particularly important, as podocyte injury may significantly alter podocyte phenotype and attenuate antibody recognition. This future work is proposed in general terms to allow the greatest flexibility following the work proposed in Section 5.2.2.

Nanoparticle panel design. A wide size range of NPs (20-200 nm) have been reported for kidney targeting applications, [20,21] but have not been systemically examined for podocyte targeting. We will investigate NPs of size 20 nm, 100 nm, and 200 nm, as these NP sizes capture a wide range of *in vivo* behavior.[18,22] Fluorescently labeled block copolymer NPs (as in Chapter 4) or unimolecular dendrimers for stability and controllable size will be conjugated with control or

podocyte IgG at comparable densities. NPs will then be injected into normal and diseased mice (DOX or antiglomerular antibody-induced).

Metrics. NPs will be evaluated for biodistribution and podocyte targeting by whole-organ imaging and fluorescence microscopy, respectively. Notably, a podocyte stain (nephrin) will be utilized to normalize NP fluorescence by podocyte, rather than glomerular, surface area, as podocyte density is expected to decrease during disease induction.[23] NP fluorescence in glomerular podocytes will be compared across disease states and various sizes to determine the conditions that best promote podocyte targeting.

Significance. There is a lack of design criteria for NP targeting to glomerular podocytes. This study would be the first to systematically evaluate the effects of NP size and disease state on NP podocyte accumulation, as well as evaluate if targeting ligands can still recognize podocytes during diseases that attack these cells.

5.3 Acknowledgments

This work was supported by the Office of the Assistant Secretary of Defense for Health Affairs through the Peer Reviewed Medical Research Program under Award Numbers PR151175 and PR151965, and by the National Science Foundation Graduate Research Fellowship Program under Grant No. DGE-1256082 to GWL. Opinions, interpretations, conclusions, and

recommendations are those of the authors and are not necessarily endorsed by the Department of Defense or the National Science Foundation.

References

1. Guan, X., *et al.* Autophagy protects renal tubular cells against ischemia / reperfusion injury in a time-dependent manner. *Cell Physiol Biochem* **36**, 285-298 (2015).
2. Kalogeris, T., Baines, C.P., Krenz, M. & Korthuis, R.J. Cell biology of ischemia/reperfusion injury. *Int Rev Cell Mol Biol* **298**, 229-317 (2012).
3. Park, J., *et al.* Single-cell transcriptomics of the mouse kidney reveals potential cellular targets of kidney disease. *Science* **360**, 758-763 (2018).
4. Li, J., Kim, S.G. & Blenis, J. Rapamycin: one drug, many effects. *Cell Metab* **19**, 373-379 (2014).
5. Meier-Kriesche, H.U. & Kaplan, B. Toxicity and efficacy of sirolimus: relationship to whole-blood concentrations. *Clin Ther* **22 Suppl B**, B93-100 (2000).
6. Zarbock, A., Koyner, J.L., Hoste, E.A.J. & Kellum, J.A. Update on Perioperative Acute Kidney Injury. *Anesth Analg* **127**, 1236-1245 (2018).
7. Liu, G.W., *et al.* Glomerular disease augments kidney accumulation of synthetic anionic polymers. *Biomaterials* **178**, 317-325 (2018).
8. Rayner, S.G., *et al.* Reconstructing the Human Renal Vascular-Tubular Unit In Vitro. *Adv Healthc Mater* **7**, e1801120 (2018).
9. Ligresti, G., *et al.* A Novel Three–Dimensional Human Peritubular Microvascular System. *Journal of the American Society of Nephrology* **27**, 2370-2381 (2016).
10. Nolin, A.C., *et al.* Proteinuria causes dysfunctional autophagy in the proximal tubule. *Am J Physiol Renal Physiol* **311**, F1271-F1279 (2016).
11. Mensah, G.A. & Brown, D.W. An overview of cardiovascular disease burden in the United States. *Health Aff (Millwood)* **26**, 38-48 (2007).
12. Boffa, C., *et al.* Transplantation of Kidneys From Donors With Acute Kidney Injury: Friend or Foe? *Am J Transplant* **17**, 411-419 (2017).
13. Zhang, J., *et al.* Podocyte repopulation by renal progenitor cells following glucocorticoids treatment in experimental FSGS. *Am J Physiol Renal Physiol* **304**, F1375-1389 (2013).
14. Mallipattu, S.K., *et al.* Krüppel–Like Factor 15 Mediates Glucocorticoid-Induced Restoration of Podocyte Differentiation Markers. *Journal of the American Society of Nephrology* **28**, 166-184 (2017).
15. Li, L., *et al.* Role of Myeloid-Derived Suppressor Cells in Glucocorticoid-Mediated Amelioration of FSGS. *Journal of the American Society of Nephrology* **26**, 2183-2197 (2015).
16. Comper, W.D. Is the LPS-mediated proteinuria mouse model relevant to human kidney disease? *Nature Medicine* **15**, 133 (2009).

17. Reiser, J. & Mundel, P. Is the LPS-mediated proteinuria mouse model relevant to human kidney disease? *Nature Medicine* **15**, 133 (2009).
18. Rooman, R., Koster, G., Bloemen, R., Gresnigt, R. & van Buul-Offers, S.C. The effect of dexamethasone on body and organ growth of normal and IGF-II-transgenic mice. *J Endocrinol* **163**, 543-552 (1999).
19. Wang, C.E., Stayton, P.S., Pun, S.H. & Convertine, A.J. Polymer nanostructures synthesized by controlled living polymerization for tumor-targeted drug delivery. *J Control Release* **219**, 345-354 (2015).
20. Bruni, R., *et al.* Ultrasmall polymeric nanocarriers for drug delivery to podocytes in kidney glomerulus. *J Control Release* **255**, 94-107 (2017).
21. Maeda, K., *et al.* CaMK4 compromises podocyte function in autoimmune and nonautoimmune kidney disease. *J Clin Invest* **128**, 3445-3459 (2018).
22. Blanco, E., Shen, H. & Ferrari, M. Principles of nanoparticle design for overcoming biological barriers to drug delivery. *Nat Biotechnol* **33**, 941-951 (2015).
23. Eng, D.G., *et al.* Glomerular parietal epithelial cells contribute to adult podocyte regeneration in experimental focal segmental glomerulosclerosis. *Kidney Int* **88**, 999-1012 (2015).

Part II

Engineering renal progenitor cells

to regenerate lost podocytes

Chapter 6

Renal progenitor cell therapy for podocyte regeneration

Abstract

Podocyte loss is exacerbated by the fact that podocytes are terminally differentiated and non-proliferative. In kidney diseases, the rate of podocyte loss is greater than that of regeneration by endogenous podocyte progenitors, leading to glomerulosclerosis and end-stage renal disease. Therefore, supplementing the endogenous reservoir of podocyte progenitors could be a therapeutic strategy for regenerating lost podocytes. In particular, human $CD133^{+}CD24^{+}$ renal progenitor cells have been shown to engraft to damaged glomeruli and differentiate into podocytes in mouse models of podocyte loss, making these cells attractive for cell therapy applications. This work seeks to improve the functionality of these cells through non-viral gene transfer and nanoengineering to improve their functionality *in vivo*.

6.1 Kinetics of podocyte loss

Humans are born with their maximum number of podocytes (~600/glomerulus), and under normal conditions lose about 0.5% or 3 podocytes per year.[1] While podocytes themselves are incapable of proliferation,[2] various endogenous podocyte progenitors have been described that likely regenerate the podocytes lost at this basal rate.[3,4]

Experimental animal models have shown that an abrupt depletion of up to 20% of podocytes leads to transient proteinuria and recovery, and that greater depletion leads to focal segmental glomerulosclerosis (FSGS) and persistent proteinuria in rats.[5] These findings suggest that at a critical podocyte number threshold, podocyte loss overwhelms regeneration, and that therapeutic interventions to regenerate even a relatively small number of podocytes could significantly improve disease outcomes. For example, the average number of podocytes per glomerulus in rats and adult humans is approximately 135 and 560, respectively.[6,7] A 20% loss in podocyte number corresponds to 27 and 112 podocytes per glomerulus, respectively. At this threshold, regeneration of 2 or 6 podocytes per glomerulus (corresponding to 1%), respectively, could profoundly alter the disease course from glomerulosclerosis to repair.

The importance of podocyte number in renal function and health motivates new interventions to arrest podocyte loss and restore podocyte number. Renal progenitor cells (RPCs) have been shown to migrate onto injured glomeruli and differentiate into *de novo* podocytes after systemic injection, and are readily sourced from patient urine. Given the clinical potential of RPCs, this work focuses on engineering these cells for regenerating lost podocytes.

6.2 Renal progenitor cell biology

During disease when podocyte loss overwhelms regeneration, supplementing the natural reservoir of endogenous podocyte progenitors could lead to improved disease outcomes. Substantial progress has been made in elucidating the origin, culture conditions, and *in vivo* functionality and tissue repair ability of human RPCs. RPCs are identified by CD133 and CD24 labeling, both of which are considered markers of stem or progenitor cells.[8-10]

6.2.1 Origin, niche, and organization

RPCs are a subset of parietal epithelial cells (PECs) lining the Bowman's capsule, and exhibit a gradated phenotype depending on location between the urinary and vascular poles. Uncommitted RPCs do not express the podocyte protein podocalyxin (PDX),[11] reside near the urinary pole of the glomerulus, and are phenotypically $CD133^{+}CD24^{+}PDX^{-}$. More committed $CD133^{+}CD24^{+}PDX^{+}$ transitional cells reside between the urinary and the vascular pole. Differentiated $CD133^{-}CD24^{-}PDX^{+}$ podocyte-like cells localize at the vascular pole and are contiguous with glomerular podocytes (**Figure 5.1**).[4,12,13]

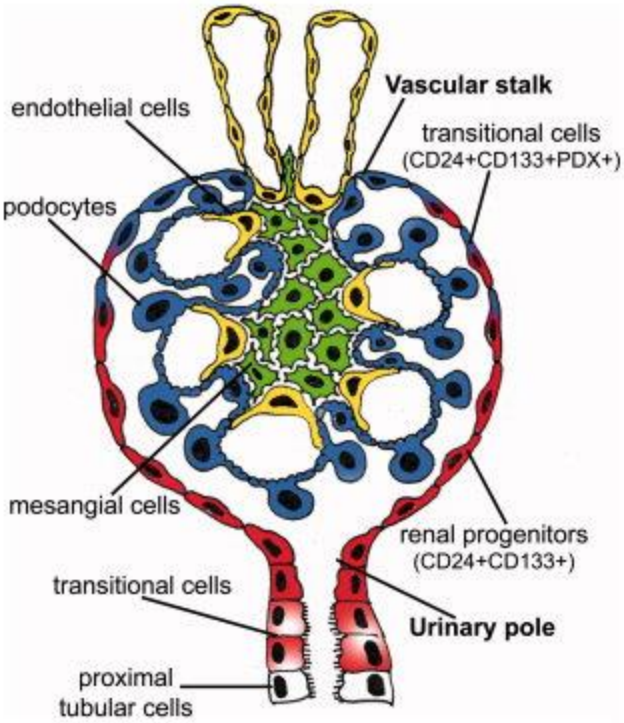

Figure 6.1 Organization of renal progenitors in the glomerulus. Figure reproduced with permission from reference 13.

6.2.2 Cell isolation methods and behavior in culture

Initial reports of isolating $CD133^{+}CD24^{+}$ RPCs were from nephrectomized kidney fragments.[4,12] Single-cell suspensions were generated through mechanical and enzymatic means, depleted of $CD45^{+}$ and $CD31^{+}$ cells, and then sorted for $CD133^{+}$ by magnetic bead separation to obtain RPCs. Cells were able to be clonally expanded, and exhibited expression of podocyte-specific proteins nephrin and synaptopodin after culture in podocyte-differentiating media VRAD.[4]

RPCs are also able to be isolated from the urine (uRPCs) of pediatric and adult patients with active nephrotic syndrome. First, urine-derived cells were cultured and expanded before magnetic bead separation (using anti-CD133 magnetic beads) or fluorescence-activated cell

sorting (staining for CD133 and CD24).[14] uRPCs were able to be maintained in large cultures for 2-3 months. In our experience, uRPCs are able to be frozen and thawed without remarkable changes in the percent of $CD133^{+}CD24^{+}$ cells or *in vivo* functionality. These cells also expressed podocyte-specific nephrin, podocyte, and synaptopodin protein expression after culture in podocyte-differentiating media VRAD.

Moreover, RPCs can be generated from iPSCs.[15] Derived cells expressed CD133 and CD24, engrafted into damaged tubules, and improved renal health in an animal model of acute kidney injury.

When RPCs were cultured in conditions that favored tubulogenic, osteogenic, adipogenic, or neurogenic differentiation, cells exhibited mRNA and protein expression characteristic of those cell types.[12]

6.2.3 *In vivo* functionality

The *in vivo* efficacy of intravenously injected RPCs appears to be through localization of the transplanted cells at the site of kidney injury. In various murine models of kidney injury, RPCs were found to migrate to the kidney at disease sites and adopt markers of differentiated cells.

In a mouse model of doxorubicin HCl-induced nephropathy, tissue- and urine-derived RPCs (administered intravenously) significantly reduced proteinuria compared to control cells or untreated controls.[4,14] Fluorescently labeled uRPCs were shown to localize to glomeruli and

acquired podocyte-specific podocin and nephrin staining. Notably, injected cells did not home or engraft to glomeruli in normal animals, and $CD133^{-}$ cells did not home to glomeruli in doxorubicin HCl nephropathy animals. These findings indicate that both molecular cues from the injury site and cellular phenotype drive RPC homing and engraftment.

In a mouse model of rhabdomyolysis-induced acute renal failure, animals treated with RPCs exhibited significantly reduced blood urea nitrogen levels compared to untreated and $CD133^{-}$ cell-treated animals. RPC-treated animals exhibited evidence of tubular repair and reduced scarring.[12,16]

6.2.4 Homing and engraftment

RPC homing and engraftment seem to be mediated in part by SDF-1, a key regulator of stem cell retention, migration, survival, and mobilization that is upregulated in injured tissues.[16-20] *In vitro*, RPCs express CXCR4 and CXCR7, both known to be receptors of SDF-1.[21,22] In a model of rhabdomyolysis-induced acute renal failure, pre-treatment with antibodies to block CXCR4 or CXCR7 prevented tissue regeneration by transferred RPCs and reduced the number of engrafted cells. Further *in vitro* studies revealed that CXCR4 is essential for RPC migration, and that CXCR7 is essential for transendothelial migration and endothelial cell adhesion.[16]

While the CXCR4-SDF-1 axis drives the migration of exogenous transferred RPCs onto the glomerular tuft, it acts to maintain quiescence of endogenous Bowman's capsule RPCs. Podocytes are the main producer of SDF-1 in the glomerulus. In normal and disease conditions,

SDF-1 inhibits Bowman's capsule RPC migration and differentiation due to a lack of a chemotactic gradient within the urinary space between the glomerular tuft and the Bowman's capsule.[23] Blockade of SDF-1 using antibodies enhanced podocyte regeneration in a model of podocyte injury.

6.2.5 Pharmacological modulation

The GSK3s inhibitor 6-bromo-indirubin-3'-oxime (BIO) enhances the sensitivity of human RPCs to the podocyte-differentiating effects of retinoic acid.[24] Animals with doxorubicin HCl-induced nephropathy treated with BIO exhibited significantly reduced proteinuria and glomerulosclerosis compared to untreated animals. BIO treatment also resulted in more $Pax2^{+}$ PECs and newly generated podocytes per kidney glomeruli, suggesting that BIO can promote podocyte differentiation *in vivo*.

All-trans retinoic acid (ATRA) induces nephrin mRNA and protein expression in human RPCs and cultured podocytes.[25,26] In multiple models of nephrosis, ATRA significantly reduced proteinuria, and increased the number of RPCs/PECs that exhibited podocyte marker staining.[26,27]

Glucocorticoids are widely used in the clinic to induce remission of proteinuria. In addition to direct drug effects on podocytes, glucocorticoids exhibit effects on PECs. In an animal model of experimental FSGS, prednisone treatment increased the number of PECs lining the Bowman's capsule, as well as increased the expression of pro-survival p-ERK signaling in PECs.[28]

Recent findings suggest that miR-193a plays an important role in the transdifferentiation of PECs into podocytes.[29] Knockdown of miR-193a in immortalized human PECs increased expression of podocyte-specific WT1, podocalyxin, synaptopodin, α-actinin-4, and nephrin mRNA and protein, and decreased expression of PEC-specific Pax-8, claudin-1, and UCH-L1 mRNA and protein. Moreover, blockade of miR-193a using complementary locked nucleic acid resulted in increased synaptopodin expression in PECs *in vivo*. These findings suggest that miR-193a controls the phenotype of PECs, and that modulation of miR-193a may be a clinical strategy for regenerating lost podocytes.

SDF-1 blockade via antibodies has been reported to enhance RPC migration and podocyte regeneration in an animal model of podocyte injury.[23] This is likely due to the reduction of SDF-1 within the urinary space, generating a steeper SDF-1 gradient that subsequently triggers RPC migration. While this strategy may be effective in augmenting the reparative activity of endogenous Bowman's capsule RPCs, doing so for intravenously transferred RPCs may severely inhibit cellular migration onto the glomerular tuft.[16]

6.3 Engineering renal progenitor cells

The standard treatment for podocytopathies is long-term immunosuppression that does not effectively address the fundamental problem of podocyte loss and subsequent disease advancement to kidney failure. Part II of the thesis work seeks to develop a novel reparative therapy that regenerates lost podocytes using uRPCs that are functionally augmented through

bioengineering methods. uRPCs are a particularly attractive candidate for cell therapies, as they can be collected non-invasively in urine and are a readily available autologous progenitor source.

6.3.1 Method optimization

First, methods were optimized to isolate and characterize uRPCs from patient urine (Chapter 7). uRPCs significantly reduced proteinuria and exhibited evidence of glomerular integration and podocyte differentiation in a model of experimental FSGS. These methods and experimental strategies will be further employed in future work.

6.3.2 Non-viral gene delivery

Methods for non-viral gene transfer to uRPCs could lead to new therapeutic strategies for treating kidney diseases. For example, uRPCs may be genetically modified to secrete therapeutic proteins, or to overexpress homing receptors to enhance tissue homing and engraftment. In Chapter 8, non-viral gene delivery methods were optimized for uRPC transfection. Efficient short and long-term transgene expression was achieved, and these methods were employed to overexpress CXCR4 in these cells. This chapter is currently a manuscript in preparation.

6.3.3 Future perspectives

Small molecule adjuvants can augment the functionality of cell therapies, but require high systemic concentrations that may cause significant adverse side effects. Loading cells with drug-

loaded nanoscale “backpacks” could result in focused and sustained drug delivery to the carrier cell. In Chapter 9, preliminary results are shown for nanoscale backpack formulations and *in vitro* characterization, with future work proposed to evaluate backpack-loaded uRPC efficacy in a model of experimental FSGS. Other future works proposed are: evaluating the glomerular homing of CXCR4-transfected uRPCs compared to controls, and generating a nephrin-reporting uRPC for high-throughput interrogation of new biological agents that modulate podocyte differentiation.

6.4 Acknowledgments

This work was supported by the Office of the Assistant Secretary of Defense for Health Affairs through the Peer Reviewed Medical Research Program under Award Numbers PR151175 and PR151965, and by the National Science Foundation Graduate Research Fellowship Program under Grant No. DGE-1256082 to GWL. Opinions, interpretations, conclusions, and recommendations are those of the authors and are not necessarily endorsed by the Department of Defense or the National Science Foundation.

References

1. Kikuchi, M., Wickman, L., Rabah, R. & Wiggins, R.C. Podocyte number and density changes during early human life. *Pediatr Nephrol* **32**, 823-834 (2017).
2. Lasagni, L., Lazzeri, E., Shankland, S.J., Anders, H.J. & Romagnani, P. Podocyte mitosis - a catastrophe. *Curr Mol Med* **13**, 13-23 (2013).

3. Lichtnekert, J., *et al.* Renin-Angiotensin-Aldosterone System Inhibition Increases Podocyte Derivation from Cells of Renin Lineage. *J Am Soc Nephrol* **27**, 3611-3627 (2016).
4. Ronconi, E., *et al.* Regeneration of glomerular podocytes by human renal progenitors. *J Am Soc Nephrol* **20**, 322-332 (2009).
5. Wharram, B.L., *et al.* Podocyte depletion causes glomerulosclerosis: diphtheria toxin-induced podocyte depletion in rats expressing human diphtheria toxin receptor transgene. *J Am Soc Nephrol* **16**, 2941-2952 (2005).
6. Bai, X.Y. & Basgen, J.M. Podocyte number in the maturing rat kidney. *Am J Nephrol* **33**, 91-96 (2011).
7. Puelles, V.G., *et al.* Podocyte Number in Children and Adults: Associations with Glomerular Size and Numbers of Other Glomerular Resident Cells. *J Am Soc Nephrol* **26**, 2277-2288 (2015).
8. Angelotti, M.L., Lazzeri, E., Lasagni, L. & Romagnani, P. Only anti-CD133 antibodies recognizing the CD133/1 or the CD133/2 epitopes can identify human renal progenitors. *Kidney Int* **78**, 620-621; author reply 621 (2010).
9. Jiang, W., *et al.* CD24: a novel surface marker for PDX1-positive pancreatic progenitors derived from human embryonic stem cells. *Stem Cells* **29**, 609-617 (2011).
10. Jimenez-Quevedo, P., *et al.* Selected CD133(+) progenitor cells to promote angiogenesis in patients with refractory angina: final results of the PROGENITOR randomized trial. *Circ Res* **115**, 950-960 (2014).
11. Shankland, S.J., Smeets, B., Pippin, J.W. & Moeller, M.J. The emergence of the glomerular parietal epithelial cell. *Nat Rev Nephrol* (2014).
12. Sagrinati, C., *et al.* Isolation and characterization of multipotent progenitor cells from the Bowman's capsule of adult human kidneys. *J Am Soc Nephrol* **17**, 2443-2456 (2006).
13. Romagnani, P. Toward the identification of a "renopoietic system"? *Stem Cells* **27**, 2247-2253 (2009).
14. Lazzeri, E. & Romagnani, P. Podocyte biology: Differentiation of parietal epithelial cells into podocytes. *Nat Rev Nephrol* **11**, 7-8 (2015).
15. Imberti, B., *et al.* Renal progenitors derived from human iPSCs engraft and restore function in a mouse model of acute kidney injury. *Sci Rep* **5**, 8826 (2015).
16. Mazzinghi, B., *et al.* Essential but differential role for CXCR4 and CXCR7 in the therapeutic homing of human renal progenitor cells. *J Exp Med* **205**, 479-490 (2008).
17. Lapidot, T., Dar, A. & Kollet, O. How do stem cells find their way home? *Blood* **106**, 1901 (2005).
18. Cottler-Fox, M.H., *et al.* Stem Cell Mobilization. *ASH Education Program Book* **2003**, 419-437 (2003).
19. Lange, C., *et al.* Administered mesenchymal stem cells enhance recovery from ischemia/reperfusion-induced acute renal failure in rats. *Kidney Int* **68**, 1613-1617 (2005).
20. Togel, F.E. & Westenfelder, C. Role of SDF-1 as a regulatory chemokine in renal regeneration after acute kidney injury. *Kidney International Supplements* **1**, 87-89 (2011).
21. Burns, J.M., *et al.* A novel chemokine receptor for SDF-1 and I-TAC involved in cell survival, cell adhesion, and tumor development. *J Exp Med* **203**, 2201-2213 (2006).
22. Ratajczak, M.Z., *et al.* The pleiotropic effects of the SDF-1-CXCR4 axis in organogenesis, regeneration and tumorigenesis. *Leukemia* **20**, 1915-1924 (2006).

23. Romoli, S., *et al.* CXCL12 blockade preferentially regenerates lost podocytes in cortical nephrons by targeting an intrinsic podocyte-progenitor feedback mechanism. *Kidney Int* **94**, 1111-1126 (2018).
24. Lasagni, L., *et al.* Podocyte Regeneration Driven by Renal Progenitors Determines Glomerular Disease Remission and Can Be Pharmacologically Enhanced. *Stem Cell Reports* **5**, 248-263 (2015).
25. Takano, Y., *et al.* Recovery and maintenance of nephrin expression in cultured podocytes and identification of HGF as a repressor of nephrin. *Am J Physiol Renal Physiol* **292**, F1573-1582 (2007).
26. Peired, A., *et al.* Proteinuria impairs podocyte regeneration by sequestering retinoic acid. *J Am Soc Nephrol* **24**, 1756-1768 (2013).
27. Zhang, J., *et al.* Retinoids augment the expression of podocyte proteins by glomerular parietal epithelial cells in experimental glomerular disease. *Nephron Exp Nephrol* **121**, e23-37 (2012).
28. Zhang, J., *et al.* Podocyte repopulation by renal progenitor cells following glucocorticoids treatment in experimental FSGS. *Am J Physiol Renal Physiol* **304**, F1375-1389 (2013).
29. Kietzmann, L., *et al.* MicroRNA-193a Regulates the Transdifferentiation of Human Parietal Epithelial Cells toward a Podocyte Phenotype. *J Am Soc Nephrol* **26**, 1389-1401 (2015).

Chapter 7

Isolation, characterization, and efficacy of human urinary renal progenitor cells (uRPCs)

Gary W. Liu, Diana G. Eng, Jeffrey W. Pippin, Stuart J. Shankland, and Suzie H. Pun

Abstract

As podocytes are unable to proliferate, replenishment of podocyte number must come from podocyte progenitors. Urinary renal progenitor cells (uRPCs) are podocyte progenitors that can be derived from the urine of proteinuric patients and have been shown to repair injured glomeruli in nephrotic animals, highlighting the clinical potential of uRPCs as a cell therapy to regenerate lost podocytes. In this work, we optimized methods for isolating uRPCs from patient urine, characterized uRPCs for progenitor cell features *in vitro*, and validated uRPC functionality *in vivo* in a mouse model of focal segmental glomerulosclerosis (FSGS). uRPCs were isolated by fluorescence-activated cell sorting, and expressed greater Ki-67, Pax-8, and Sox-9 protein compared to uRPCs treated with podocyte-differentiating media. Podocyte-differentiated uRPCs expressed greater and more organized F-actin protein, and greater synaptopodin mRNA compared to untreated uRPCs. Biological functionality was validated in mice with experimental FSGS, induced with an optimized dose of cytotoxic anti-podocyte antibody that results in abrupt podocyte dysfunction and depletion. Animals treated with uRPCs exhibited significantly reduced proteinuria compared to animals treated with PBS. Moreover, uRPCs were observed to migrate to injured glomeruli and adopt podocyte-like features. Collectively, these data provide evidence that the isolated cells are uRPCs capable of differentiating into podocyte-like cells, and the methods developed here will be employed for later testing of engineered uRPCs.

7.1 Introduction

Reduction in podocyte number underlies glomerulosclerosis and chronic kidney disease,[1] emphasizing the importance of maintaining and increasing podocyte number as a therapeutic goal to prevent kidney failure. As podocytes are unable to productively proliferate,[2] replenishment of podocyte number during health and disease must come from podocyte progenitors.[3,4] However, disease conditions result in an accelerated rate of podocyte loss that overwhelms endogenous regeneration, leading to glomerulosclerosis and kidney failure.[5] Supplementing the endogenous reservoir of podocyte progenitors through cell transfer could be clinically strategic in regenerating lost podocytes and preventing glomerulosclerosis.

Renal progenitor cells (RPCs) are an endogenous podocyte progenitor population lining the Bowman's capsule and contiguous with the glomerular vascular stalk.[3] These cells exhibit a graded phenotype from the uncommitted RPCs near the urinary pole to the podocyte-committed RPCs near the vascular pole. The latter, podocyte-committed RPCs are thought to migrate upon the glomerulus to replace lost podocytes.[3,6] Important findings by the Romagnani group have highlighted RPCs as an attractive podocyte progenitor source for cell therapy. First, RPCs are shed into the urine of kidney disease patients, and may be isolated by fluorescence-activated cell sorting or magnetic bead sorting methods and expanded *ex vivo*.[6,7] This presents an accessible and facile avenue of sourcing autologous podocyte progenitors for patient-specific therapies. Second, intravenously administered RPCs are able to migrate onto injured glomeruli and differentiate into podocyte-like cells. During doxorubicin HCl-induced nephrosis,[8] which induces podocyte loss and focal segmental glomerulosclerosis (FSGS), mice administered human

RPCs exhibited reduced proteinuria compared to saline-treated animals. Within the kidneys, RPCs were found within glomeruli and co-stained for podocyte proteins podocin, nephrin, and synaptopodin in injured animals.[6,7] Injected uRPCs were not found in the glomeruli of normal mice. These observations suggest that exogenous uRPCs are capable of homing to injured glomeruli and adopting a podocyte-like phenotype in conditions of glomerular injury, which leads to a reduction in proteinuria.

Given the clinical potential of RPCs, the work in this chapter sought to recapitulate these key findings for later testing of engineered RPCs. First, $CD133^{+}CD24^{+}$ urinary renal progenitor cells (uRPCs) were collected and cultured. These cells have been reported to be isolated from the urine of pediatric patients diagnosed with a variety of glomerular diseases including steroid-resistant and steroid-sensitive nephrotic syndrome, congenital nephrotic syndrome, and IgA nephropathy.[7] Moreover, active proteinuria increased the probability of isolating cells from urine, and urines from normal donors did not yield these cells. Based on these observations, our inclusion criteria for human subjects were: steroid-sensitive or steroid-resistant pediatric (ages 1-17) and adult (18-50) patients, with active proteinuria at the time of urine collection. As urine samples are routinely collected in the nephrology clinic, this provides a unique opportunity for non-invasively collecting these cells.

Our inclusion criteria included steroid-resistant nephrotic syndrome (SRNS), as these are typically caused by genetic mutations: 85% of SRNS cases that develop by age 3 months and 66% of cases that develop by age 1 year can be explained by mutations in nephrin, podocin, laminin β2, and Wilms tumor 1, which broadly play critical roles in podocyte attachment and

ultrastructure.[9] Notably, uRPCs derived from patients with genetic causes of nephrotic syndrome do not differentiate into morphological podocytes.[7] Genetic editing of these cells could present a therapeutic avenue for these patients to regenerate functional podocytes.

Here, we sought to develop and optimize experimental methods for uRPC engineering by validating the *in vivo* functionality of unmodified uRPCs in a mouse model of FSGS. To induce FSGS, a cytotoxic anti-podocyte antibody that causes abrupt podocyte dysfunction and depletion was administered to mice. This model was selected over doxorubicin HCl, as it produces more consistent proteinuria between animals with reduced morbidity and mortality. The goals of this work were to (*1*) optimize methods for isolating uRPCs, (*2*) phenotype the collected cells for progenitor and differentiated cell markers, and (*3*) validate that uRPCs reduce proteinuria and home to glomeruli during experimental FSGS.

7.2 Materials and methods

7.2.1 Human subjects

All human studies were approved by the Institutional Review Board at the University of Washington (STUDY00000973). Informed consent was obtained from all subjects. Urine was collected from actively proteinuric pediatric and adult patients with focal segmental glomerulosclerosis, membranous nephropathy, or minimal change disease during routine

nephrologist visits. Samples were stored at 4 °C until processing, typically within an hour of sample collection.

7.2.2 $CD133^{+}CD24^{+}$ urinary renal progenitor cell (uRPC) isolation

uRPCs were isolated as previously described with modifications.[6,7] Briefly, fresh patient urine samples were collected by centrifugation, washed with PBS, and plated with EGM-MV+20% FBS (Lonza) supplemented with antibiotics on T-75 flasks. Cells were allowed to grow for 6-8 d until confluence. For sorting, cells were lifted with Accutase (Millipore), stained with anti-CD133-APC (clone 293C3, Miltenyi Biotec) and anti-CD24-FITC (clone SN3, ThermoFisher Scientific) antibodies, and then sorted for double-positive cells (BD FACSAria III, UW Pathology Flow Cytometry Core). Isotype-stained cells were used to establish gates. After, sorted $CD133^{+}CD24^{+}$ cells were plated on T75 flasks and allowed to grow to confluence. Multiple cell stocks were frozen in 5% DMSO/95% FBS (passage 2) or allowed to grow for another passage before freezing (passage 3).

7.2.3 uRPC differentiation

For differentiation studies, $5\text{-}10\times10^{3}$ $CD133^{+}CD24^{+}$ cells were plated on human laminin (Corning)-coated 12-mm glass coverslips in 24-well plates for fluorescence microscopy, or 1.5×10^{5} cells plated on 100-mm tissue culture dishes for RT-qPCR, until ~75% confluence. After, cells were either maintained in EGM-MV+20% FBS or switched to podocyte-

differentiating VRADD media (DMEM/F12+10% FBS, 50 μM all-trans retinoic acid, 100 nM vitamin D_3, 100 nM dexamethasone) for 5 d.[6,7,10]

7.2.4 Fluorescence microscopy

The following antibodies and dilutions were used: 1:100 anti-Ki67 (clone SP6, ThermoFisher Scientific); 1:500 anti-PAX8 (clone EPR18715, abcam); 1:50 anti-SOX9 (clone EPR14335, abcam). Briefly, cells were fixed with 4% PFA, permeabilized with 0.1% Triton X-100/PBS, blocked with 1% BSA/PBS, and then incubated with primary antibodies overnight at 4 °C. After, cells were washed with 0.1% Triton X-100/PBS, stained with the appropriate secondary antibodies, FITC-phalloidin, and DAPI, and then mounted.

7.2.5 RT-qPCR

Cell RNA was isolated with an RNA NucleoSpin kit (Macherey-Nagel), and cDNA synthesized using the SuperScript III First-Strand Synthesis System (ThermoFisher Scientific) with random hexamer primers. The following primers were used for qPCR analysis (all sequences 5' to 3'): Pax8 fw: CAGGTCTACGATGCGCTG, rev: TGCCTCACAACTCCATCAGA; Sox9 fw: GTACCCGCACTTGCACAAC, rev: TCTCGCTCTCGTTCAGAAGTC; CD24 fw: TGCTCCTACCCACGCAGATT, rev: GGCCAACCCAGAGTTGGAA; CD133 fw: CAGAGTACAACGCCAAACCA, rev: AAATCACGATGAGGGTCAGC; synaptopodin fw: ATGGAGGGGTACTCAGAGGAG; rev: CTCTCGGTTTTGGGACAGGTG; GAPDH fw: ACCACAGTCCATGCCATCAC, rev: TCCACCACCCTGTTGCTGTA. qPCR was performed

with a 7300 Real Time PCR System (Applied Biosystems). Relative mRNA levels of VRADD-treated uRPCs compared to untreated uRPCs were calculated using the $2^{-\Delta\Delta Ct}$ method.[11]

7.2.6 uRPC culture

uRPCs were isolated, sorted for $CD133^{+}CD24^{+}$ expression by fluorescence-activated cell sorting, and frozen as previously reported.[6,7] For *in vivo* experiments, cells were thawed, plated on T-75 flasks, and maintained in EGM-MV+20% FBS (Lonza) for 6 d with regular media changes.

7.2.7 Experimental FSGS induction and timeline

For optimization studies, animals (n = 2 each, 8-10 weeks old) were administered 7, 8, 10, or 11 mg anti-podocyte antibody/20 g via two intraperitoneal injections 24 h apart on days −1 and 0. Kidney biopsies were performed on days 7 and 14, and animals were sacrificed on day 28. Spot urines were collected at baseline and on days 7, 14, 21, and 28 after antibody administration.

For uRPC testing, experimental FSGS was induced in 9-week old BALB/c SCID (Jackson Laboratory) via two intraperitoneal injections (7 mg antibody/20 g mouse) of anti-podocyte antibody 24 h apart on days −1 and 0. Spot urines were collected on days −4 (baseline), 1, 3, 6, and 8, and cells were injected via tail vein on days 1 (target cell number = 7.5×10^5) and 4 (target cell number = 5.7×10^5). All animals were sacrificed on day 8, and organ (heart, lungs, liver, spleen, kidneys) fluorescence was quantified by Xenogen IVIS using ex/em = 605/660 nm.

7.2.8 uRPC processing for injection

Cultured uRPCs were washed with PBS, lifted with Accutase (Millipore), and resuspended in pre-warmed RPMI to 1.0×10^6 cells/mL for fluorescence labeling by DiD Vybrant (ex/em = 644/665 nm, Thermo Fisher Scientific) according to manufacturer instructions. After washing, cells were resuspended in PBS to 2.5×10^6 or 1.9×10^6 cells/mL for injection on days 1 or 4, respectively. Cells (3.75×10^5–7.5×10^5 cells in 300 μL) were loaded into a 1-mL syringe and slowly injected using a 27G×1/2" needle via tail vein.

7.2.9 Tissue processing and staining

For fluorescence, kidney tissues were fixed in 4% PFA, washed with PBS, and incubated overnight with 30% sucrose/PBS at 4 °C. Tissues were then embedded in OCT and snap-frozen in an ethanol/dry ice bath. Kidney sections (4 μm) were washed with PBS, blocked with 1% BSA/PBS, and stained overnight using 1:100 sheep anti-nephrin (R&D AF4269). After, tissues were washed in PBS, stained with a donkey anti-sheep secondary antibody (Jackson ImmunoResearch Labs) and DAPI, and mounted using Fluoromount-G (Southern Biotech). Images were collected using an EVOS microscope.

7.2.10 Urine albumin and creatinine quantification

Urine albumin content was quantified by radial immunodiffusion as previously described,[12] and creatinine quantified using a creatinine assay kit (Cayman Chemical).

7.3 Results and discussion

7.3.1 Urine collection from kidney disease patients

Urines from adult and pediatric patients with active proteinuria were collected, processed, and assayed for $CD133^{+}CD24^{+}$ cells by flow cytometry. A majority of the adult urine samples (11/19) exhibited cell growth, while neither of the pediatric patient urine samples (0/2) exhibited cell growth (**Table 7.1**).

No correlations were observed between patient characteristics (age, presentation, sex, urine volume) and presence of urinary cell growth. The percentage of $CD133^{+}CD24^{+}$ cells after growth, as tested by flow cytometry, varied between 10-70% depending on donor.

7.3.2 uRPC isolation by fluorescence-activated cell sorting

Previous attempts to sort cells using a variety of magnetic column-based sorting methods produced low-quality cell yields and purity. To address these challenges, fluorescence-activated cell sorting (FACS) was utilized for high purity and throughput sorting. Urinary cell outgrowths were stained for CD133 and CD24, and double-positive cells were sorted using isotype-stained cells to establish gates. A typical sort results in $3\text{-}9\times10^{5}$ $CD133^{+}CD24^{+}$ cells from $1\text{-}2\times10^{6}$ urinary cells, depending on the donor, with purity ranging 90-96% (**Figure 7.1**). Moreover, cells were able to be frozen without major viability loss, and maintained CD133 and CD24 expression after thawing.

Table 7.1 Patient urine samples and urinary cell outgrowth. MN, membranous nephropathy; FSGS, focal segmental glomerulosclerosis; MCD, minimal change disease; NS, nephrotic syndrome. Samples denoted with "UWMC" indicate adult patients; samples denoted with "SCH" indicate pediatric patients. "Untested" indicates that cellular growths were present but not yet tested for $CD133^+CD24^+$ cells.

Patient	Presentation	$CD133^+CD24^+$ cells
UWMC1	MN	yes
UWMC2	MN	no
UWMC3	FSGS	yes
UWMC4	MN	untested
UWMC5	MN	yes
UWMC6	MN	yes
UWMC7	FSGS	untested
UWMC8	MN	untested
UWMC5-2	MN	yes
UWMC9	MCD	yes
UWMC10	MN	no
UWMC11	FSGS	yes
UWMC12	MN	no
UWMC14	MCD	no
UWMC15	MN	no
UWMC16	FSGS	yes
UWMC17	MN	no
UWMC18	FSGS	no
UWMC19	FSGS	no
SCH1	MCD	no
SCH2	NS	no

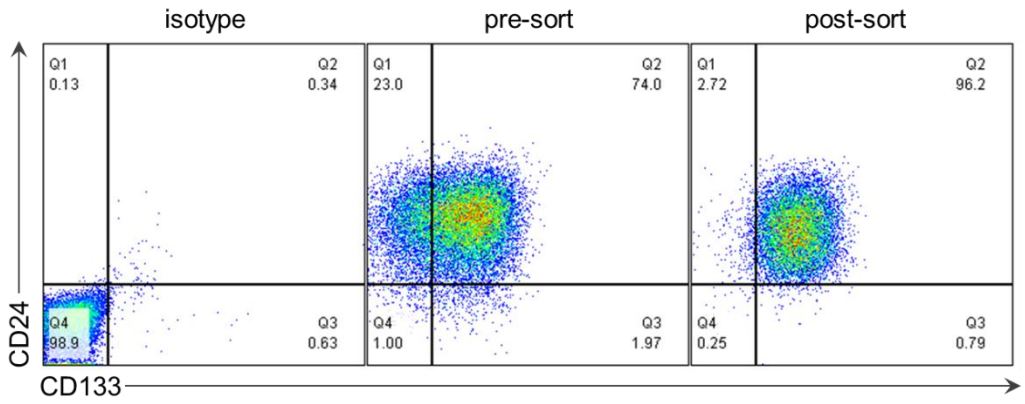

Figure 7.1 CD133 and CD24 staining of urinary cells before and after FACS.

7.3.3 uRPC differentiation by fluorescence microscopy

To test the differentiation ability of uRPCs, cells were cultured in DMEM/F12 containing vitamin D3, retinoic acid, and dexamethasone (VRADD media), which has been shown to differentiate uRPCs towards a podocyte-like phenotype[6,7,10,13] as well as increase mRNA levels of podocyte genes nephrin and NEPH-1 in cultured podocytes.[10] First, cells were stained for F-actin after VRADD treatment to examine differences in F-actin organization (**Figure 7.2**).

VRADD-treated uRPCs exhibited overall greater F-actin staining, with greater cortical actin staining and increased number and organization of F-actin fibers that resemble podocyte morphology in culture.[14,15]

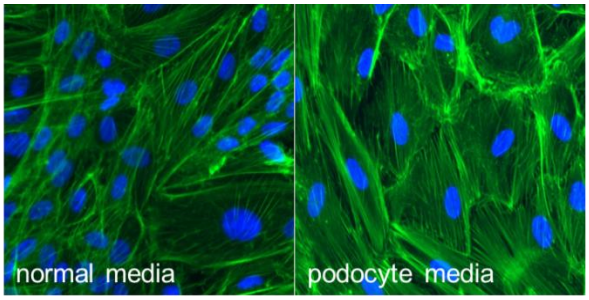

Figure 7.2 F-actin staining of untreated uRPCs and VRADD-treated uRPCs. Left, uRPCs maintained in uRPC media; right, uRPCs cultured in podocyte-differentiating media VRADD. Green, F-actin; blue, DAPI.

Untreated uRPCs and VRADD-treated uRPCs were also stained for Ki-67, a proliferation marker; Pax-8, a transcription factor critical for kidney development and a marker of parietal epithelial cells (PECs);[16-18] and Sox-9, a transcription factor critical for kidney regeneration and a marker of progenitor cells in the kidneys.[19] By fluorescence microscopy, uRPCs expressed greater Ki-67, Pax-8, and Sox-9 staining compared to VRADD-treated uRPCs (**Figure 7.3**). Moreover, uRPCs maintained in VRADD exhibited reduced proliferation, as evidence by lack of Ki-67 staining as well as reduced nuclei/field by fluorescence microscopy. These observations are consistent with previous reports: uRPCs are progenitor cells thought to be a subset of PECs,[3,6,7,13] and podocytes are non-proliferative and terminally differentiated cells.[20,21] Collectively, these data provide evidence to support that the isolated $CD133^{+}CD24^{+}$ cells are renal progenitor cells.

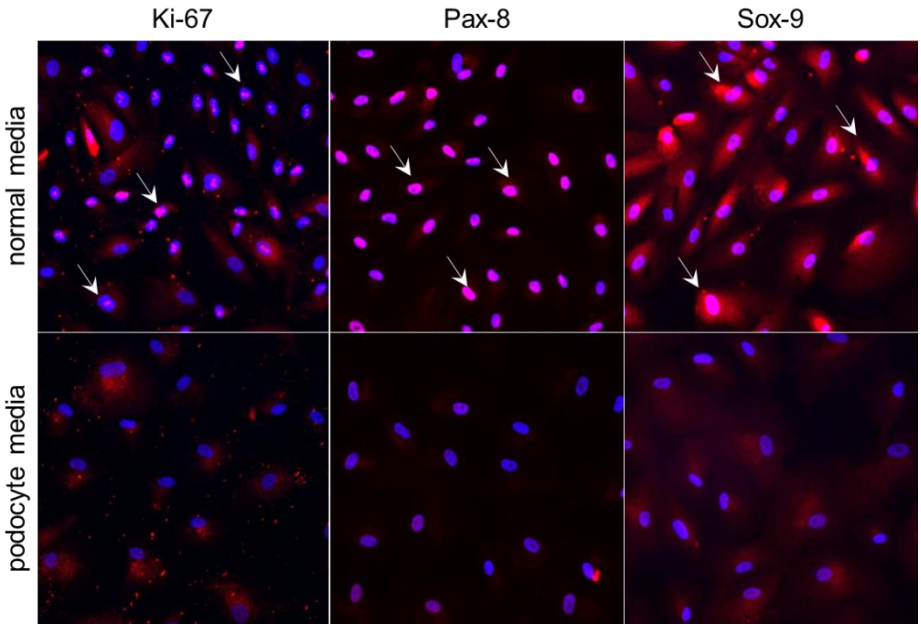

Figure 7.3 Ki-67, Pax-8, and Sox-9 staining of untreated uRPCs and VRADD-treated uRPCs. Top row: uRPCs that were maintained in uRPC media; bottom row: uRPCs cultured in podocyte-differentiating media VRADD. Red, Ki-67, Pax-8, or Sox-9; blue, DAPI. Arrows indicate examples of transcription factor-positive nuclei.

.

7.3.4 uRPC differentiation by RT-qPCR

In a preliminary study (n = 1), relative mRNA expression of selected genes was compared between VRADD-treated uRPCs and untreated uRPCs, with GAPDH as a reference gene. While VRADD-treated uRPCs expressed more synaptopodin mRNA, an actin-associated protein highly expressed in podocytes,[22] they also expressed more Sox-9, CD24, and CD133 mRNA compared to untreated uRPCs. uRPCs expressed slightly more Pax-8 than VRADD-treated uRPCs.

Table 7.2 Relative gene expression of VRADD-treated uRPCs compared to untreated uRPCs.

Gene	Protein description	Fold-expression (VRADD/untreated)
Pax-8	transcription factor parietal epithelial cell marker	0.85
Sox-9	transcription factor progenitor cell marker	1.45
CD24	cell surface glycoprotein renal progenitor cell marker	1.18
CD133	cell surface glycoprotein renal progenitor cell marker	4.48
synaptopodin	actin-associated protein podocyte marker	3.16

There is some discrepancy between Sox-9 mRNA and protein expression levels in VRADD-treated uRPCs and untreated uRPCs. Guhr *et al*. reported that cultured PECs exhibit less active proteasomal activity and autophagosomal/lysosomal degradation compared to cultured podocytes,[23] which may partially explain the observation here that untreated uRPCs express more Sox-9 protein but less mRNA compared to VRADD-treated uRPCs.

7.3.5 Optimization of an antibody-induced podocyte loss animal model

A cytotoxic anti-podocyte antibody was used to induce experimental FSGS. This antibody specifically causes apoptosis of glomerular podocytes,[18,24,25] leading to albuminuria, a clinical signature of a damaged glomerular filtration barrier due to podocyte loss or dysfunction.[26] Therefore, this model was selected to validate the reported functionality of the isolated uRPCs,

using urinary albumin/creatinine ratio (ACR) as a clinical readout. Severe combined immune deficiency (SCID) mice, which lack functional T- and B-cells, were used to mitigate immune rejection of the human uRPCs.[27,28]

First, BALB/c SCID mice were administered a panel of antibody doses (7, 8, 10, or 11 anti-podocyte antibody/20 g mouse) to determine the optimal dose for uRPC studies. We sought an antibody dose that resulted in podocyte loss and proteinuria as a clinical readout, with observable endogenous repair that might suggest the presence of molecular cues and scaffolds required for cellular trafficking and engraftment. In advanced disease, extensive glomerular scarring leads to remodeling of the extracellular matrix, which would presumably obliterate or suppress a pro-regenerative response.[29] Mice administered 10 and 11 mg antibody/20 g exhibited more extensive podocyte loss, global sclerosis, and damaged capillaries than other mouse strains at equivalent doses (data not shown). Moreover, these animals did not exhibit repair by day 28.

Mice administered 7 and 8 mg antibody/20 g did exhibit functional repair of glomeruli, with proteinuria and glomerular disease decreasing over time (**Figure 7.4**). Based on these studies, the

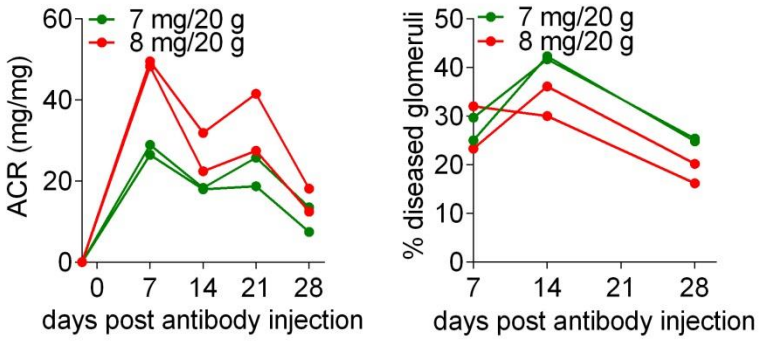

Figure 7.4 Urine albumin/creatinine ratios (ACR) and percent diseased glomeruli of BALB/c SCID mice treated with cytotoxic anti-podocyte antibody. Mice were treated with either 7 or 8 mg antibody/20 g of antibody (n = 2 each).

7 mg antibody/20 g dose was selected for uRPC testing, as this was the lowest tested dose that still exhibited podocyte loss, proteinuria, and glomerular injury with evidence of endogenous recovery.

7.3.6 *In vivo* efficacy of uRPC treatment

Animals were administered the optimized antibody dose (7 mg antibody/20 g) on days −1 and 0 to induce experimental FSGS, and then received either PBS or uRPCs (n = 5 each) on days 1 and 4 via tail vein injection. Urines were analyzed for albumin and creatinine. No statistically significant differences were observed in urine ACRs before day 8 between the two treatment groups (**Figure 7.5**). On day 8 however, uRPC-treated mice exhibited significantly lower urine ACR compared to PBS-treated mice (p-value = 0.0117). This observation is consistent with previous reports using uRPCs in a doxorubicin HCl-induced model of nephrosis,[6-8] indicating the reproducible functionality of these cells.

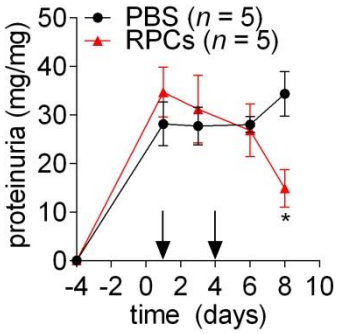

Figure 7.5 Urine albumin/creatinine ratios (ACR) of experimental FSGS mice treated with PBS or uRPCs. Arrows indicate cell injection on days 1 and 4. Bars represent means ± SEM. *p-value = 0.0117.

Notably, animals that received fewer cells still exhibited a reduction in urine ACR. On day 1, two animals received 6.25×10^5 and 3.75×10^5 cells instead of the intended 7.5×10^5 (based on previous reports[6,7]) due to injection difficulties. On day 4, all mice received 5.7×10^5 cells instead of the intended 7.5×10^5 due to limited cell number. All uRPC-treated animals responded regardless of the cell dose, suggesting that the cell dose may be reduced.

As this model of experimental FSGS causes podocyte loss and downstream proteinuria, these findings suggest that the injected uRPCs may be adopting a podocyte-like phenotype[6,7] and/or secreting reparative paracrine factors. Whole-organ fluorescence and kidney tissue fluorescence microscopy were employed to further study the *in vivo* behavior and morphology of these cells.

7.3.7 Biodistribution of fluorescently labeled uRPCs

uRPCs were labeled with a membrane-binding fluorescent DiD dye[30] for *in vivo* fluorescence monitoring. After animals were sacrificed on day 8, whole-organ fluorescence was observed using a Xenogen IVIS (**Figure 7.6**). This is the timepoint in which uRPCs reduce proteinuria.

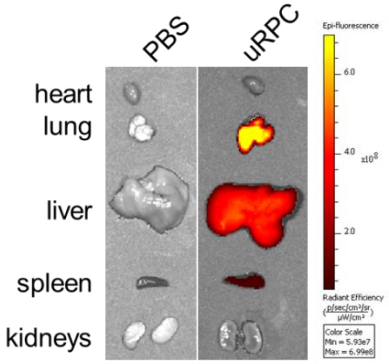

Figure 7.6 Representative fluorescent images of major organs after intravenous administration of PBS or fluorescently labeled uRPCs.

High fluorescence was observed in the lungs and liver, suggesting high uRPC accumulation in these organs. Indeed, the pulmonary "first pass effect" has been reported to initially trap a majority (50-60%) of intravenously injected stem cells in the lungs.[31] This effect appears to be size-, receptor-, and time-dependent,[31-33] with cells redistributing to the liver and spleen afterwards. Moreover, nodules were observed on the livers of uRPC-treated mice (data not shown), suggesting that uRPCs may have been trapped and proliferated in the liver.

7.3.8 Kidney distribution of fluorescently labeled uRPCs

Kidney sections (day 8) from experimental FSGS animals treated with uRPCs were stained for nephrin, a podocyte-specific slit diaphragm protein,[34] to observe uRPC trafficking and engraftment behavior *in vivo*. uRPCs were observed to distribute in injured parts of glomeruli, indicated by areas of reduced nephrin staining, and were not exclusively found in capillary loops, suggesting that the uRPCs were migrating and engrafting onto the glomerular tuft (**Figure 7.7**). Moreover, some of these cells appeared to have protrusions, similar to podocyte morphology, and exhibited some evidence of nephrin co-staining. Approximately 5% of all glomeruli contained uRPCs, of which 70-80% of the glomeruli are injured.

From these observations, the injected uRPCs appear to migrate to injured glomeruli and adopt a podocyte-like morphology. These observations are consistent with previous reports.[6,7]

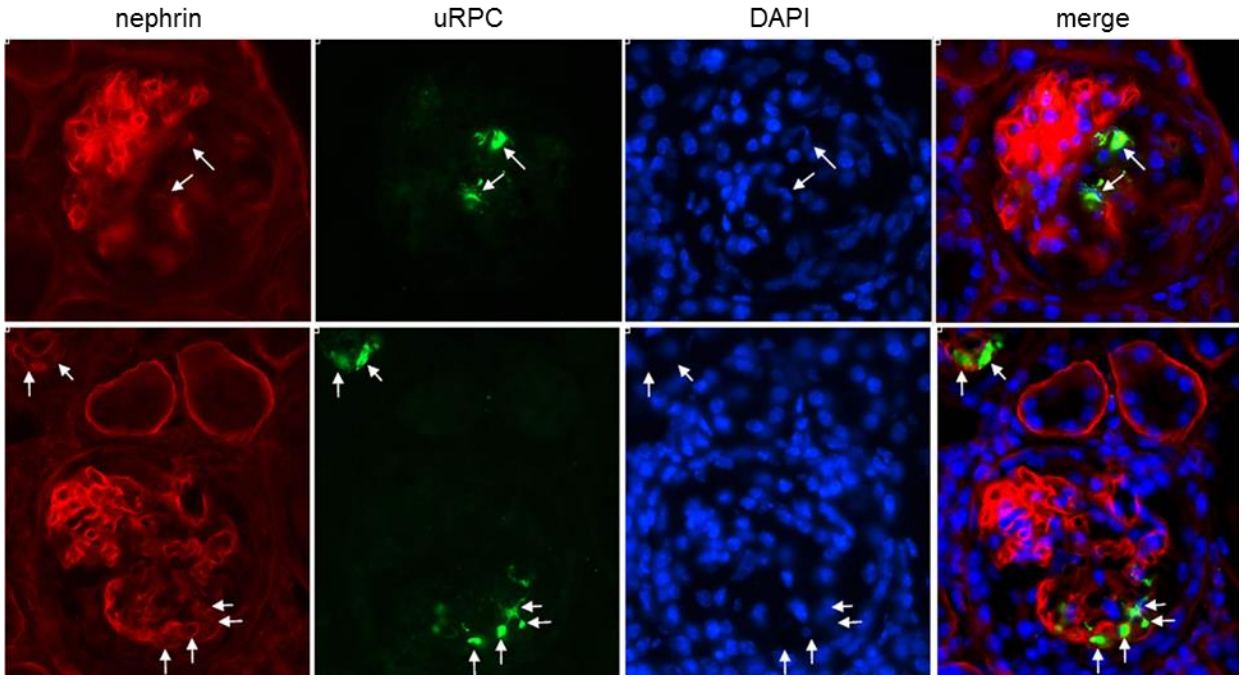

Figure 7.7 Fluorescent images of injured glomeruli containing fluorescently labeled uRPCs. Kidneys were harvested and analyzed on day 8. Red, nephrin; green, DiD membrane-labeled uRPC; blue, DAPI.

7.4 Conclusions

The objective of this work was to isolate and characterize $CD133^{+}CD24^{+}$ urinary renal progenitor cells. These cells were found in a majority of urine samples from adult patients with active proteinuria, and were readily isolated by FACS. Fluorescence staining revealed that $CD133^{+}CD24^{+}$ cells expressed Ki-67, Pax-8, and Sox-9, indicating that these cells exhibited a progenitor phenotype. Treatment with podocyte-differentiating media VRADD induced major changes in F-actin content and organization, as well as decreased protein expression of Ki-67, Pax-8, and Sox-9. RT-qPCR studies revealed differences in mRNA expression after VRADD treatment, with VRADD-treated cells expressing more synaptopodin, a podocyte-specific

protein. Collectively, these data largely recapitulate previous reports on uRPC behavior *in vitro*. Optimized *in vitro* methods for isolating and characterizing uRPCs for later cell engineering studies have been developed.

Human $CD133^{+}CD24^{+}$ uRPCs were also validated for *in vivo* functionality. Cells were fluorescently labeled and intravenously injected into mice with experimental FSGS. uRPCs significantly reduced urine albuminuria, a clinical sign of glomerular filtration barrier damage, compared to PBS-treated animals. While biodistribution analysis showed that the majority of injected cells accumulated in off-target organs (lungs and liver), fluorescence microscopy of kidney tissue revealed that fluorescently labeled uRPCs homed to injured glomeruli, with some adopting a podocyte-like stellate morphology and nephrin expression.

Together, these data confirm that the uRPC isolation, sorting, culture, and experimentation methods developed here are valid in generating quantifiable differences in urine ACR. These methods will be leveraged for future experiments in engineering and genetically manipulating these cells.

7.5 Acknowledgments

This work was supported by the Office of the Assistant Secretary of Defense for Health Affairs through the Peer Reviewed Medical Research Program under Award Numbers PR151175 and PR151965, and by the National Science Foundation Graduate Research Fellowship Program

under Grant No. DGE-1256082 to GWL. Opinions, interpretations, conclusions, and recommendations are those of the authors and are not necessarily endorsed by the Department of Defense or the National Science Foundation. We would also like to thank Donna Prunkard and Ngoc-Han Thi Nguyen (UW Pathology) for assistance with FACS.

References

1. Kriz, W. & Lemley, K.V. A potential role for mechanical forces in the detachment of podocytes and the progression of CKD. *J Am Soc Nephrol* **26**, 258-269 (2015).
2. Lasagni, L., Lazzeri, E., Shankland, S.J., Anders, H.J. & Romagnani, P. Podocyte mitosis - a catastrophe. *Curr Mol Med* **13**, 13-23 (2013).
3. Shankland, S.J., Smeets, B., Pippin, J.W. & Moeller, M.J. The emergence of the glomerular parietal epithelial cell. *Nat Rev Nephrol* (2014).
4. Pippin, J.W., *et al.* Cells of renin lineage are progenitors of podocytes and parietal epithelial cells in experimental glomerular disease. *Am J Pathol* **183**, 542-557 (2013).
5. Lasagni, L., *et al.* Podocyte Regeneration Driven by Renal Progenitors Determines Glomerular Disease Remission and Can Be Pharmacologically Enhanced. *Stem Cell Reports* **5**, 248-263 (2015).
6. Ronconi, E., *et al.* Regeneration of glomerular podocytes by human renal progenitors. *J Am Soc Nephrol* **20**, 322-332 (2009).
7. Lazzeri, E., *et al.* Human Urine-Derived Renal Progenitors for Personalized Modeling of Genetic Kidney Disorders. *J Am Soc Nephrol* (2015).
8. Pippin, J.W., *et al.* Inducible rodent models of acquired podocyte diseases. *Am J Physiol Renal Physiol* **296**, F213-229 (2009).
9. Lovric, S., Ashraf, S., Tan, W. & Hildebrandt, F. Genetic testing in steroid-resistant nephrotic syndrome: when and how? *Nephrol Dial Transplant* **31**, 1802-1813 (2016).
10. Takano, Y., *et al.* Recovery and maintenance of nephrin expression in cultured podocytes and identification of HGF as a repressor of nephrin. *Am J Physiol Renal Physiol* **292**, F1573-1582 (2007).
11. Livak, K.J. & Schmittgen, T.D. Analysis of relative gene expression data using real-time quantitative PCR and the 2(-Delta Delta C(T)) Method. *Methods* **25**, 402-408 (2001).
12. Marshall, C.B., Krofft, R.D., Pippin, J.W. & Shankland, S.J. CDK inhibitor p21 is prosurvival in adriamycin-induced podocyte injury, in vitro and in vivo. *Am J Physiol Renal Physiol* **298**, F1140-1151 (2010).
13. Romagnani, P., *et al.* Next generation sequencing and functional analysis of patient urine renal progenitor-derived podocytes to unravel the diagnosis underlying refractory lupus nephritis. *Nephrol Dial Transplant* **31**, 1541-1545 (2016).

14. Macconi, D., *et al.* Permselective dysfunction of podocyte-podocyte contact upon angiotensin II unravels the molecular target for renoprotective intervention. *Am J Pathol* **168**, 1073-1085 (2006).
15. Ransom, R.F., Lam, N.G., Hallett, M.A., Atkinson, S.J. & Smoyer, W.E. Glucocorticoids protect and enhance recovery of cultured murine podocytes via actin filament stabilization. *Kidney Int* **68**, 2473-2483 (2005).
16. Narlis, M., Grote, D., Gaitan, Y., Boualia, S.K. & Bouchard, M. Pax2 and pax8 regulate branching morphogenesis and nephron differentiation in the developing kidney. *J Am Soc Nephrol* **18**, 1121-1129 (2007).
17. Kietzmann, L., *et al.* MicroRNA-193a Regulates the Transdifferentiation of Human Parietal Epithelial Cells toward a Podocyte Phenotype. *J Am Soc Nephrol* **26**, 1389-1401 (2015).
18. Kaverina, N.V., Eng, D.G., Schneider, R.R., Pippin, J.W. & Shankland, S.J. Partial podocyte replenishment in experimental FSGS derives from nonpodocyte sources. *Am J Physiol Renal Physiol* **310**, F1397-1413 (2016).
19. Kang, H.M., *et al.* Sox9-Positive Progenitor Cells Play a Key Role in Renal Tubule Epithelial Regeneration in Mice. *Cell Rep* **14**, 861-871 (2016).
20. Griffin, S.V., Petermann, A.T., Durvasula, R.V. & Shankland, S.J. Podocyte proliferation and differentiation in glomerular disease: role of cell-cycle regulatory proteins. *Nephrol Dial Transplant* **18 Suppl 6**, vi8-13 (2003).
21. Hagen, M., *et al.* Cell cycle re-entry sensitizes podocytes to injury induced death. *Cell Cycle* **15**, 1929-1937 (2016).
22. Asanuma, K., *et al.* Synaptopodin regulates the actin-bundling activity of alpha-actinin in an isoform-specific manner. *J Clin Invest* **115**, 1188-1198 (2005).
23. Guhr, S.S., *et al.* The expression of podocyte-specific proteins in parietal epithelial cells is regulated by protein degradation. *Kidney Int* **84**, 532-544 (2013).
24. Eng, D.G., *et al.* Glomerular parietal epithelial cells contribute to adult podocyte regeneration in experimental focal segmental glomerulosclerosis. *Kidney Int* **88**, 999-1012 (2015).
25. Kaverina, N.V., *et al.* WT1 Is Necessary for the Proliferation and Migration of Cells of Renin Lineage Following Kidney Podocyte Depletion. *Stem Cell Reports* **9**, 1152-1166 (2017).
26. Jefferson, J.A., Alpers, C.E. & Shankland, S.J. Podocyte biology for the bedside. *Am J Kidney Dis* **58**, 835-845 (2011).
27. Zhan, Y., *et al.* Activated macrophages require T cells for xenograft rejection under the kidney capsule. *Immunol Cell Biol* **81**, 451-458 (2003).
28. Richmond, A. & Su, Y. Mouse xenograft models vs GEM models for human cancer therapeutics. *Dis Model Mech* **1**, 78-82 (2008).
29. Atala, A., Irvine, D.J., Moses, M. & Shaunak, S. Wound Healing Versus Regeneration: Role of the Tissue Environment in Regenerative Medicine. *MRS Bull* **35**(2010).
30. Majkowski, M., Poda, P., Kulbacka, J., Saczko, J. & Sikorski, A.F. Alternation of fluorescent spectra of membrane markers DiI C18(3) and DiI C18(5) evoked by laser illumination. *J Histochem Cytochem* **60**, 789-791 (2012).
31. Fischer, U.M., *et al.* Pulmonary passage is a major obstacle for intravenous stem cell delivery: the pulmonary first-pass effect. *Stem Cells Dev* **18**, 683-692 (2009).

32. Schrepfer, S., *et al.* Stem cell transplantation: the lung barrier. *Transplant Proc* **39**, 573-576 (2007).
33. Kang, W.J., *et al.* Tissue distribution of 18F-FDG-labeled peripheral hematopoietic stem cells after intracoronary administration in patients with myocardial infarction. *J Nucl Med* **47**, 1295-1301 (2006).
34. Ruotsalainen, V., *et al.* Nephrin is specifically located at the slit diaphragm of glomerular podocytes. *Proceedings of the National Academy of Sciences* **96**, 7962-7967 (1999).

Chapter 8

Optimized non-viral gene delivery to primary urinary renal progenitor cells for enhanced cell migration

Gary W. Liu, Soren L. Johnson, Ritika Jain, David J. Peeler, Yilong Cheng, Jeffrey W. Pippin, Stuart J. Shankland, and Suzie H. Pun

Abstract

Progressive loss of glomerular podocytes during kidney disease leads to irreversible kidney failure, and is exacerbated by the fact that podocytes are terminally differentiated and unable to proliferate. Regeneration of lost podocytes must therefore come from non-podocyte sources. Human urine-derived renal progenitor cells (uRPCs) are attractive podocyte progenitors for cell therapy due to their ability to migrate to injured glomeruli and differentiate into *de novo* podocytes after intravenous administration, and accessible sourcing from patient urine. As gene delivery has emerged as an important strategy to augment the functionality and survival of cell therapies prior to injection, in this work we optimized non-viral gene delivery conditions (cell density, DNA dose, % FBS, and transfection material composition) to primary uRPCs. Using the cationic polymer-peptide conjugate VIPER, we achieve efficient transgene expression (up to 55% transfected cells) as well as stable transgene expression (>65% integration efficiency) lasting up to 10 days. With these methods, we transfected uRPCs to overexpress CXCR4, an important chemokine receptor that mediates uRPC migration to the kidneys after intravenous injection.

[1]Manuscript in preparation.

8.1 Introduction

New therapies to arrest chronic kidney disease (CKD) progression and prevent end stage renal disease are urgently needed as the cost of treating these patients approaches a staggering $114 billion per year in the United States.[1] A leading cause of CKD is injury and loss of glomerular podocytes, highly specialized and differentiated epithelial cells that are an integral component of the glomerular filtration barrier.[2,3] As podocytes are terminally differentiated and unable to proliferate, replenishment of podocyte number during physiological and pathological podocyte loss is entirely dependent on cellular regeneration by non-podocyte sources.[4-6] In disease conditions when podocyte loss is aggravated (e.g., by circulating factors, autoreactive antibodies, genetic mutations of key podocyte cytoskeletal proteins),[7-9] the rate of podocyte loss overwhelms the regenerative capacity of endogenous podocyte progenitors. Continuous net podocyte depletion leads to focal, then global, glomerulosclerosis that deteriorates kidney filtration.[2] Maintaining podocyte number is critical for kidney function, and autologous transfer of podocyte progenitors that have been expanded *ex vivo*, to supplement the endogenous progenitor reservoir, may be clinically strategic in meeting the increased regenerative demand during disease and halt CKD progression.

Renal progenitor cells (RPCs) are an attractive candidate for podocyte cell therapies due to their ability to integrate into injured glomeruli and differentiate into *de novo* podocytes after intravenous administration, and ease of sourcing. Within the nephron, RPCs are a subset of parietal epithelial cells (PECs) that line the Bowman's capsule and are characterized as $CD133^{+}CD24^{+}$, which are markers of stem and progenitor cells.[10] Bowman's capsule RPCs are

contiguous with glomerular podocytes, and exhibit a gradient in phenotype from multipotent RPCs near the urinary pole to podocyte-committed RPCs near the vascular pole. Clinically, RPCs are shed into urine during active proteinuria,[11] presenting a non-invasive avenue of collecting and expanding these cells for therapeutic applications. Intravenous infusion of urine-derived RPCs (uRPCs) in an animal model of doxorubicin HCl-induced nephropathy significantly reduced proteinuria, and uRPCs integrated into glomeruli and expressed podocyte proteins synaptopodin, nephrin, and podocin, suggesting differentiation into *de novo* podocytes.[11,12]

Gene delivery is often applied to cell therapies to augment the functionality and survival of the transferred cells: in cancer immunotherapy, the FDA-approved T-cell therapies Yescarta and Kymriah recognize B-cell leukemias through viral transduction of CD19 chimeric antigen receptors. An interesting candidate for gene delivery to RPCs is the chemokine receptor CXCR4, which is expressed on multiple cell types (e.g., hematopoietic stem cells, leukocytes) and mediates cellular migration through binding to its ligand, SDF-1,[13] which is often locally upregulated in diseased or injured tissues.[14,15] In RPCs, CXCR4 mediates migration to the kidneys during disease: blocking CXCR4 on transferred RPCs with antibodies significantly reduces cell recruitment to the kidneys and efficacy in a mouse model of acute renal failure, as well as transendothelial migration *in vitro*.[16] CXCR4 overexpression through gene delivery has been shown to augment the migration of mesenchymal stem cells to glioblastoma multiforme tumors and the engraftment of human pluripotent stem cell-derived hematopoietic progenitor cells into bone marrow.[17,18] Similarly, we hypothesize that CXCR4 overexpression via gene

delivery methods in transferred uRPCs could enhance cellular homing to injured glomeruli and subsequent podocyte regeneration.

Given the clinical potential of uRPCs in regenerating lost podocytes, we developed methods for non-viral gene delivery to uRPCs using a cationic polymer-peptide gene delivery conjugate, VIPER (virus-inspired polymer for endosomal release), for both transient and stable transgene expression.[19,20] First, we optimized transfection conditions (cell seeding density, media FBS content, DNA dose, VIPER composition) to achieve efficient transgene expression (up to 55%) in primary uRPCs. Through co-transfection with *Sleeping Beauty* transposon and transposase, we attained long-term (10 day) transgene expression. In translational work, we transfected uRPCs to overexpress CXCR4, and show that transfection significantly increases CXCR4 expression compared to untransfected and mock-transfected cells.

8.2 Materials and methods

8.2.1 Plasmids

A tdTomato-T2A-DHFRdm plasmid that carries the T3 SB transposon cassette containing an EF1α promoter, tdTomato, *Thosea asigna* virus 2A cleavable peptide (T2A), and a double-mutant of dihydrofolate reductase (DHFRdm) insensitive to methotrexate (MTX) was constructed using the previously reported pMC_T3/mCherry-T2A-DHFRdm construct as a backbone and standard molecular biology cloning techniques.[21] A tdTomato-containing plasmid

(generous gift from Michael Jensen, Seattle Children's Research Institute) and the NTC9385R-MCS plasmid (Nature Technology)[22] were used as templates for PCR. R6K-RNA-OUT origin of replication and selection gene were amplified with complementary ends and ligated to the transposon. The plasmid was transformed into electrocompetent bacteria according to manufacturer instructions (Nature Technology) and purified using a Plasmid Maxi Kit (Qiagen). SB100× minicircle was described previously.[23] pmaxGFP plasmid was purchased from Lonza, and CXCR4 plasmid was purchased from Addgene (plasmid 66262).

8.2.2 VIPER synthesis

The cationic polymer-peptide conjugate VIPER (virus-inspired polymer for endosomal release) was synthesized and characterized as previously described by reversible addition-fragmentation chain transfer polymerization.[19,20] VIPER is a diblock copolymer and contains the general block formula p(OEGMA-*co*-DMAEMA)-*b*-p(DIPAMA-*co*-PDSEMA), where OEGMA is oligo(ethylene glycol) monomethyl ether methacrylate, DMAEMA is 2-(dimethylamino)ethyl methacrylate, DIPAMA is 2-diisopropylaminoethyl methacrylate, and PDSEMA is poly(pyridyl disulfide ethyl methacrylate). After polymerization, copolymers were functionalized with the membrane-lytic peptides melittin, FL-20, CMA-2, C6M3, or MEP-2 as previously described.[20]

8.2.3 Renal progenitor cell isolation

Human RPCs were isolated from patient urine as previously described with modifications[11,12] and with approval from the University of Washington Institutional Review Board. Briefly, fresh

patient urine samples were collected, washed with PBS, and plated with EGM-MV+20% FBS (Lonza) supplemented with antibiotics on T-75 flasks. Cells were allowed to grow for 6-8 d until confluence. For sorting, cells were lifted with Accutase (Millipore), stained with anti-CD133-APC (clone 293C3, Miltenyi Biotec) and anti-CD24-FITC (clone SN3, ThermoFisher Scientific) antibodies, and then sorted for double-positive cells (BD FACSAria III, UW Pathology Flow Cytometry Core). Isotype-stained cells were used to establish gates. After, sorted $CD133^{+}CD24^{+}$ cells were plated on T75 flasks and allowed to grow to confluence. Multiple cell stocks were frozen in 5% DMSO/95% FBS or allowed to grow for another passage before freezing.

8.2.4 Transfection

In a typical transfection experiment, RPCs were thawed and either plated directly or first allowed to proliferate and then plated in a 24-well plate for experiments. RPCs were transfected after 18-21 h incubation. For polyplex formulation, VIPER polymer dissolved in 10 μL H_2O at the appropriate nitrogen/phosphate (N/P) mass ratio was added to 1 μg plasmid dissolved in 10 μL H_2O, mixed, and incubated at room temperature for 30 min. After, 180 μL media was added to the polyplexes. Cells were then washed with 500 μL PBS, and polyplexes were immediately added. After 4 h incubation with polyplexes at 37 °C, cells were washed with PBS and incubated in fresh media for 24-48 h.

The tdTomato-T2A-DHFRdm plasmid was co-transfected with SB100× transposase minicircle for genome-integration studies using the methods described above. The total DNA amount was fixed at 1 μg at various transposon:transposase ratios (1:0-1:4). Transient and stable tdTomato

expression was quantified by flow cytometry on days 1 and 10, respectively. Percent integration was calculated as the percent tdTomato+ cells on day 10 divided by the percent tdTomato+ cells on day 1. MTX selection was performed by adding various concentrations of MTX (0-500 nM).

For flow cytometry analysis, cells were washed with PBS, lifted with trypsin for 5 min, resuspended in PBS, stained with Zombie Violet viability dye (BioLegend) according to manufacturer instructions, and resuspended in 1% BSA in PBS. Flow cytometry was performed using an Attune NxT flow cytometer (ThermoFisher Scientific), and data was analyzed using FlowJo software. Statistical analysis was performed using GraphPad Prism 6. To quantify CXCR4 expression, CXCR4-transfected cells were lifted and incubated with mouse anti-CXCR4 monoclonal primary antibody (eBioscience, clone 12G5) for 30 min at 4 °C, followed by staining with Alexa Fluor 488-labeled donkey anti-mouse antibody (Jackson ImmunoResearch Laboratories, Inc.) for 30 min at 4 °C. Cells were evaluated for CXCR4 protein expression by flow cytometry as described above, using secondary antibody-stained controls to establish negative gates.

8.3 Results and discussion

8.3.1 Optimization of non-viral gene delivery

Plasmids of minimal size were generated with the short (<500 bp) expression and antiobiotic-free selection sequence from the Nanoplasmid platform, as transfection efficiency increases with

decreasing plasmid size.[24,25] To evaluate transient and long-term transfection, plasmids containing the *Sleeping Beauty* transposon system (SBTS) that we have previously reported were generated, but with a tdTomato fluorescent reporter.[21] Briefly, the transposon expresses tdTomato and a double-mutant of dihydrofolate reductase (DHFRdm) that confers resistance to methotrexate (MTX) metabolic inhibition. The SBTS is a non-viral gene transfer method currently used in clinical trials for adoptive T-cell therapy.[26] Compared to viral vectors, SBTS is less costly, easier to produce, and exhibits a reduced risk of insertional mutagenesis.[26] Short-term transfection may be evaluated by transfection of the plasmid alone, while long-term gene integration may be evaluated by co-transfection with transposase, which recognize the inverted terminal repeats flanking the transposon and integrates the transposon into the genome. Subsequent MTX addition could provide an avenue to select for integrated cells for a more homogeneous cell population.[21]

.

The cationic polymer-peptide conjugate, VIPER (virus-inspired polymer for endosomal release), was utilized for these gene delivery experiments. This polymer complexes and condenses with plasmid DNA, self-assembling into nanoparticle polyplexes, and was engineered to be pH-sensitive. After cellular internalization into acidic endosomes and lysosomes, the polyplexes linearize and unpackage to expose conjugated membrane-lytic mellitin peptides that mediate endosomal escape and gene delivery into the cytoplasm.[19] This delivery technology enables efficient gene delivery *in vitro* and *in vivo*, and in subsequent studies we have developed a panel of VIPER variants with alternative membrane-lytic peptides and pH-dependent membrane lysis.[20] Here, we screened this panel of VIPER polymers to identify the formulation that enables efficient gene delivery.

Initial experiments screened for the effect of cell density, DNA dose, media FBS content, and VIPER composition on transfection efficiency and viability using design of experiments optimization as we have previously reported.[27] First, uRPC density (2.5×10^4 or 5.0×10^4 cells/well) and DNA dose (1 or 2 μg) were optimized. At each of the nitrogen (VIPER) to phosphate (DNA) (N/P) ratios tested, transfection with 1 μg DNA resulted in greater viability and number of tdTomato+ cells compared to transfection with 2 μg DNA, likely due to less VIPER polymer used. Notably, transfections at N/P > 3 with 5.0×10^4 cells/well resulted in greater than double the viability and number of tdTomato+ cells compared to transfections with 2.5×10^4 cells/well (**Figure 8.1**). Therefore, future transfections were performed using 1 μg DNA and 5.0×10^4 cells/well.

Next, media conditions (reduced serum OptiMEM or media containing 10% FBS) were optimized. Generally, the presence of serum improves cellular viability, but decreases transfection efficiency. Transfections in complete media containing 20% FBS were not pursued, as preliminary experiments in complete media resulted in poor transgene expression (data not shown). We hypothesized that transfection in media containing 10% FBS would improve transfection efficiency and cellular viability at higher N/P ratios. Indeed, at greater N/P, transfections performed in media containing 10% FBS exhibited greater viability and comparable transfection efficiency compared to those performed in OptiMEM (**Figure 8.2**). Accordingly, future transfection experiments were performed in 10% FBS.

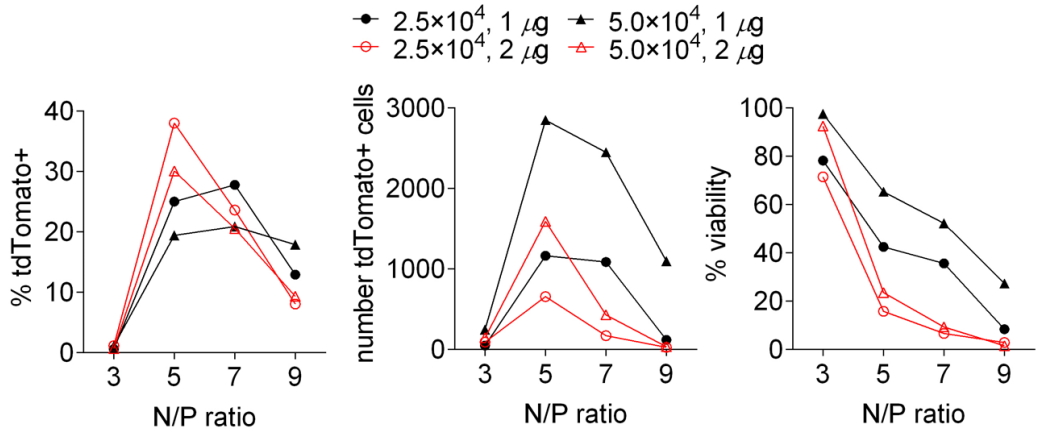

Figure 8.1 Effect of cell density and DNA amount on transfection efficiency. RPCs (n = 1 each) were transfected with VIPER/DNA polyplexes in OptiMEM at four N/P ratios, 2.5×10^4 or 5.0×10^4 cells/well, and 1 or 2 μg DNA, and then analyzed for % tdTomato+ cells (left), number of tdTomato+ cells (middle), and % viability (right) after 2 d by flow cytometry.

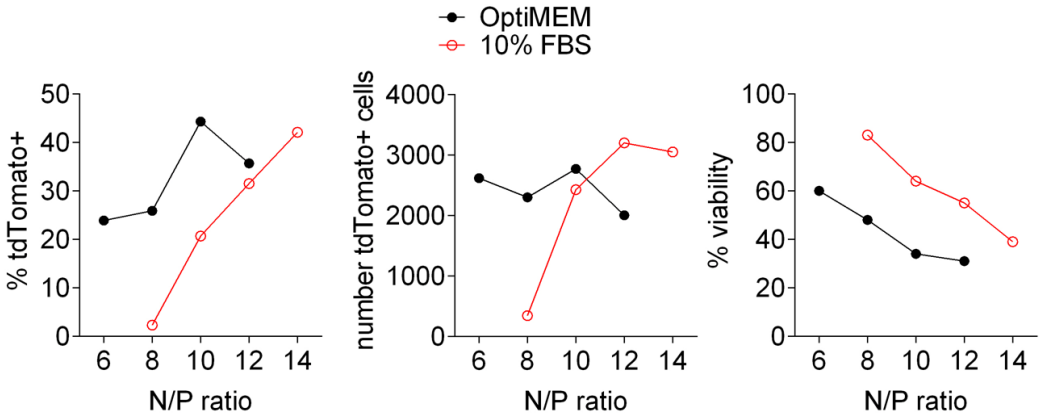

Figure 8.2 Effect of serum on transfection efficiency at higher N/P ratios. RPCs (n = 1 each) were transfected with VIPER/DNA polyplexes in OptiMEM or media containing 10% FBS at various N/P ratios, 5.0×10^4 cells/well, and 1 μg DNA, and then analyzed for % tdTomato+ cells (left), number of tdTomato+ cells (middle), and % viability (right) after 2 d by flow cytometry.

A panel of VIPER variants with different membrane-lytic peptides was tested to identify the best-performing VIPER formulation. Cell types exhibit different rates of endosomal acidification which may affect the performance of VIPER unpackaging and plasmid delivery;[28,29] for example, human T-cells exhibit a higher endosomal pH compared to Jurkats and HeLas. To

account for potential variances in endosomal pH and VIPER performance, a VIPER panel with the following membrane-lytic peptides and corresponding EC50 of membrane lysis at pH 5.5 was screened: mellittin (original VIPER, 5 μM), FL-20 (16 μM), CMA-2 (14 μM), C6M3 (6 μM), and MEP-2 (12 μM). These variants capture a range of optimal membrane-lytic activity pH and exhibit robust transfection *in vivo* in the brain after subventricular zone injection.[20] Transfection at N/P 10 and 12 with this VIPER panel revealed that VIPER mellittin, CMA-2, and MEP-2 variants resulted in a higher number of transfected cells than the other variants (**Figure 8.3**). As the original VIPER mellittin resulted in the greatest percent transfection and number of transfected cells, this variant was used in subsequent optimization studies.

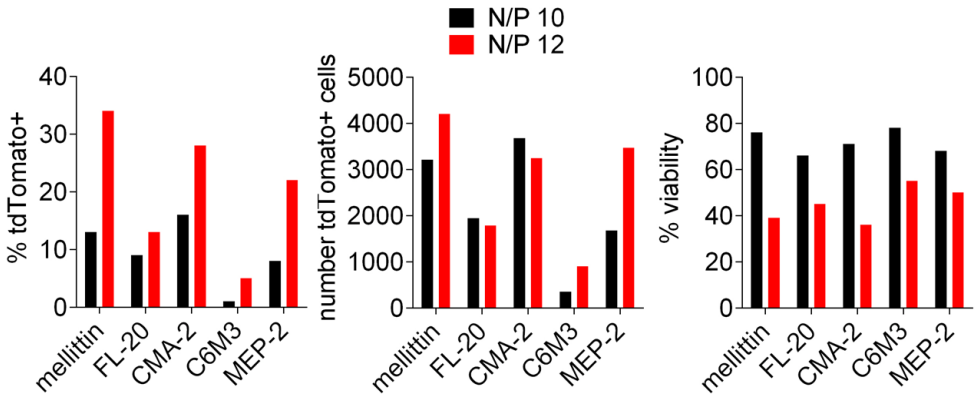

Figure 8.3 VIPER panel transfection efficiency. RPCs (n = 1 each) were transfected with VIPER/DNA polyplexes in media containing 10% FBS at N/P 10 or 12, 5.0×10^4 cells/well, and 1 μg DNA, and then analyzed for % tdTomato+ cells (left), number of tdTomato+ cells (middle), and % viability (right) after 2 d by flow cytometry.

Having optimized cell density, DNA amount, media conditions, and VIPER peptide, transfection experiments were performed in triplicate for statistical analysis and to optimize VIPER/DNA N/P ratio. Five N/P ratios were tested (**Figure 8.4**). Transfection at N/P 12, 14, and 16 resulted in greater than 7500 tdTomato+ cells, with no significant differences among the three ratios. Notably, transfection at N/P 14 resulted in significantly higher transfection efficiency than other ratios without major loss of cellular viability, whereas doubling the N/P ratio from 8 to 16

resulted in a significant decrease in viability from 79.4±10.6% to 45.2±10.9 and no significant increase in transfection efficiency over N/P 14. Therefore, N/P 14 was used for further transfection experiments. Additional experiments using a smaller plasmid, pmaxGFP, yielded 32.7, 55.1, and 44.3% transfection at N/P 10, 15, and 20, respectively (**Figure S8.1**).

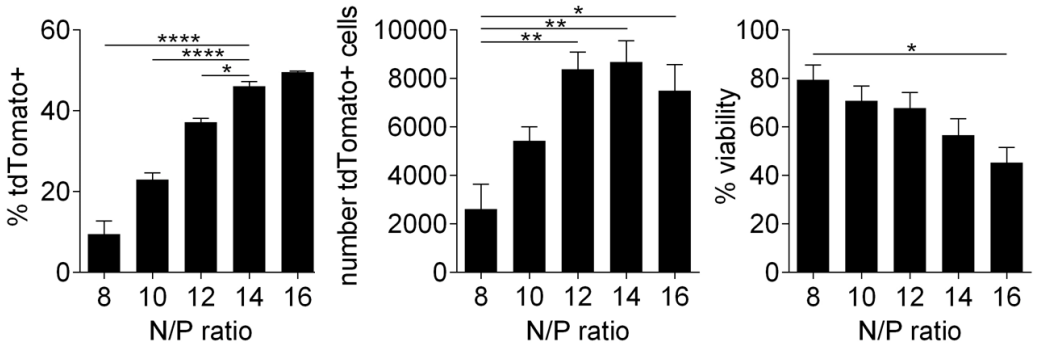

Figure 8.4 Optimization of transfection N/P ratios. RPCs (n = 3 each) were transfected with VIPER/DNA polyplexes in media containing 10% FBS at various N/P ratios, 5.0×10^4 cells/well, and 1 μg DNA, and then analyzed for % tdTomato+ cells (left), number of tdTomato+ cells (middle), and % viability (right) after 2 d by flow cytometry. Statistical analysis was performed using a one-way ANOVA with post-hoc Tukey's multiple comparisons test. Select comparisons are shown. Bars represent means ± SEM. *p-value < 0.05, **p-value < 0.01, ****p-value < 0.0001.

8.3.2 Gene integration

Gene integration efficiency was studied by co-transfecting tdTomato-T2A-DHFRdm transposon and SB100× transposase at various mole ratios in a total of 1 μg DNA using the optimized methods. Transient tdTomato expression was analyzed on day 1, and stable expression was analyzed on day 10. Notably, in the absence of transposase, minimal tdTomato expression (2.1 ± 0.5%) was observed after 10 days, whereas 12.3 ± 3.5, 15.9 ± 4.3%, 14.5 ± 1.6%, and 18.6 ± 1.4% expression was observed for transposon:transposase 4:1, 2:1, 1:1, and 1:2, respectively (**Figure 8.5**). Integration efficiency was calculated by dividing % expression on day 10 by that of

day 1. The highest genome integration (68.0 ± 2.6%) was achieved at transposon:transposase 1:2, which was significantly greater than that of 4:1 (42.3 ± 10.6%) and 1:0 (6.9 ± 1.3). Therefore, addition of transposase results in stable gene expression.

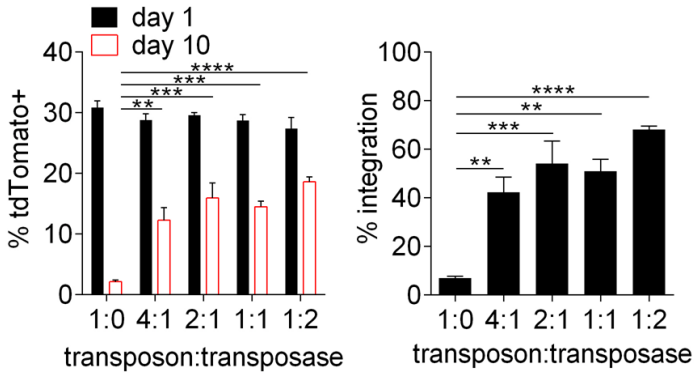

Figure 8.5 *Sleeping Beauty* transposase for stable gene expression. RPCs (n = 3) were transfected with VIPER/DNA polyplexes at five mole ratios of tdTomato-T2A-DHFRdm transposon to SB100× transposase. Left: cells were analyzed for transient expression 1 day after transfection (black) and stable expression after 10 days (red). Statistical tests were performed comparing to transposon:transposase 1:0, day 10. Right: percent integration was calculated as the % tdTomato+ after 10 days divided by the % tdTomato+ after 1 day. Statistical analysis was performed using a one-way ANOVA with post-hoc Tukey's multiple comparisons test. Bars represent means ± SEM. ***p*-value < 0.01, ****p*-value < 0.001, *****p*-value < 0.0001.

8.3.3 Methotrexate selection of transfected cells

The transposon contains a double-mutant of DHFR, which renders the mutant DHFR 10,000-fold less susceptible to MTX inhibition. Therefore, MTX may be used to enrich uRPCs for those stably transfected with the tdTomato-T2A-DHFRdm transposon construct. With methods to stably transfect RPCs at greater than 50% integration efficiency, we next sought to optimize the MTX concentration needed to enrich stably expressing cells over time. To maximize proliferation time and therefore susceptibility to MTX inhibition, cells were plated directly in a

24-well plate after thawing and then transfected using the optimized methods described above. After 24 h, transfected cells were pooled. A portion of the cells was used to analyze transient tdTomato expression on day 1, while the rest were re-plated in MTX-containing media. Cells continuously treated with MTX were analyzed again on days 6 and 16 to assess the selection efficiency of MTX. On day 1, greater than 51.5% RPCs transiently expressed tdTomato, which decreased to 41-42% after 5 days culture in MTX, regardless of concentration. After an additional 10 days, 21.8, 29.8, and 30.1% RPCs grown in 0, 100, and 500 nM MTX, respectively, expressed tdTomato (**Figure S8.2**). These findings suggest that in the conditions tested, MTX does not induce robust (>90%) enrichment of stably transfected RPCs. Alternative selection mechanisms, such as puromycin or G418, may improve the selection mechanism.

8.3.4 Overexpression of CXCR4

We then sought to generate CXCR4-overexpressing uRPCs using these optimized non-viral gene delivery methods, as transient CXCR4 expression may be clinically useful to promote the migration of transferred uRPCs onto the glomerular tuft during systemic circulation. To generate CXCR4-uRPCs, cells were transfected with CXCR4 plasmid or tdTomato plasmid as a mock transfection at N/P 14, and analyzed for CXCR4 expression by flow cytometry. Untransfected cells were also analyzed to establish baseline CXCR4 expression. Transfection with CXCR4 plasmid resulted in the greatest percentage of CXCR+ cells (~35%) compared to mock transfection (~4%) (**Figure 8.6**). CXCR4 expression observed in mock transfection conditions may be due to non-specific antibody binding rather than true gene expression. Interestingly, a low percentage of untransfected uRPCs expressed CXCR4+ (<1%), whereas Mazzinghi *et al.*

have reported that RPCs abundantly express CXCR4 at both the protein and mRNA level.[16] This may be due to cell sourcing differences: here, RPCs were collected from urine, while Mazzinghi *et al*. isolated RPCs from nephrectomized kidney tissue of patients with renal cell carcinoma. A particular phenotype of RPCs may be more predisposed to be denuded or migrate off of the Bowman's capsule during disease and shed into the urine, resulting in predominantly CXCR4-low-expressing RPCs in the urine. Extended residence in protein-dense urine may also contribute to an altered phenotype.[30]

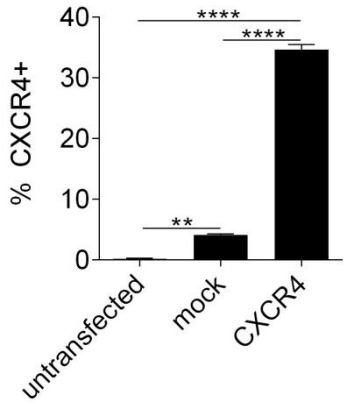

Figure 8.6 CXCR4 transfection. RPCs (n = 3 each) were transfected with tdTomato (mock) or CXCR plasmid and compared for CXCR4 expression with untransfected cells. Statistical analysis was performed using a one-way ANOVA with post-hoc Tukey's multiple comparisons test. Bars represent means ± SEM. ***p*-value < 0.01, *****p*-value < 0.0001.

The progressive loss of glomerular podocytes during disease overwhelms the regenerative capacity of endogenous podocyte progenitors and directly underlies CKD and end stage renal disease. Cell therapies leveraging RPCs, capable of engrafting onto injured kidney glomeruli and differentiating into new podocytes after intravenous infusion,[11,12] may be clinically strategic in enhancing the rate of endogenous podocyte regeneration and arresting CKD progression. These new therapies will likely utilize gene delivery methods to augment the therapeutic efficacy of the transferred cells. In this work, we optimized non-viral gene delivery conditions to primary RPCs.

Non-viral gene delivery presents with many advantages compared to viral gene delivery, including unrestricted plasmid size, reduced cost, and reduced risk of immunogenicity.[27]

We identified uRPC culture conditions and VIPER composition that lead to optimal non-viral gene delivery for both short-term and long-term transgene expression. After 48 h post-transfection, we observed up to 55% transfected cells, which decreases to <3% over 10 days. Clinically, transient expression may be useful to temporarily confer transferred stem cells with transgenes that promote migration and homing to diseased tissue, but desist after cells adopt differentiated and reparative phenotypes. Given the importance of CXCR4 in mediating RPC migration to the injured kidney,[16] we demonstrate that transfected CXCR4-uRPCs exhibit greater CXCR4 expression compared to mock-transfected and untransfected cells. Non-viral gene delivery has been an important strategy in augmenting stem cell migration and function: microporation of mesenchymal stem cells (MSCs) with CXCR4 minicircle enhances cell migration towards skin injuries;[31] and TRAIL-overexpressing adipose-derived stem cells[32] and MSCs,[33] mediated by polyplexes, localize to tumors and reduce tumor burden.

Using the *Sleeping Beauty* transposon system (SBTS), we also achieved long-term (up to 10 days) gene expression with >65% gene integration efficiency. Here, incorporation of methotrexate selection via a double-mutant of dihydrofolate reductase did not result in significant enrichment of transfected cells. An alternative strategy may be to expand transfected single-cell clones,[11] although new agents to reverse and prevent cellular senescence after expansion are needed to maintain the function of these cells. Genetic manipulation of RPCs *ex vivo* may present an avenue to repair genetically caused podocyte dysfunction. Mutations in key

podocyte ultrastructure and attachment proteins such as nephrin, podocin, and laminin β2 lead to podocyte dysfunction[34] and kidney failure. These patients often fail to respond to frontline steroid therapy, and 50% develop end-stage kidney disease within 15 years.[35] While autologous transfer of uRPCs may present an attractive strategy to restore podocyte number, the same genetic mutations would prevent differentiation into functional podocytes. Indeed, Lazzeri *et al* have shown that uRPCs derived from patients with genetic mutations in *NPHS2* differentiate into podocytes with severe cytoskeletal F-actin defects and disruption of nephrin and podocin protein expression.[11] The methods developed here could enable genomic integration of wildtype gene variants or CRISPR/Cas9 delivery that correct genetic mutations in uRPCs and therefore lead to differentiation into functional podocytes *in vivo*.

Recent work by the Romagnani group has revealed the different effects of SDF-1 on endogenous and transferred RPCs. Within the glomerulus, podocytes are the main producer of SDF-1, which under normal and disease conditions maintains quiescence of and inhibits podocyte differentiation by RPCs on the Bowman's capsule.[36,37] Interestingly, systemic blockade of SDF-1 in animals reduces proteinuria and increases podocyte regeneration by PECs during doxorubicin HCl-induced nephropathy compared to untreated animals, likely due to disruption of SDF-1-mediated PEC quiescence and inhibition.[36] While blockade of intraglomerular SDF-1 may promote podocyte differentiation by endogenous PECs, the CXCR4-SDF-1 axis is still critical in mediating glomerular engraftment of transferred RPCs.[16]

8.4 Conclusions

We report efficient non-viral gene delivery methods (up to 55% transfected cells) to primary uRPCs through optimizing cell density, DNA dose, media FBS content, and VIPER transfection reagent composition. While co-transfection with transposase resulted in >65% integration efficiency, we did not observe significant enrichment of integrated cells with MTX selection. Transfection with CXCR4 plasmid resulted in greater CXCR4 expression compared to control transfections, and we are currently evaluating migration of transfected cells in response to SDF-1. Future work will assess migration and therapeutic efficacy of transfected RPCs in animal models of podocyte loss. Given the clinical potential of uRPCs as a cell therapy to regenerate glomerular podocytes, the methods reported here may be useful in future manufacturing applications to augment the survival and differentiation ability of uRPCs. Such gene delivery to uRPCs may be clinically strategic in regenerating functional podocytes in patients with genetic causes of podocyte dysfunction.

8.5 Acknowledgments

This work was supported by the Office of the Assistant Secretary of Defense for Health Affairs through the Peer Reviewed Medical Research Program under Award Numbers PR151175 and PR151965, and by the National Science Foundation Graduate Research Fellowship Program under Grant No. DGE-1256082 to GWL. Opinions, interpretations, conclusions, and recommendations are those of the authors and are not necessarily endorsed by the Department of

Defense or the National Science Foundation. We would like to thank Ian Blumenthal and Michael Jensen for their generous gift of tdTomato-containing plasmid.

References

1. Saran, R., *et al.* US Renal Data System 2018 Annual Data Report: Epidemiology of Kidney Disease in the United States. *American Journal of Kidney Diseases* **73**, A7-A8 (2019).
2. Wharram, B.L., *et al.* Podocyte depletion causes glomerulosclerosis: diphtheria toxin-induced podocyte depletion in rats expressing human diphtheria toxin receptor transgene. *J Am Soc Nephrol* **16**, 2941-2952 (2005).
3. Matsusaka, T., *et al.* Genetic engineering of glomerular sclerosis in the mouse via control of onset and severity of podocyte-specific injury. *J Am Soc Nephrol* **16**, 1013-1023 (2005).
4. Lasagni, L., Lazzeri, E., Shankland, S.J., Anders, H.J. & Romagnani, P. Podocyte mitosis - a catastrophe. *Curr Mol Med* **13**, 13-23 (2013).
5. Kaverina, N.V., Eng, D.G., Schneider, R.R., Pippin, J.W. & Shankland, S.J. Partial podocyte replenishment in experimental FSGS derives from nonpodocyte sources. *Am J Physiol Renal Physiol* **310**, F1397-1413 (2016).
6. Shankland, S.J., Pippin, J.W. & Duffield, J.S. Progenitor cells and podocyte regeneration. *Semin Nephrol* **34**, 418-428 (2014).
7. Hahm, E., *et al.* Bone marrow-derived immature myeloid cells are a main source of circulating suPAR contributing to proteinuric kidney disease. *Nat Med* **23**, 100-106 (2017).
8. Beck, L.H., *et al.* M-Type Phospholipase A2 Receptor as Target Antigen in Idiopathic Membranous Nephropathy. *New England Journal of Medicine* **361**, 11-21 (2009).
9. Patrakka, J., *et al.* Congenital nephrotic syndrome (NPHS1): features resulting from different mutations in Finnish patients. *Kidney Int* **58**, 972-980 (2000).
10. Shankland, S.J., Smeets, B., Pippin, J.W. & Moeller, M.J. The emergence of the glomerular parietal epithelial cell. *Nat Rev Nephrol* (2014).
11. Lazzeri, E., *et al.* Human Urine-Derived Renal Progenitors for Personalized Modeling of Genetic Kidney Disorders. *J Am Soc Nephrol* (2015).
12. Ronconi, E., *et al.* Regeneration of glomerular podocytes by human renal progenitors. *J Am Soc Nephrol* **20**, 322-332 (2009).
13. Kucia, M., *et al.* CXCR4-SDF-1 signalling, locomotion, chemotaxis and adhesion. *J Mol Histol* **35**, 233-245 (2004).
14. Deng, Q.J., Xu, X.F. & Ren, J. Effects of SDF-1/CXCR4 on the Repair of Traumatic Brain Injury in Rats by Mediating Bone Marrow Derived Mesenchymal Stem Cells. *Cell Mol Neurobiol* **38**, 467-477 (2018).

15. Chen, L.H., *et al.* SDF-1/CXCR4 signaling preserves microvascular integrity and renal function in chronic kidney disease. *PLoS One* **9**, e92227 (2014).
16. Mazzinghi, B., *et al.* Essential but differential role for CXCR4 and CXCR7 in the therapeutic homing of human renal progenitor cells. *J Exp Med* **205**, 479-490 (2008).
17. Jiang, X., Wang, C., Fitch, S. & Yang, F. Targeting Tumor Hypoxia Using Nanoparticle-engineered CXCR4-overexpressing Adipose-derived Stem Cells. *Theranostics* **8**, 1350-1360 (2018).
18. Reid, J.C., *et al.* CXCL12/CXCR4 Signaling Enhances Human PSC-Derived Hematopoietic Progenitor Function and Overcomes Early In Vivo Transplantation Failure. *Stem Cell Reports* **10**, 1625-1641 (2018).
19. Cheng, Y., Yumul, R.C. & Pun, S.H. Virus-Inspired Polymer for Efficient In Vitro and In Vivo Gene Delivery. *Angew Chem Int Ed Engl* **55**, 12013-12017 (2016).
20. Peeler, D.J., *et al.* pH-sensitive polymer micelles provide selective and potentiated lytic capacity to venom peptides for effective intracellular delivery. *Biomaterials* **192**, 235-244 (2019).
21. Kacherovsky, N., Liu, G.W., Jensen, M.C. & Pun, S.H. Multiplexed gene transfer to a human T-cell line by combining Sleeping Beauty transposon system with methotrexate selection. *Biotechnol Bioeng* **112**, 1429-1436 (2015).
22. Luke, J., Carnes, A.E., Hodgson, C.P. & Williams, J.A. Improved antibiotic-free DNA vaccine vectors utilizing a novel RNA based plasmid selection system. *Vaccine* **27**, 6454-6459 (2009).
23. Kacherovsky, N., Harkey, M.A., Blau, C.A., Giachelli, C.M. & Pun, S.H. Combination of Sleeping Beauty transposition and chemically induced dimerization selection for robust production of engineered cells. *Nucleic Acids Res* **40**, e85 (2012).
24. Suschak, J.J., Williams, J.A. & Schmaljohn, C.S. Advancements in DNA vaccine vectors, non-mechanical delivery methods, and molecular adjuvants to increase immunogenicity. *Hum Vaccin Immunother* **13**, 2837-2848 (2017).
25. Levacic, A.K., Morys, S., Kempter, S., Lachelt, U. & Wagner, E. Minicircle Versus Plasmid DNA Delivery by Receptor-Targeted Polyplexes. *Hum Gene Ther* **28**, 862-874 (2017).
26. Aronovich, E.L., McIvor, R.S. & Hackett, P.B. The Sleeping Beauty transposon system: a non-viral vector for gene therapy. *Hum Mol Genet* **20**, R14-20 (2011).
27. Olden, B.R., Cheng, Y., Yu, J.L. & Pun, S.H. Cationic polymers for non-viral gene delivery to human T cells. *J Control Release* **282**, 140-147 (2018).
28. Olden, B.R., Cheng, E., Cheng, Y. & Pun, S.H. Identifying key barriers in cationic polymer gene delivery to human T cells. *Biomater Sci* **7**, 789-797 (2019).
29. Rybak, S.L. & Murphy, R.F. Primary cell cultures from murine kidney and heart differ in endosomal pH. *J Cell Physiol* **176**, 216-222 (1998).
30. Zhai, T., *et al.* Alteration of podocyte phenotype in the urine of women with preeclampsia. *Sci Rep* **6**, 24258 (2016).
31. Mun, J.-Y., Shin, K.K., Kwon, O., Lim, Y.T. & Oh, D.-B. Minicircle microporation-based non-viral gene delivery improved the targeting of mesenchymal stem cells to an injury site. *Biomaterials* **101**, 310-320 (2016).
32. Jiang, X., *et al.* Nanoparticle engineered TRAIL-overexpressing adipose-derived stem cells target and eradicate glioblastoma via intracranial delivery. *Proc Natl Acad Sci U S A* **113**, 13857-13862 (2016).

33. Han, J., Hwang, H.S. & Na, K. TRAIL-secreting human mesenchymal stem cells engineered by a non-viral vector and photochemical internalization for pancreatic cancer gene therapy. *Biomaterials* **182**, 259-268 (2018).
34. Lovric, S., Ashraf, S., Tan, W. & Hildebrandt, F. Genetic testing in steroid-resistant nephrotic syndrome: when and how? *Nephrol Dial Transplant* **31**, 1802-1813 (2016).
35. Ha, T.S. Genetics of hereditary nephrotic syndrome: a clinical review. *Korean J Pediatr* **60**, 55-63 (2017).
36. Romoli, S., *et al.* CXCL12 blockade preferentially regenerates lost podocytes in cortical nephrons by targeting an intrinsic podocyte-progenitor feedback mechanism. *Kidney Int* **94**, 1111-1126 (2018).
37. Sayyed, S.G., *et al.* Podocytes produce homeostatic chemokine stromal cell-derived factor-1/CXCL12, which contributes to glomerulosclerosis, podocyte loss and albuminuria in a mouse model of type 2 diabetes. *Diabetologia* **52**, 2445-2454 (2009).

Supporting information

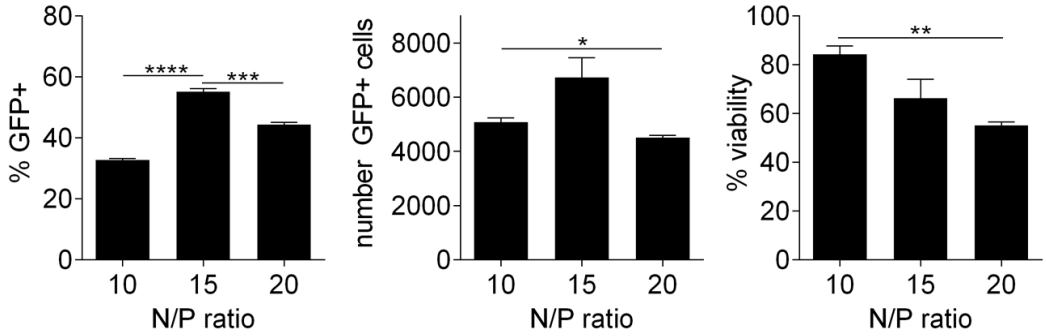

Figure S8.1 Transfection of RPCs with pmaxGFP. RPCs (n = 3 each) were transfected 19 h after thawing with VIPER/DNA polyplexes in media containing 10% FBS at various N/P ratios, 5.0×10^4 cells/well, and 1 μg DNA, and then analyzed for % GFP+ cells (left), number of GFP+ cells (middle), and % viability (right) after 1 d by flow cytometry. Statistical analysis was performed using a one-way ANOVA with post-hoc Tukey's multiple comparisons test. Select comparisons are shown. Bars represent means ± SEM. *p-value < 0.05, **p-value < 0.01, ***p-value < 0.001, ****p-value < 0.0001.

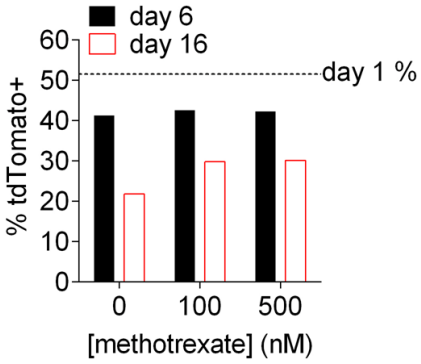

Figure S8.2 Effect of methotrexate selection on transfected cell enrichment. RPCs (n = 1) were transfected with transposon:transposase ratio 1:1 and analyzed for tdTomato expression after 1 (dotted line), 6 (black bars), and 16 days (red bars). MTX was added after day 1.

Chapter 9

Major findings and future perspectives

Abstract

In this chapter, major findings from Chapters 7 and 8 are summarized, and future work to test uRPCs engineered with nanoscale drug “backpacks” and gene delivery are proposed.

9.1 Summary of major findings

The completed work sought to engineer urine-derived renal progenitor cells (uRPCs) as a cell therapy for podocyte regeneration.

9.1.1 Isolation and functionality of urinary renal progenitor cells (uRPCs)

The work described in Chapter 7 sought to isolate and characterize renal progenitor cells from human patient urine (uRPCs), with the priority of demonstrating *in vivo* rescue in an animal model of podocyte loss. uRPCs were efficiently sorted and isolated, and exhibited changes in actin cytoskeleton and progenitor markers when cultured in podocyte-differentiating media. In an antibody-induced model of podocyte loss, animals treated with uRPCs exhibited significantly less proteinuria compared to PBS-treated animals. Tissue imaging confirmed uRPC migration to injured glomeruli and podocyte-like features. These cells exhibit therapeutic effects during kidney disease, and are ideal for cell engineering applications as a cell therapy.

9.1.2 Optimized non-viral gene delivery methods to uRPCs

Gene delivery to uRPCs could enhance the therapeutic efficacy of these cells by enhancing migration towards injured tissues and correcting genetic mutations. Work in Chapter 8 optimized non-viral gene delivery conditions of cell density, DNA dose, FBS content, and transfection reagent composition to achieve efficient (up to 55%) and long-term (10 day) transgene expression using cationic polymer-peptide conjugates. With these methods, uRPCs were

transfected to overexpress CXCR4, an important receptor that mediates the migration of these cells.

9.2 Future perspectives

9.2.1 Nanoscale drug "backpacks" to augment uRPC therapy

Rationale. A recognized challenge in clinical cell therapies across various cell types (e.g., stem cells, hepatocytes, and T cells) is maintaining cellular viability and persistence *in vivo*.[1-3] Factors such as anoikis, ischemia, and reactive oxygen species at the engraftment site contribute to poor viability of transplanted cells.[3-5] Strategies to mitigate these factors and improve cell survival include cellular encapsulation within biomaterial scaffolds,[2,6,7] pre-treatment with pro-survival cues,[8,9] and genetic manipulation to enhance cell engraftment.[10] Small molecule drugs have also been concomitantly infused as adjuvants to boost the efficacy of cell therapies: in cancer immunotherapy, small molecule drugs are used to enhance T cell survival and tumor-homing.[11]

Glucocorticoids are routinely utilized in the nephrology clinic to treat glomerular diseases.[12] Recent reports have shown that the clinical efficacy of glucocorticoids may be due to direct drug effects on glomerular cells, rather than its systemic anti-inflammatory effects. In experimental focal segmental glomerulosclerosis (FSGS), glucocorticoids enhanced podocyte regeneration by increasing the number and p-ERK pro-survival signaling of renal progenitor cells lining the Bowman's capsule.[13] Therefore, glucocorticoids are attractive to boost the functionality of

injected uRPCs. However, long-term glucocorticoid therapy causes significant side effects. To overcome these clinical challenges, one strategy is to focus adjuvant drug effects directly on the transferred uRPCs through loading of drug-loaded nanoscale "backpacks."

Due to the direct action of glucocorticoids on RPCs, we hypothesize that focused delivery of glucocorticoids to transferred uRPCs through drug "backpacks" could augment the survival and differentiation ability of uRPCs during cell therapy (**Figure 9.1**).

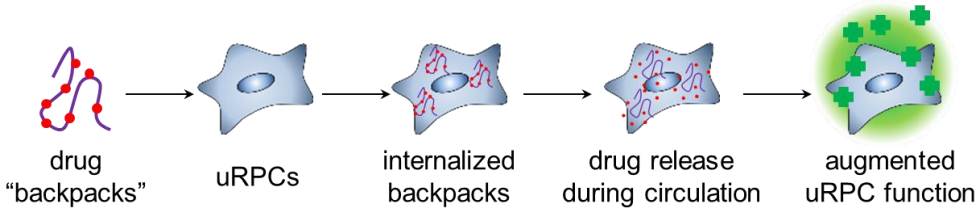

Figure 9.1 Overview of proposed design. Urinary renal progenitor cells (uRPCs) are loaded with nanoscale drug "backpacks" that release glucocorticoids, which protect cell viability and enhance differentiation during injection and engraftment into injured glomeruli. Red circles represent drug cargo; purple lines represent polymer "backpacks."

Preliminary data. Polymer-DEX conjugates were synthesized by reversible addition-fragmentation chain transfer of the monomers *N*-(2-hydroxypropyl) methacrylamide (HPMA) and *N*-[3-(dimethylamino)propyl]methacrylamide (DMAPMA), a tertiary amine-containing monomer that mediates cellular internalization via electrostatic interactions with the negatively charged cell membrane.[14] Dexamethasone (DEX) was used as a model glucocorticoid due to its reported *in vivo* effects in glomerular disease models,[15,16] and was first modified to contain a carboxylic acid as previously described[17] for ester bond formation with polymer hydroxyl groups via EDC/DMAP chemistry. Ester bonds were selected due to its esterase-sensitivity and

controlled drug release profile.[18] Two DEX-containing polymers were synthesized and are summarized in **Table 9.1**.

Table 9.1 Summary of DEX-containing copolymers. M_n, number average molecular weight; $Đ$, dispersity.

Polymer	Composition	M_n (Da)	$Đ$	DEX loading (% w/w)
P1-DEX	p($HPMA_{75}$-*co*-$DMEPMA_5$)	11.1 kDa	1.01	16.9
P2-DEX	p($HPMA_{250}$-*co*-$DMEPMA_{25}$)	34.4 kDa	1.04	14

Next, polymer-DEX conjugates were characterized for cell loading, internalization, cytotoxicity, and non-specific protein adsorption *in vitro*. An immortalized human parietal epithelial cell line (PEC)[19] was used for these characterization studies due to limited quantities of primary uRPCs. To simulate polymer loading before intravenous injection, cells were incubated with fluorescently labeled P1-DEX or P2-DEX (0.1-10 mg/mL, corresponding to DEX concentrations of 0.035-4.3 mM) for 30 min with mixing every 10 min as previously described.[11] After, cells were evaluated for polymer loading by flow cytometry (**Figure 9.2A**). Uniform polymer loading into cells was observed with polymer concentrations as low as 0.1 mg/mL, and loading increased with increasing polymer concentration. By confocal microscopy studies, polymers were internalized into intracellular vesicles, as evidenced by punctate polymer staining, and a subset was trafficked through the endolysosomal pathway (**Figure 9.2B**). Importantly, polymers did not exhibit significant cytotoxicity against immortalized PECs up to 48 h after polymer loading (**Figure 9.2C**).

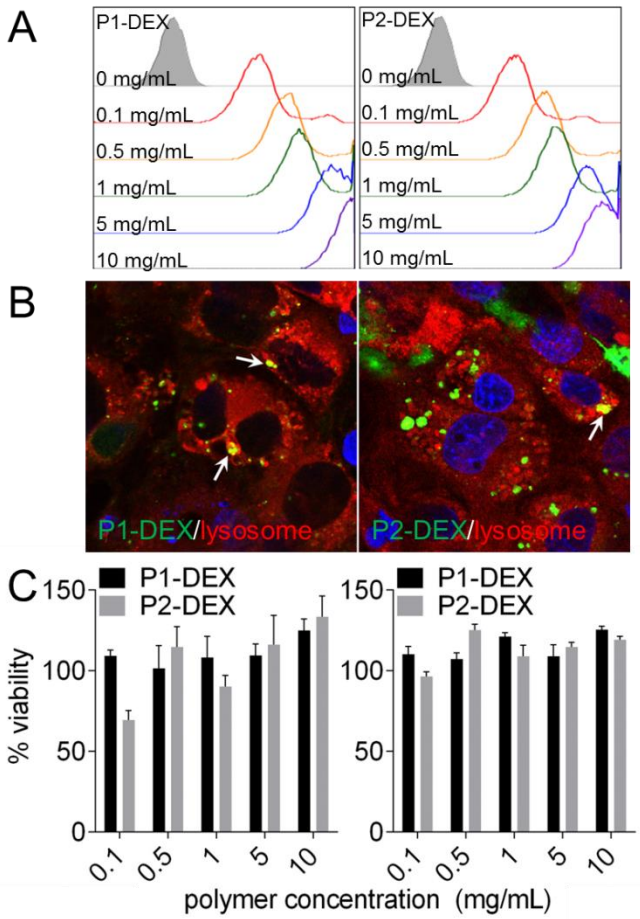

Figure 9.2 Polymer-DEX conjugate behavior *in vitro*. **A.** Intensity plots of fluorescent polymers loaded onto immortalized human parietal epithelial cells (PECs) at various concentrations (0.1-10 mg/mL). **B.** Representative fluorescent images of PECs 24 h after loading with polymers. Arrows indicate colocalization. Blue, DAPI; green, DEX-polymer; red, lysosomes. **C.** Viability of PECs loaded with polymers after 24 (left) or 48 (right) h. Bars represent means ± SEM.

In our experience, cationic polymers can alter cell membrane charge and cause artificial binding of negatively charged macromolecules such as albumin and siRNA. This could lead to non-specific cell adherence to negatively charged endothelial cells and protein adsorption that dramatically alters the *in vivo* functionality of these cells. To investigate this potential issue, cells were incubated with fluorescently labeled albumin immediately after polymer loading and washing to simulate injection conditions. While loading with P1-DEX (11 kDa) did not effect a

general trend in albumin adsorption, loading with P2-DEX (34 kDa) resulted in greater albumin adsorption with increasing polymer concentration (**Figure 9.3**). As drug loading efficiencies for the P1-DEX and P2-DEX polymers are similar (16.9% and 14%, respectively), future studies will proceed with the P1-DEX polymer due to its reduced potential to alter the cell membrane.

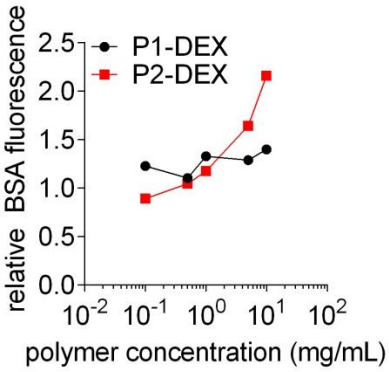

Figure 9.3 Albumin adsorption to polymer-loaded cells. Median fluorescence intensity of bovine serum albumin adsorption after loading human parietal epithelial cells with polymers. Intensities were normalized to untreated cells.

The preliminary data indicate that cationic DEX-polymer conjugates are readily loaded onto cells, are internalized, and are not cytotoxic. Future work will investigate the therapeutic efficacy of these materials loaded into uRPCs.

Therapeutic animal model. Polymer-loaded uRPCs will be tested in the antibody-induced model of podocyte loss described in Chapter 7. On days 1 and 4, animals will be treated with the following: (*i*) PBS; (*ii*) uRPCs only; (*iii*) uRPCs + DEX given systemically; and (*iv*) P1-DEX-uRPCs. The DEX dose will be equivalent at 1 mg/kg (per prior work[13,15,16]) across all relevant treatments. At least 3.75 $\times 10^5$ cells will be injected each time, and cells will be fluorescently labeled to enable cellular quantification as described in Chapter 7.

Metrics. Urine proteinuria, glomerular podocyte density, and glomerular uRPC density will be quantified to evaluate treatment efficacy. We expect P1-DEX-uRPCs to outperform other treatments in proteinuria reduction, maintenance of glomerular podocyte density, and increased glomerular engraftment during podocyte loss due to focused and localized intracellular DEX delivery.

Significance. Podocyte loss is a leading cause of end-stage kidney failure, and new interventions to regenerate lost podocytes are urgently needed for these patients. uRPCs are a promising cell therapy candidate, and nanotechnology can significantly enhance the efficacy of these cells. The proposed work develops a new method of extending the viability and functionality of transferred uRPCs in a manner that focuses drug delivery to these cells, optimizing drug pharmacokinetics to reduce systemic side effects.

9.2.2 Gene delivery to uRPCs for augmented cell homing

Rationale. The CXCR4-SDF-1 axis is critical in mediating uRPC homing to injured glomeruli. As the therapeutic efficacy of uRPC transfer is dependent on cellular migration and subsequent differentiation into *de novo* podocytes, gene delivery strategies to overexpress CXCR4 on uRPCs could be strategic in increasing cell homing to glomeruli. This strategy is based on an established field of gene delivery to stem cells for increased migration to tumors and injury sites, and the work described in Chapter 8 validates that uRPCs can be manipulated to overexpress CXCR4.

Therapeutic animal model. First, historical kidney tissue will be validated for SDF-1 expression in injured glomeruli in our antibody-induced model of podocyte loss. On days 1 and 4, after antibody-induced podocyte injury, animals will be treated with the following: (*i*) PBS; (*ii*) uRPCs only; (*iii*) mock-transfected uRPCs; and (*iv*) CXCR4-transfected uRPCs. At least 3.75 $\times 10^5$ cells will be injected each time, and cells will be fluorescently labeled to enable cellular quantification. Urines will be collected regularly throughout.

Metrics. Urine proteinuria and glomerular uRPC density will be quantified to evaluate treatment efficacy as well as uRPC migration onto the glomerular tuft. We expect all treatments to significantly reduce proteinuria. If CXCR4 promotes uRPC migration, then we may observe an earlier or more sustained reduction of proteinuria compared to other treatments. This will be correlated with glomerular uRPC quantification.

Significance. Gene delivery to these cells establishes an important precedent for new podocyte-regenerative therapies that replace dysfunctional podocytes in genetic causes of podocyte loss. Here, we targeted the CXCR-SDF-1 axis, as it is well-established broadly in stem/progenitor cell migration as well as uRPCs. If effective, this strategy could be implemented in the clinic to enhance the effectiveness of uRPC therapies.

9.2.3 Nephrin-reporter uRPCs for high-throughput screening

Rationale. uRPCs are an attractive cell source for cell therapies to regenerate lost podocytes due to their easy sourcing (collection from urine) and ability to differentiate into *de novo* podocytes

after systemic administration. This cell platform can therefore have various applications in drug delivery and regenerative medicine. Here, we propose the development of nephrin-reporting uRPCs (via fluorescence or luminescence) for high-throughput screening methods to identify drugs (small molecules, proteins) that induce a podocyte fate. Identification of such drugs is urgently needed to promote the differentiation ability of both transferred and endogenous renal progenitor cells. Moreover, identification of protein modulators of podocyte differentiation can enable new therapeutics that genetically edit transferred cells to secrete these agents in an auto- and paracrine manner. Such a screening method has been effective in identifying small molecule modulators of nephrin expression in podocytes.[20]

Overall strategy. A tdTomato fluorescent reporter will be generated under the nephrin promoter. Nephrin was selected as it is a classical podocyte gene essential to the function of the slit diaphragm. RPCs will be permanently integrated with this reporter by viral transduction, and transduced cells will be identified and isolated via limiting dilution and PCR. Cells will then be expanded for high-throughput screening assays. The area of potential greatest impact may be protein modulators of RPC survival and differentiation, as protein secretion may be genetically encoded for cell therapy applications. A library of proteins will be screened for RPC survival (quantified by viability assays) and podocyte differentiation (quantified by reporter fluorescence) in normal and high albumin challenge (shown to inhibit RPC differentiation). Positive controls DEX and retinoic acid will be included in the screen as positive controls.

Significance. While some pharmacological modulators of RPC survival and differentiation (DEX,[13] BIO,[21] retinoic acid[22]) have been identified, these have mostly been small molecules.

Protein modulators can potentially offer great utility in the management of kidney diseases due to genetic engineering strategies and greater specificity compared to small molecule drugs. Moreover, these reporters can be utilized in animal models of podocyte loss to study the kinetics and conditions of *de novo* podocyte differentiation.

9.3 Acknowledgments

This work was supported by the Office of the Assistant Secretary of Defense for Health Affairs through the Peer Reviewed Medical Research Program under Award Numbers PR151175 and PR151965, and by the National Science Foundation Graduate Research Fellowship Program under Grant No. DGE-1256082 to GWL. Opinions, interpretations, conclusions, and recommendations are those of the authors and are not necessarily endorsed by the Department of Defense or the National Science Foundation.

References

1. Nguyen, P.K., Neofytou, E., Rhee, J.W. & Wu, J.C. Potential Strategies to Address the Major Clinical Barriers Facing Stem Cell Regenerative Therapy for Cardiovascular Disease: A Review. *JAMA Cardiol* **1**, 953-962 (2016).
2. Lee, A.S., *et al.* Prolonged survival of transplanted stem cells after ischaemic injury via the slow release of pro-survival peptides from a collagen matrix. *Nature Biomedical Engineering* **2**, 104-113 (2018).
3. Lee, S., Choi, E., Cha, M.J. & Hwang, K.C. Cell adhesion and long-term survival of transplanted mesenchymal stem cells: a prerequisite for cell therapy. *Oxid Med Cell Longev* **2015**, 632902 (2015).
4. Chang, W., *et al.* Anti-death strategies against oxidative stress in grafted mesenchymal stem cells. *Histol Histopathol* **28**, 1529-1536 (2013).

5. Gilmore, A.P. Anoikis. *Cell Death And Differentiation* **12**, 1473 (2005).
6. Hill, E., Boontheekul, T. & Mooney, D.J. Regulating activation of transplanted cells controls tissue regeneration. *Proc Natl Acad Sci U S A* **103**, 2494-2499 (2006).
7. Zhong, J., *et al.* Hydrogel matrix to support stem cell survival after brain transplantation in stroke. *Neurorehabil Neural Repair* **24**, 636-644 (2010).
8. Hu, S., *et al.* Novel microRNA prosurvival cocktail for improving engraftment and function of cardiac progenitor cell transplantation. *Circulation* **124**, S27-34 (2011).
9. Rota, C., *et al.* Human amniotic fluid stem cell preconditioning improves their regenerative potential. *Stem Cells Dev* **21**, 1911-1923 (2012).
10. Yang, J.X., *et al.* CXCR4 receptor overexpression in mesenchymal stem cells facilitates treatment of acute lung injury in rats. *J Biol Chem* **290**, 1994-2006 (2015).
11. Stephan, M.T., Moon, J.J., Um, S.H., Bershteyn, A. & Irvine, D.J. Therapeutic cell engineering with surface-conjugated synthetic nanoparticles. *Nat Med* **16**, 1035-1041 (2010).
12. Mallipattu, S.K., *et al.* Kruppel-Like Factor 15 Mediates Glucocorticoid-Induced Restoration of Podocyte Differentiation Markers. *J Am Soc Nephrol* **28**, 166-184 (2017).
13. Zhang, J., *et al.* Podocyte repopulation by renal progenitor cells following glucocorticoids treatment in experimental FSGS. *Am J Physiol Renal Physiol* **304**, F1375-1389 (2013).
14. Cheng, Y., *et al.* Boronic Acid Copolymers for Direct Loading and Acid-Triggered Release of Bis-T-23 in Cultured Podocytes. *ACS Biomaterials Science & Engineering* **4**, 3968-3973 (2018).
15. Mallipattu, S.K., *et al.* Krüppel–Like Factor 15 Mediates Glucocorticoid-Induced Restoration of Podocyte Differentiation Markers. *Journal of the American Society of Nephrology* **28**, 166-184 (2017).
16. Li, L., *et al.* Role of Myeloid-Derived Suppressor Cells in Glucocorticoid-Mediated Amelioration of FSGS. *Journal of the American Society of Nephrology* **26**, 2183-2197 (2015).
17. Everts, M., *et al.* Selective intracellular delivery of dexamethasone into activated endothelial cells using an E-selectin-directed immunoconjugate. *J Immunol* **168**, 883-889 (2002).
18. Howard, M.D., Ponta, A., Eckman, A., Jay, M. & Bae, Y. Polymer micelles with hydrazone-ester dual linkers for tunable release of dexamethasone. *Pharm Res* **28**, 2435-2446 (2011).
19. Kietzmann, L., *et al.* MicroRNA-193a Regulates the Transdifferentiation of Human Parietal Epithelial Cells toward a Podocyte Phenotype. *J Am Soc Nephrol* **26**, 1389-1401 (2015).
20. Yamauchi, K., *et al.* Screening and identification of substances that regulate nephrin gene expression using engineered reporter podocytes. *Kidney International* **70**, 892-900 (2006).
21. Lasagni, L., *et al.* Podocyte Regeneration Driven by Renal Progenitors Determines Glomerular Disease Remission and Can Be Pharmacologically Enhanced. *Stem Cell Reports* **5**, 248-263 (2015).
22. Peired, A., *et al.* Proteinuria impairs podocyte regeneration by sequestering retinoic acid. *J Am Soc Nephrol* **24**, 1756-1768 (2013).